TRANSNUCLEAR
AN AREVA COMPANY

August 17, 2011
E-31368

U. S. Nuclear Regulatory Commission
Attn: Document Control Desk
One White Flint North
11555 Rockville Pike
Rockville, MD 20852

Subject: Revision 1 to Transnuclear, Inc. (TN) Application for Approval of the TN-LC Transportation Package, Response to Request for Supplemental Information (Docket No. 71-9358; TAC No. L24543)

Reference: Letter from Pierre Saverot (NRC) to Kamran Tavassoli (TN), "Request for Supplemental Information for the Model No. TN-LC Package (TAC No. L24543)," July 26, 2011

The letter referenced above advised TN that NRC staff had completed an acceptance review of our June 7, 2011 application for Approval of the TN-LC Transportation Package and that supplemental information is needed for the staff to continue their review. The information needed was enclosed in the letter as Requests for Supplemental Information (RSIs). The letter also included observations to allow TN to start earlier on items containing the potential to be asked at a later date. TN was advised that responses to the observations are not required for the staff to begin a detailed technical review.

The purpose of this submittal is to respond to the RSIs and the observations.

- Enclosure 1 provides the proprietary version of the TN responses to the Request for Supplemental Information.
- Enclosure 2 provides the non-proprietary version of the TN responses to the Request for Supplemental Information.
- Enclosure 3 provides a list of changes in the Safety Analysis Report (SAR) associated with the RSI responses.
- Enclosure 4 provides instructions for the SAR page replacement.
- Enclosures 5 and 6 include the changed SAR pages for the proprietary and non-proprietary SAR versions, respectively. The changed areas are indicated by revision bars in the right margin and italics for inserted text.
- Enclosure 7 provides the references associated with the RSI responses. A list of these references is also provided in Enclosure 7.
- Enclosure 8 is the signed Affidavit Pursuant to 10 CFR 2.390.

Transnuclear looks forward to working with the NRC staff on this application. TN is prepared to meet with the staff to resolve any questions you might have. Should the NRC staff require additional information to support review of this application, please do not hesitate to contact Mr. Kamran Tavassoli at 410-910-6944 or me at 410-910-6881.

7135 Minstrel Way, Suite 300, Columbia, MD 21045
Phone: 410-910-6900 ◆ Fax: 410-910-6902

NMSS01
NMSS

Sincerely,

Jayant Bondre, PhD
Vice President - Engineering

cc: Pierre Saverot, Project Manager, NRC SFST, as follows:
- Two paper copies of this cover letter and Enclosures 1, 3 through 5, and 7 through 8
- Seven DVDs containing this cover letter and all Enclosures
- One DVD containing this cover letter and Enclosures 2 through 4, and 6 through 8 for the publicly available information

Enclosures:

1. Responses to Request for Supplemental Information, Proprietary Version
2. Responses to Request for Supplemental Information, Non-proprietary Version
3. List of changed pages of the SAR associated with RSI responses
4. SAR Page Replacement Instructions
5. Changed Pages for the Safety Analysis Report, Revision 1, Proprietary Version
6. Changed Pages for the Safety Analysis Report, Revision 1, Non-proprietary Version
7. References associated with the RSI responses
8. Affidavit Pursuant to 10 CFR 2.390

Enclosure 2 to TN E-31368

Responses to Request for Supplemental Information

(Non-proprietary Version)

DOCKET NO. 71-9358

REQUEST FOR SUPPLEMENTAL INFORMATION (RSI) FOR THE MODEL NO. TN-LC PACKAGE

RSI 1 Re-evaluate the closure lid and cask top flange interface design and perform the necessary numerical simulation analysis to substantiate the statement, "The maximum separation between the lid and cask body during the impact is 0.047 in. This gap occurs for a short duration, and the gap is closed subsequently." See Appendix 2.13.7, Page No. 2.13.7-8.

Considering the maximum calculated separation or bolt elongation of 0.047", the twenty (20) 4-inch long by 1-inch diameter SA-540 Graded B23 Class 1 bolts shown in Drawing 65200-71-01 appear to have undergone inelastic deformation during the 30-ft cask free end-drop hypothetical accident condition. Evidence of the inelastic deformation is shown by a permanent lid separation of more than 0.02" between the lid and cask body, as displayed in Figures 2.13.7-14 and -21. The calculated permanent lid separation of the 30-ft cask end-drop accident, per 10 CFR 71.73(c)(1), does not meet the regulations because "inelastic deformation of the containment closure system (e.g., bolts and flanges) is unacceptable for the containment evaluation."

This information is needed to demonstrate compliance with 10 CFR 71.73(c)(1).

TN RSI 1 RESPONSE:

Proprietary Information Withheld Pursuant to 10 CFR 2.390.

RSI 2 Revise the analysis implied by the bullet statement, "A nodal force time history is applied to the cask mass, corresponding to the peak deceleration of the TN-LC transport cask impact limiter at -40°F," to ensure that the fuel rod end drop analysis methodology is appropriate. See Appendix 2.13.11, Page No. 2.13.11-11.

The staff notes that the boundary condition as stated in the bullet is inconsistent with the approach of the recently approved TN-40 transportation cask in which no force time history is applied to the cask mass; instead, a terminal velocity of 527.4 in/sec corresponding to the 30-ft drop is applied to the fuel rod and the cask supported by the cask-to-ground spring.

This information is needed to demonstrate compliance with 10 CFR 71.73(c)(1).

TN RSI 2 RESPONSE:

Proprietary Information Withheld Pursuant to 10 CFR 2.390.

RSI 3 Include in the application the force-deflection curves which represent the characteristic spring behavior for evaluating fuel rod structural performance under the cask end-drop hypothetical accident condition. The impact limiter force-deflection curves for the springs shown on Figure 2.13.11-12 have not been presented.

This information is needed to demonstrate compliance with 10 CFR 71.73(c)(1).

TN RSI 3 RESPONSE:

Per the request, the plots for the impact limiter force-deflection curves for the cask to ground springs are provided in the Figure 2.13.11-12a of SAR.

RSI 4 Demonstrate that pieces of the poison plate material will maintain their configuration during normal and accident conditions.

Note 12 on Sheet 1 of Licensing Drawing 65200-71-90 states that the poison plates can be made of multiple pieces of material.

There is no analysis in the Safety Analysis Report of how these pieces could reconfigure under normal and accident conditions. Spaces between poison plate pieces and overlapping of those pieces may significantly alter the criticality analysis, particularly under accident conditions.

This information is needed to demonstrate compliance with 10 CFR 71.55(b).

TN RSI 4 RESPONSE:

Note 12 on Sheet 1 of Licensing Drawing 65200-71-90 statement is modified to "Each plate (Item 4) may consist of multiple segments in the longitudinal direction. Each segment must be attached by minimum of two studs (Item 3)."

Poison plates are entrapped between the stainless steel of 1" thick compartment and rails which are attached through bolts. Evaluation is performed to demonstrate that the poison plates do not shear and therefore overlapping of poison plates will not occur which is addressed in new SAR Section 2.13.8.5.6.

The effect of these bolt holes (through the poison plate) on the criticality of the TN-LC-1FA basket is evaluated in section 6.10.4.4.1 of Appendix 6.10.4 of the SAR. The result of this evaluation indicates that the effect is statistically insignificant although the highest calculated k_{eff} (that includes the effect of the poison plate bolt holes) is employed as the design basis k_{eff} for the TN-LC-1FA basket.

RSI 5 Demonstrate that both normal and accident conditions of transport will not substantially alter the geometric form of non-commercial spent nuclear fuel and assemblies of commercial high burn up spent fuel.

The mechanical properties of non-commercial spent nuclear fuel and high burn assemblies (> 45 GWd/MTU) of commercial spent fuel are not well established.

This information is needed to demonstrate compliance with 10 CFR 71.43(f).

TN RSI 5 RESPONSE:

Proprietary Information Withheld Pursuant to 10 CFR 2.390.

RSI 6 Provide descriptions of the alternate but equivalent weld joint configurations or unspecified welding geometries listed throughout the licensing drawings, e.g., Note 14 of licensing drawing 65200-71-20, Note 19 on Sheet 2 of licensing drawing 65200-71-01, etc. Alternatively, justify how all of these joint configurations and welding geometries are not important to safety.

This information is needed to demonstrate compliance with 10 CFR 71.33(a)(5)(iii).

TN RSI 6 RESPONSE:

The drawing notes are revised with the following note added to each applicable drawing, in order to ensure that any alternate welding configuration will be analyzed prior to implementation and compared with the allowable stresses defined in the safety analysis, to ensure compliance with Part 71 requirements. The revised note reads:

> "Partial penetration weld sizes shown are the required effective throat. All weld preparation grooves to be sized accordingly. Minimum weld sizes are specified on all drawings. Alternate weld configurations conforming to applicable ASME code may be used upon TN approval, provided the stresses calculated for the alternate weld configurations are bounded by the allowable stresses defined in the safety analysis with safety factors equal to or greater than those used in the safety analysis".

Regarding Note 14 of drawing 65200-71-20 rev. 0: as mentioned in the note, the sole safety function of this weld is to ensure leak tightness of the impact limiter shell, in order to maintain the moisture content of the wood inside the impact limiter to the range of values specified on the drawing in Note 10.

The particular area of the impact limiter this note is pointing to is the junction between three components of the impact limiter: the inner shell (item 2 of drawing 65200-71-20 rev. 0), the outer cover segment (item 10 of drawing 65200-71-20 rev. 0) and the bolt sleeve (item 8 of drawing 65200-71-20 rev. 0), where the weld might prove difficult to make because of the geometry of the joint. The purpose of note 14 is to clarify the design intent of the weld

(impact limiter leak tightness) for the purpose of facilitating fabrication. Note 14 of drawing 65200-71-20 has been revised to clarify this requirement.

RSI 7 Justify that an upper limit of -31°C on the temperature of retraction of the elastomer seal is sufficient to maintain containment at -40°C.

Discussions with vendors of elastomer seals have lead the staff to find that a temperature of retraction no greater than -35°C is necessary to maintain a static seal at -40°C.

This information is needed to demonstrate compliance with 10 CFR 71.43(f).

TN RSI 7 RESPONSE:

The elastomer chosen for use in the TN-LC is based on the manufacturer's rating which states that the elastomer will function at -40°C. One parameter used to determine suitability for use is the temperature of retraction, TR-10. This temperature is determined by stretching a test sample approximately 50% at room temperature and then cooling to a temperature such that it does not retract when released. The TR-10 value is determined by raising the temperature until the sample has retracted by 10%. This temperature is defined as the TR-10 value. The TR-10 value for the TN-LC O-ring material is given as -31°C in Reference 8 of Chapter 4 of the SAR.

Multiple other references state that for a static seal, the sealing performance is maintained as low as 15°C below the TR-10 value. This value is then -46°C which is below the limit of -40°C. Three of these references are provided below:

http://machinedesign.com/article/relating-material-tests-to-seal-performance-0323

http://www.pspglobal.com/prop-thermal-stability.html

http://www.rlhudson.com/O-Ring%20Book/selecting-thermal3.html

Note again that this value applies to a static seal configuration reflecting the TN-LC design. In addition, the pressures expected at the low temperatures are also low since the design pressures are based on design heat loads at hot ambient conditions.

RSI 8 Justify that the absorbed dose will not significantly affect the elastomer seals used for containment, citing sources in literature.

In general, the staff finds that the radiation damage threshold for elastomer materials is 10^6 rads. However, the radiation threshold for fluoropolymers is significantly lower, approximately 1×10^4 rads, The maximum calculated dose of 2×10^4 rads to the seals is above this number.

This information is needed to demonstrate compliance with 10 CFR 71.43(d).

TN RSI 8 RESPONSE:

Data described in Reference 8 of SAR Chapter 4, Section 4.5 indicate that the effect of radiation on Viton-type elastomers is such that the seals used in the TN-LC are adequate. This reference was produced to evaluate O-ring seal material for a package with similar requirements to those of the TN-LC. A notable difference, however, is that long-term performance was required for the subject evaluation. The radiation resistance at exposure levels expected for the TN-LC was noted to be of secondary interest compared to oxidization and temperature effects. Figures 11 through 13 of this reference demonstrate this by showing time and temperature to be the most important variables at the radiation levels predicted. The effect of oxidation is not a concern for the TN-LC application because the containment seal is kept in a helium environment for the duration of the shipment. Note also that the TN-LC seals are used in a static application and are required to seal a relatively low-pressure containment vessel.

RSI 9 Provide additional information for the neutron shield resin tubes installed around the outer steel shell of the cask, describing:

a. How the resin tubes are attached to the cask body,

b. How the maximum gap size is determined,

c. How the gap size might be expected to change in response to changing conditions (e.g., thermal cycling of ambient conditions, differential thermal expansion due to different package contents, or mechanical stresses during NCT and HAC).

The neutron shield resin tubes are installed around the outer steel shell of the cask in a manner "controlled to maximize the tube-to-tube contact, thus minimizing gaps between adjacent tubes" (see Chapter No. 5, Section No. 5.3.3). In Chapter No. 3, the thermal analysis uses a uniform value of 0.01 inch for the gap between the steel shell and the aluminum tubes containing the resin, and for the gap between the resin tubes and the outer steel skin of the package. The character of this gap has an important effect on radial temperature gradients through the cask body, and there is not sufficient information in the application to demonstrate that this assumed value is conservative and bounding for both NCT and HAC.

This information is needed to demonstrate compliance with 10 CFR 71.33 (a)(5)(v).

TN RSI 9 RESPONSE:

Proprietary Information Withheld Pursuant to 10 CFR 2.390.

Since the thermal expansion coefficient of aluminum is larger than stainless steel, the gap sizes will not be changed when the cask is loaded. Therefore, assuming a radial gap of 0.01 inch between neutron shield resin tubes and adjacent shells is conservative.

In the thermal model of the TN-LC transport cask, the assumed gaps between the neutron shield aluminum tubes and adjacent shells are removed during the fire accident (the properties changed to the properties of one of the adjacent components) and then restored after the fire accident as described in the SAR Section 3.4.2 and Table 3-21. This approach maximizes the heat input from the fire to the cask during fire accident and maximizes the cask thermal resistance during the cool-down period to result in conservative maximum component temperatures.

Two thermal tests were performed on the TN-32 casks at PCC and at RANOR. The test results were summarized and sent to NRC for review via TN letter E-18576 (TN-32 Cask Thermal Testing, Docket 72-1021) dated December 1, 2000. A copy of this letter is included in Enclosure 7 to this submittal.

The thermal tests demonstrated that the assumed gaps are conservative using fabrication method at RANOR and acceptable using fabrication method at PCC.

It should be noted that the thermal analysis of the TN-LC transport cask determines a margin of 134°F to the temperature limit of 400°F for research reactor spent nuclear fuels and a margin of 210°F to the temperature limit of 752°F for the commercial spent nuclear fuels as shown in Table 3-2 of the SAR. These large margins provide additional assurance for the safety of the TN-LC transport cask.

RSI 10 Provide information from references, including other application's documents, directly, either as additional attachments to the submitted package application, or by simply reproducing the referenced information within the current application.

The thermal analyses in Chapter No. 3 make multiple references to other application's documents, some of which are currently under review by NRC. This approach of referencing other documents for important technical information fragments the presentation of information in the application, and could lead to gaps in required information to perform this review (particularly if information in documents currently under NRC review change during the course of the review.)

This information is needed to ensure compliance with 10 CFR 71.31.

TN RSI 10 RESPONSE:

Information from references, including other application's documents, is provided in Enclosure 7 to this submittal.

RSI 11 Provide 2-D depletion analyses or validation studied in support of the SAS2H analysis of BWR and PWR fuel assemblies.

In Section No. 5.2 of the application, the applicant states: "the SAS2H module of the SCALE4.4 code package is used to compute the gamma and neutron source terms for BWR and PWR fuel assemblies and rods." Given the fact that the SAS2H is no longer supported by the developer, the applicant can perform a 2-D depletion analysis sequence which could provide more accurate source terms calculations.

Alternatively, the applicant can provide validation studies or benchmark experiments that quantify the accuracy for the nuclides of importance for shielding calculations (such as Co-60, Cs-134, Cs-137, Eu-154, Pr-144, Cm-242, and Cm-244), and any bias in the calculations that should be incorporated in a margin for safety.

This information is needed to ensure compliance with 10 CFR 71.7.

TN RSI 11 RESPONSE:

Appendix 5.6.4, section 5.6.4.2 is amended to include discussion regarding the analysis of the system with TRITON, an uncertainty and validation analysis for SAS2H, and quantification of conservatisms in the source term for commercial fuel in the TN-LC-1FA shielding analysis. The conservatisms in the shielding analysis are sufficient to cover for these uncertainties.

The NCT maximum package surface dose rate shown in Table 5.6.4-1 is 582 mrem/hour and corresponds to the underside of the package at the location of the shear key where the neutron shielding is replaced with steel. This results in an increase in neutron dose rates at a location where the surface is not accessible. This does not have any impact on the calculation of the maximum dose rate 2 m from the vehicle surface. Therefore, the reported dose rate results (the change in the maximum dose rate from cask surface to 2 m from vehicle surface) in Table 5.6.4-1 are justified.

RSI 12 Clarify whether partial and/or preferential flooding has been addressed for each of the four TN-LC basket designs (TN-LC-NRUX, TN-LC-MTR, TN-LC-TRIGA, and TN-LC-1FA). Demonstrate that partial and preferential flooding is less reactive than modeling flooding in all areas of the package at the most reactive density.

The staff recognizes that partial flooding was considered for one basket design based on a statement in Section 6.10.3.3.1 for the TN-LC-TRIGA basket that states "While it is possible that the cask could be partially filled with water, with some fuel assemblies submerged and others uncovered, this scenario was not modeled because it is less reactive (due to less moderation) than the case in which all fuel assemblies are submerged." It is not apparent that this statement is necessarily true for all cases involving HEU. In addition, no statements were made regarding the other basket designs (e.g., TN-LC-MTR). Clarify that this statement applies to the other TN-LC basket designs and provide further justification for making this conclusion for all cases involving HEU.

Similarly, the staff recognizes that preferential flooding was considered for one basket design based on a statement in Section 6.10.2.3.1 for the TN-LC-NRUX basket that states "Because the cask is designed for wet loading, water drains freely inside the

basket, and no preferential draining scenarios are considered. Therefore, water is always modeled at the same density in all basket regions of the model." Clarify that this statement applies to the other TN-LC basket designs.

The staff needs such clarifications and demonstrations to determine if k_{eff} has been calculated with the maximum reactivity.

This information is needed to ensure compliance with 10 CFR 71.55(b).

TN RSI 12 RESPONSE:

The TN-LC cavity and all baskets have been designed to drain freely. Therefore, preferential flooding that could result in a more reactive configuration is not credible for any of the baskets. However, the cavity could be partially flooded. Because the baskets drain freely, if the TN-LC cavity is partially flooded, the only credible scenario is that some fuel would be submerged in water, and the remaining fuel would remain unsubmerged. Therefore, any partial flooding scenarios would result in unmoderated fuel. All fuels transported in the TN-LC, including the HEU fuels, show lower reactivity in the absence of moderation. Therefore, any partial flooding would uncover fuel and decrease the reactivity. This effect is demonstrated explicitly for NRU fuel in Appendix 6.10.2 of the SAR.

Although partial and/or preferential flooding that could result in a more reactive configuration is not credible, cases are run with reduced water density in the package cavity for each of the fuel and basket types. For each fuel type, full-density water results in the most reactive condition, which supports the statement that uncovering fuel will reduce the reactivity.

A discussion on partial and/or preferential flooding is added to the criticality analysis for each of the four basket/fuel types – Appendix 6.10.1, Section 6.10.1.3.1 for TN-LC-MTR basket, Appendix 6.10.2, Section 6.10.2.2.1 for TN-LC-NRUX basket, Appendix 6.10.3, Section 6.10.3.3.1 for TN-LC-TRIGA basket, and Appendix 6.10.4, Section 6.10.4.3.1 for TN-LC-1FA basket.

Observations

1. Clarify the notations, such as 8D and 5C on page No. 2.13.1-18, Figure Nos. 2.13.1-20 and -21, used in the formula for calculating the axial component reaction pressure estimates, R_E and R_I, for the cask body structural analysis. Also, explain why the reaction force proration is conservative, which appears to have no consideration for an impact limiter deformation-compatible stress distribution force boundary condition.

The staff notes that, if reaction force, R_I, is overestimated, stresses in the cask bottom or cask lid may not be conservatively calculated. The basis for prorating the reaction pressure must be justified for the cask body structural analysis.

TN OBSERVATION 1 RESPONSE:

Notations refer to the item number in the drawings shown in Chapter 1, such as 8D refers to Gamma Shielding in drawing 65200-71-01, sheet 11, Section Y-Y and 5C refers to gamma shielding in drawing 65200-71-01, sheet 8, Section H-H.

The bounding condition for the HAC end and corner drops is Load Combination 29, End Drop on Lid End, and the maximum $P_L + P_B$ stress for the Lid Assembly is 44.6 ksi (Table 2.13.1.43).

An axisymmetric ANSYS evaluation of the lid assembly is performed where the lid is simply supported at the bolt location. The total load on the lid is evaluated considering the impact limiter wood orientation. Assuming the deflection in the impact limiter is constant through the different wood orientations, the force exerted by the center section of the balsa is $A_{B\perp}.X$, where $A_{B\perp}$ is section area and X is the reaction pressure applied. Similarly the reaction forces exerted by other segments are equal to the area of the segment and the reaction pressure applied. The crush stress of redwood and balsa in the parallel direction are a factor of 18.5 and 5.0 greater than balsa in the perpendicular direction (Appendix 2.13.12). Given that the reaction pressure is directly proportional to the crush stress of wood, the net reaction force applied by the impact limiter to the cask is

$$W_cG = A_{B\perp} X + 18.5A_{R\parallel} X + 5.0 A_{B\parallel} X$$

Where,

W_c = Weight of the TN-LC cask with one impact limiter

G = Maximum g-load deceleration during end drop

$A_{B\perp}$ = Section area for Balsa wood in perpendicular direction

$A_{R\parallel}$ = Section area for Redwood in parallel direction

$A_{B\parallel}$ = Section area for Balsa wood in parallel direction

X = Reaction pressure applied

The maximum bending stress in the Lid assembly is at the center of the Lid and is 17.2 ksi. Conservatively, adding this stress to the bounding Lid assembly stress from Appendix 2.13.1, (44.6 +17.2 = 61.8 ksi), is still below the allowable of $P_L + P_B$ of 65.1 ksi. Thus, the maximum stress in the lid does not exceed the ASME code allowables.

2. Provide sufficient description and justification for physical attributes of the dummy composite volume used to evaluate the structural performance of the closure lid and bolt for the delayed impact.

Assumptions, as presented on page No. 2.13.7-3, for the Young's modulus, Poisson ratio, and mass density for the "dummy volume" are insufficient for evaluating its mass and axial stiffness effects on the cask closure lid and bolts for the delayed impact event. Physical attributes of the dummy volume (e.g., size, dimensions, distribution, gaps, etc.) should clearly be described in the application.

TN OBSERVATION 2 RESPONSE:

Proprietary Information Withheld Pursuant to 10 CFR 2.390.

3. For end-drop hypothetical accident condition (HAC), explain how the stress category S_y is considered for evaluating the MTR basket bucket side wall and TRIGA basket tubes and wraps. See Table Nos. 2.13.8-9 and 2.13.8-12, respectively.

   Table No. 2-3 of the application, "Cask Basket Stress Limits," does not recognize the "stress category" S_y for evaluating basket structural performance for the HAC end drop event.

TN OBSERVATION 3 RESPONSE:

The stress category S_y is removed for evaluating the MTR basket bucket side wall and TRIGA basket tubes and wraps for end-drop hypothetical accident condition (HAC) and the stresses are compared with "Cask Basket Stress Limits," specified in Chapter 2, Table 2-3.

4. Justify the use of an initial internal pressure of 2,020 psi for analyzing the PWR and BWR fuel rods for the cask 30-ft end drop accident. See Page No. 2.13.11, Section 2.13.11.1.4.10, Boundary Conditions.

TN OBSERVATION 4 RESPONSE:

Proprietary Information Withheld Pursuant to 10 CFR 2.390.

5. Explain the basis for selecting the sampling frequency for displaying the calculated response time history. See Figure No. 2.13.11.19, Maximum Principal Strain Time History of 14x14 Fuel Rod for HAC.

   The staff notes that, in post-processing calculated time-history response, the selection of a large time interval for reporting and displaying the results may often result in some unintended data filtering effects. A sensitivity analysis should be performed on the response sampling frequency to ensure that response data is properly reported.

TN OBSERVATION 5 RESPONSE:

Proprietary Information Withheld Pursuant to 10 CFR 2.390.

6. Clarify the sub-caption of the Table, "(1/3 Scale Test Results vs. 1/3 Scale LS-DYNA Analysis)" on Table No. 2.13.12-1, Benchmark Analysis Results. The listed results, such as acceleration values, appear to be related to a prototypical cask or cask equivalent. Explain how the displayed data is obtained and what it represents.

TN OBSERVATION 6 RESPONSE:

The accelerations are scaled by 1/3 to represent the accelerations of the full-scale cask. Impact duration and crush depth are unchanged. The above statement has been added to a note to Table 2.13.12-1.

Enclosure 3 to TN E-31368

List of SAR Page Changes Associated with Application for TN-LC Transportation Package, Revision 1

Safety Analysis Report (Proprietary Version)	
Page number	**Reason for change**
Cover Page	Update
Master TOC - v	Update TOC
1.4.5-29	RSI-11
2.13.7-i	Update TOC
2.13.7-3 and -3a	OBS-2
2.13.7-5, -6, -8, -34, and -35	RSI-1
2.13.8-i	Update TOC
2.13.8-16a	RSI-4
2.13.8-50 and -52	OBS-3
2.13.11-i through –iii	Update TOC
2.13.11-1	RSI-5
2.13.11-4	OBS-4 / OBS-5
2.13.11-10	RSI-3
2.13.11-11	RSI-2 / OBS-4
2.13.11-19a and -20	RSI-5
2.13.11-27	OBS-4
2.13.11-37a	RSI-3
2.13.11-64 through -67	OBS-4
2.13.12-18	OBS-6
5.6.4-i through –iii, -3, -3a, -9, -9a, -9b, -19, -45, -46, -56 through -58, and -90a through -90e	RSI-11
6.10.1-5 and -5a	RSI-12
6.10.2-ii, -4, -4a, -8, -26, and -35	RSI-12
6.10.3-5, -5a	RSI-12
6.10.4-iii, -2, and -3	RSI-4
6.10.4-5, and -5a	RSI-12
6.10.4-13, -14, -23, -41, -42, and -65	RSI-4

Safety Analysis Report (Non-Proprietary Version)	
Page number	**Reason for change**
Cover Page	Update
v	Update TOC
1.4.5-29	RSI-11
2.13.7-i	Update
2.13.8-i	Update
2.13.11-i and –ii	Update TOC
2.13.11-1	RSI-5
2.13.11-19a and -20	RSI-5
2.13.12-18	OBS-6
5.6.4-i through –iii, -3, -3a, -9, -9a, -9b, -19, -45, -46, -56 through -58, and -90a through -90e	RSI-11
6.10.1-5 and -5a	RSI-12
6.10.2-ii, -4, -4a, -8, -26, and -35	RSI-12
6.10.3-5, -5a	RSI-12
6.10.4-iii, -2, and -3	RSI-4
6.10.4-5, and -5a	RSI-12
6.10.4-13, -14, -23, -41, -42, and -65	RSI-4

List of SAR Page Changes Associated with Application for TN-LC Transportation Package, Revision 1

Safety Analysis Report - Drawings	
Drawing number	**Reason for change**
65200-71-01	RSI-6
65200-71-20	RSI-6
65200-71-40	RSI-6
65200-71-50	RSI-6
65200-71-60	RSI-6
65200-71-70	RSI-6
65200-71-80	RSI-6
65200-71-90	RSI-4 / RSI-6
65200-71-96	RSI-6
65200-71-102	RSI-6

Enclosure 4 to TN E-31368

SAR Page Replacement Instructions

SAR Proprietary Version	
Old page	**Revision 1 Replacement Page**
Cover Page	Cover Page
Master TOC - v	Master TOC - v
2.13.7-i	2.13.7-i
2.13.7-3	2.13.7-3
New page	2.13.7-3a
2.13.7-5	2.13.7-5
2.13.7-6	2.13.7-6
2.13.7-8	2.13.7-8
New Page	2.13.7-34
New Page	2.13.7-35
2.13.8-i	2.13.8-i
New Page	2.13.8-16a
2.13.8-50	2.13.8-50
2.13.8-52	2.13.8-52
2.13.11-i	2.13.11-i
2.13.11-ii	2.13.11-ii
2.13.11-iii	2.13.11-iii
2.13.11-1	2.13.11-1
2.13.11-4	2.13.11-4
2.13.11-10	2.13.11-10
2.13.11-11	2.13.11-11
New Page	2.13.11-19a
2.13.11-20	2.13.11-20
2.13.11-27	2.13.11-27
New Page	2.13.11-37a
2.13.11-64	2.13.11-64
2.13.11-65	2.13.11-65
2.13.11-66	2.13.11-66
2.13.11-67	2.13.11-67
2.13.12-18	2.13.12-18
5.6.4-i	5.6.4-i
5.6.4-ii	5.6.4-ii
5.6.4-iii	5.6.4-iii
5.6.4-3	5.6.4-3
New Page	5.6.4-3a
5.6.4-9	5.6.4-9
New Page	5.6.4-9a
New Page	5.6.4-9b
5.6.4-19	5.6.4-19
5.6.4-45	5.6.4-45
5.6.4-46	5.6.4-46
5.6.4-56	5.6.4-56
5.6.4-57	5.6.4-57
5.6.4-58	5.6.4-58
New Page	5.6.4-90a
New Page	5.6.4-90b
New Page	5.6.4-90c
New Page	5.6.4-90d
New Page	5.6.4-90e

SAR Page Replacement Instructions

SAR Proprietary Version	
Old page	**Revision 1 Replacement Page**
6.10.1-5	6.10.1-5
New Page	6.10.1-5a
6.10.2-ii	6.10.2-ii
6.10.2-4	6.10.2-4
New Page	6.10.2-4a
6.10.2-8	6.10.2-8
6.10.2-26	6.10.2-26
6.10.2-35	6.10.2-35
6.10.3-5	6.10.3-5
New Page	6.10.3-5a
6.10.4-iii	6.10.4-iii
6.10.4-2	6.10.4-2
6.10.4-3	6.10.4-3
6.10.4-5	6.10.4-5
6.10.4-5a	6.10.4-5a
6.10.4-13	6.10.4-13
6.10.4-14	6.10.4-14
6.10.4-23	6.10.4-23
6.10.4-41	6.10.4-41
6.10.4-42	6.10.4-42
6.10.4-65	6.10.4-65
Drawings	
65200-71-01, Rev. 0	65200-71-01, Rev. 1
65200-71-20, Rev. 0	65200-71-20, Rev. 1
65200-71-40, Rev. 0	65200-71-40, Rev. 1
65200-71-50, Rev. 0	65200-71-50, Rev. 1
65200-71-60, Rev. 0	65200-71-60, Rev. 1
65200-71-70, Rev. 0	65200-71-70, Rev. 1
65200-71-80, Rev. 0	65200-71-80, Rev. 1
65200-71-90, Rev. 0	65200-71-90, Rev. 1
65200-71-96, Rev. 0	65200-71-96, Rev. 1
65200-71-102, Rev. 0	65200-71-102, Rev. 1

SAR Page Replacement Instructions

SAR Non-Proprietary Version	
Old page	**Revision 1 Replacement Page**
Cover Page	Cover Page
Master TOC - v	Master TOC - v
1.4.5-29	1.4.5-29
2.13.7-i	2.13.7-i
2.13.8-i	2.13.8-i
2.13.11-i	2.13.11-i
2.13.11-ii	2.13.11-ii
2.13.11-1	2.13.11-1
New Page	2.13.11-19a
2.13.11-20	2.13.11-20
2.13.12-18	2.13.12-18
5.6.4-i	5.6.4-i
5.6.4-ii	5.6.4-ii
5.6.4-iii	5.6.4-iii
5.6.4-3	5.6.4-3
New Page	5.6.4-3a
5.6.4-9	5.6.4-9
5.6.4-9a	5.6.4-9a
5.6.4-19	5.6.4-19
5.6.4-45	5.6.4-45
5.6.4-46	5.6.4-46
5.6.4-56	5.6.4-56
5.6.4-57	5.6.4-57
5.6.4-58	5.6.4-58
New Page	5.6.4-90a
New Page	5.6.4-90b
New Page	5.6.4-90c
New Page	5.6.4-90d
New Page	5.6.4-90e
6.10.1-5	6.10.1-5
New Page	6.10.1-5a
6.10.2-ii	6.10.2-ii
6.10.2-4	6.10.2-4
New Page	6.10.2-4a
6.10.2-8	6.10.2-8
6.10.2-26	6.10.2-26
6.10.2-35	6.10.2-35
6.10.3-5	6.10.3-5
New Page	6.10.3-5a
6.10.4-iii	6.10.4-iii
6.10.4-2	6.10.4-2
6.10.4-3	6.10.4-3
6.10.4-5	6.10.4-5
New Page	6.10.4-5a

SAR Page Replacement Instructions

SAR Non-Proprietary Version	
Old page	**Revision 1 Replacement Page**
6.10.4-13	6.10.4-13
6.10.4-14	6.10.4-14
6.10.4-23	6.10.4-23
6.10.4-41	6.10.4-41
6.10.4-42	6.10.4-42
New Page (file after Figure 6.10.4-15)	6.10.4-65
Drawings	
65200-71-01, Rev. 0	65200-71-01, Rev. 1
65200-71-20, Rev. 0	65200-71-20, Rev. 1
65200-71-40, Rev. 0	65200-71-40, Rev. 1
65200-71-50, Rev. 0	65200-71-50, Rev. 1
65200-71-60, Rev. 0	65200-71-60, Rev. 1
65200-71-70, Rev. 0	65200-71-70, Rev. 1
65200-71-80, Rev. 0	65200-71-80, Rev. 1
65200-71-90, Rev. 0	65200-71-90, Rev. 1
65200-71-96, Rev. 0	65200-71-96, Rev. 1
65200-71-102, Rev. 0	65200-71-102, Rev. 1

Enclosure 6 to TN E-31368

Changed Pages for the Safety Analysis Report, Revision 1, Non-proprietary Version

NON-PROPRIETARY

AREVA

TRANSNUCLEAR, INC.

TN-LC
TRANSPORTATION PACKAGE

SAFETY ANALYSIS REPORT

Revision 1
August 2011

7135 Minstrel Way, Suite 300 • Columbia, MD 21045

2.13.8 TN-LC Basket Structural Evaluation 2.13.8-1
2.13.8.1 Introduction 2.13.8-1
2.13.8.2 Approach 2.13.8-2
2.13.8.3 Loading 2.13.8-3
2.13.8.4 Design Criteria 2.13.8-4
2.13.8.5 TN-LC-1FA Baskets 2.13.8-5
2.13.8.6 TN-LC-MTR Basket 2.13.8-17
2.13.8.7 TN-LC-TRIGA Basket 2.13.8-25
2.13.8.8 TN-LC-NRUX Basket 2.13.8-30
2.13.8.9 References 2.13.8-43
2.13.9 TN-LC Basket Dynamic Load Factor Determination 2.13.9-1
2.13.9.1 Introduction 2.13.9-1
2.13.9.2 Natural Frequencies during End Drop 2.13.9-2
2.13.9.3 Basket Side Drop ANSYS Analysis 2.13.9-3
2.13.9.4 Summary of Results and Conclusion 2.13.9-7
2.13.9.5 References 2.13.9-8
2.13.10 TN-LC Transport Package Thermal Expansion Evaluation 2.13.10-1
2.13.10.1 Purpose 2.13.10-1
2.13.10.2 Methodology 2.13.10-2
2.13.10.3 Results and Conclusions 2.13.10-10
2.13.10.4 References 2.13.10-11
2.13.11 TN-LC Fuel Assemblies and Fuel Elements under Impact Loads 2.13.11-1
Proprietary Information Withheld Pursuant to 10 CFR 2.390
2.13.11.2 MTR and TRIGA Fuel Element Evaluation 2.13.11-14
2.13.11.3 *Conclusion* 2.13.11-20
2.13.11.4 References *2.13.11-21*
2.13.12 TN-LC Transport Package Impact Limiter Analysis using LS-DYNA 2.13.12-1
2.13.12.1 Description of Impact Limiters and Load Path 2.13.12-1
2.13.12.2 Analysis Approach 2.13.12-2
2.13.12.3 MP197 1/3 Scale LS-DYNA Benchmark Analysis 2.13.12-3
2.13.12.4 TN-LC Impact Limiter Analysis 2.13.12-5
2.13.12.5 Sensitivity Studies 2.13.12-11
2.13.12.6 Impact Limiter Bolt Evaluation 2.13.12-12
2.13.12.7 References 2.13.12-17
2.13.13 TN-LC Transport Cask and Basket ASME Code Alternatives 2.13.13-1
2.13.13.1 Introduction 2.13.13-1
2.13.13.2 References 2.13.13-2

Notes:

- Burnup = Assembly Average burnup when loading fuel assemblies.
- Use burnup and enrichment to lookup minimum cooling time in years. Licensee is responsible for ensuring that uncertainties in fuel enrichment and burnup are correctly accounted for during fuel qualification.
- For values not explicitly listed in the tables, round burnups **up** to the first value shown, round enrichments **down**, and select the cooling time listed. Grey areas indicate fuel not analyzed for loading..
- Fuel with an initial enrichment less than 0.9 (or less than the minimum provided above for each burnup) or greater than 5.0 wt. % U-235 is unacceptable for transportation.
- Fuel assembly with a burnup greater than 62 GWD/MTU is unacceptable for transportation.
- Burnup = *Maximum* burnup when loading fuel rods.
- When transporting 25 or less fuel rods, the rods shall be placed in a specially designed 25 pin can.
- When transporting 9 or less fuel rods, the rods shall be placed in the 3x3 region of the 25 pin can.
- Fuel rods with a burnup greater than 90 GWD/MTU are unacceptable for transportation.
- Shaded areas in these Tables indicate fuel is not analyzed for loading.

Example: Per Table 1.4.5-8, a PWR assembly with an initial enrichment of 4.85 wt. % U-235 and a burnup of 41.5 GWD/MTU is acceptable for transport after a 4.1-year cooling time as defined by 4.8 wt. % U-235 (rounding down) and 42 GWD/MTU (rounding up) on the qualification table (other considerations not withstanding).

Appendix 2.13.7
TN-LC Lid Closure Evaluation Due to Delayed Impact

Proprietary Information Withheld Pursuant to 10 CFR 2.390

Appendix 2.13.8
TN-LC Basket Structural Evaluation

Proprietary Information Withheld Pursuant to 10 CFR 2.390

Appendix 2.13.11
TN-LC Fuel Assemblies and Fuel Elements under Impact Loads

TABLE OF CONTENTS

Proprietary Information Withheld Pursuant to 10 CFR 2.390

2.13.11.2 MTR and TRIGA Fuel Element Evaluation 2.13.11-14
2.13.11.2.1 Material Properties 2.13.11-14
2.13.11.2.2 TRIGA Fuel Element Methodology 2.13.11-14
2.13.11.2.3 MTR Fuel Element Methodology 2.13.11-14
2.13.11.3 Conclusion 2.13.11-20
2.13.11.4 References 2.13.11-21

LIST OF TABLES

Proprietary Information Withheld Pursuant to 10 CFR 2.390

Proprietary Information on Pages 2.13.11-ii through 2.13.11-iii
Withheld Pursuant to 10 CFR 2.390.

Appendix 2.13.11
TN-LC Fuel Assemblies and Fuel Elements under Impact Loads

NOTE: References in this Appendix are shown as [1], [2], etc., and refer to the reference list in Section 2.13.11.*4*.

Criticality analyses in Chapter 6 consider bounding re-configured/damaged fuel geometries for all conditions except for commercial fuel in NCT condition, thus, taking no credit for the structural integrity of the fuel. However, the structural integrity of the TN-LC payload fuel assemblies and fuel elements during NCT side and end drops are evaluated in this appendix. Furthermore, commercial fuel is also evaluated for HAC end drop conditions which is the bounding drop for geometric alteration. The analyses performed and results obtained form the basis to conclude that the fuel assemblies and fuel elements will maintain their structural integrity during normal and accident conditions of transportation.

While the material properties for high burnup commercial fuel cladding are unknown after long-term storage in a dry environment, the material properties after wet storage have been established and used in Reference [2] and [8]. Furthermore, the fuel may be loaded directly from spent fuel pool or from hot cell, thus decreasing the uncertainties of the material properties.

Similarly the material properties for the research reactor fuel are unknown and conservative assumptions were made in the conjecturing of the material properties, thus giving credence to the conclusion of fuel integrity during NCT and HAC loads.

The fuel evaluation was done for two separate groups of fuels. PWR, BWR, and NRU/NRX were evaluated as one group. TRIGA and MTR were evaluated separately. Different material analytical methodologies were used for the two groups, so, the evaluations are presented separately.

2.13.11.3 Conclusion

The results for the PWR, BWR, and NRU/NRX fuel assembly evaluations are summarized in Table 2.13.11-7 to Table 2.13.11-13. The maximum stress due to side drop for all cases is less than the yield stress of the cladding material and the maximum principal strain due to the end drop for all cases is less than 1%.

The MTR and TRIGA fuel element evaluations are described in Section 2.13.11.2; it concluded that the stresses in both MTR and TRIGA fuel elements are less than the yield stress of the annealed aluminum Al-6061-0 (conservative assumption). Both fuel elements are checked for buckling and it is concluded that the allowable buckling stress is higher than the calculated stresses. Therefore, both fuel elements will maintain their structurally integrity during the NCT load.

These analyses are intended to provide additional assurance that the fuel geometry will be maintained for the analyzed loads. The structural integrity of fuel/element geometry as demonstrated in the above analyses is not considered in the criticality and thermal analyses as described below:

1. *Basket structural evaluation (Appendix 2.13.8) demonstrated that the basket geometry is not altered for any fuel basket types following NCT and HAC. Each fuel element/assembly is confined within the corresponding fuel/element compartments (buckets or tubes, and end caps are used). The criticality evaluations are based on geometric configurations of the fuel element/assembly confined within their respective compartments (buckets or tubes) thereby inherently assuming fuel damage/re-configuration.*

2. *The thermal evaluation demonstrated that the maximum temperature of the research Reactor fuel element/assembly remained well below their melting points during HAC. Since each fuel element/assembly is confined within the corresponding fuel element/assembly compartments and does not grossly deform, it is not required to demonstrate the structural integrity of this fuel assembly/element for HAC.*

2.13.11.4 References

1. Final Safety Analysis Report for NUHOMS®-MP197 Transport Packaging, Revision 7.

2. Harold E. Adkins, Jr., Brian J. Koeppel and David T. Tang, "Spent Nuclear Fuel Structural Response when Subject to An End Impact Accident," PVP-Vol. 483, Transportation Storage and Disposal of Radioactive Materials, July 25-29, 2004, San Diego, CA, USA.

3. Kaufman, J.G., ed., "Properties of Aluminum Alloys: Tensile, Creep, and Fatigue Data and High and Low Temperatures," The Aluminum Association (Washington, D.C.) and ASM International (Metals Park, Ohio), 1999.

4. DOE/RW-0184, Vol 3 of 6, "Characteristics of Spent Fuel, High-Level Waste and other Radioactive Wastes Which May Require Long-Term Isolation – Physical Descriptions of LWR Fuel Assemblies," Appendix 2A, U.S. DOE, December, 1987.

5. UCID - 21246, "Dynamic Impact Effects on Spent Fuel Assemblies," Lawrence Livermore National Laboratory, October 20, 1987.

6. SCALE NUREG/CR-0200, Vol. 3, Rev. 5 (Table M8.2.4).

7. "Fuel Design Data," Nuclear Engineering International, September, 2004.

8. NUREG-1864, "A Pilot Probabilistic Risk Assessment of a Dry Cask Storage System at a Nuclear Power Plant," March 2007.

9. "Transnuclear, Inc. (TN) Application for the TN-40 Transportation Packaging for Spent Fuel, Revision 5, Docket No. 71-9313, TAC No. L24106," dated March 15, 2010.

10. LS-DYNA Version 971 R2, Rev 7600.1224, "LS-DYNA Key Word User's Manual," Livermore Software Technology Corporation (LSTC).

11. ANSYS Computer Code and User's Manuals, Rev. 10.0A1.

12. NUREG/CR-6322 UCRL-ID-119697, "Buckling Analysis of Spent Fuel Basket."

Table 2.13.12-1
Benchmark Analysis Results

(1/3 Scale Test Results vs. 1/3 Scale LS-DYNA Analysis)

		Test Results	**LS-DYNA *Analysis***
End Drop (-20°F)	Acceleration	65g	65.8g
	Impact Duration	0.010 sec.	0.012 sec.
	Wood Crush Depth	2.5"	2.5"
Side Drop	Acceleration	61g	61.5g
	Impact Duration	0.012 sec.	0.014 sec.
	Wood Crush Depth	2.69"-2.75"	2.75"
20° Slap Down 1st Impact	Acceleration at Center of Cask	17g	18.2g
	Acceleration at Bottom of Cask	36g	34.9g
	Impact Duration	0.016 sec.	0.023 sec.
	Wood Crush Depth Bottom Limiter	4.92"	5.5"
20° Slap Down 2nd Impact	Acceleration at Center of Cask	32g	41.1g
	Acceleration at Top of Cask	73g	78.4g
	Impact Duration	0.009 sec.	0.012 sec.
	Wood Crush Depth Upper Limiter	2.42"	3.0"

Note: *The accelerations are scaled by 1/3 to represent the accelerations of the full scale cask. Impact duration and crush depths are unchanged.*

Table 2.13.12-2
Analyzed Load Cases

Load Cases	**Firm Wood Properties**	**Soft Wood Properties**
30 ft End Drop	X	X
30 ft Side Drop	X	X
30 ft Slap Down 5° Angle	X	X
30 ft Slap Down 10° Angle	X	-
30 ft CG Over Corner Drop	X	X
1 ft End Drop	X	-
1 ft Side Drop	X	-

Appendix 5.6.4
TN-LC-1FA Basket Shielding Evaluation

TABLE OF CONTENTS

5.6.4.1 Description of the Shielding Design *5.6.4-1*
5.6.4.1.1 Design Features *5.6.4-1*
5.6.4.1.2 Summary Tables of Maximum Radiation Levels *5.6.4-1*
5.6.4.2 Source Specification *5.6.4-3*
5.6.4.2.1 Fuel Qualification *5.6.4-4*
5.6.4.2.2 MCNP Response Functions *5.6.4-5*
5.6.4.2.3 Design Basis Gamma and Neutron Source Terms *5.6.4-7*
5.6.4.2.4 Axial Blankets *5.6.4-8*
Proprietary Information Withheld Pursuant to 10 CFR 2.390.
5.6.4.3 Shielding Model *5.6.4-10*
5.6.4.3.1 Configuration of Source and Shielding *5.6.4-10*
5.6.4.3.2 Material properties *5.6.4-12*
5.6.4.4 Shielding Evaluation *5.6.4-13*
5.6.4.4.1 Methods *5.6.4-13*
5.6.4.4.2 Input and Output Data *5.6.4-13*
5.6.4.4.3 Flux-to-Dose-Rate Conversion *5.6.4-13*
5.6.4.4.4 External Radiation Levels *5.6.4-13*
5.6.4.5 Appendices *5.6.4-19*
5.6.4.5.1 References *5.6.4-19*
Proprietary Information Withheld Pursuant to 10 CFR 2.390.

LIST OF TABLES

Table 5.6.4-1 Summary of TN-LC-1FA NCT Dose Rates 5.6.4-34
Table 5.6.4-2 Summary of TN-LC-1FA HAC Dose Rates 5.6.4-35
Table 5.6.4-3 PWR Fuel Assembly Data 5.6.4-36
Table 5.6.4-4 BWR Fuel Assembly Data 5.6.4-37
Table 5.6.4-5 PWR B&W 15x15 Exposure Zone Materials 5.6.4-38
Table 5.6.4-6 BWR GE 7x7 Exposure Zone Materials 5.6.4-38
Table 5.6.4-7 Material Element Composition 5.6.4-39
Table 5.6.4-8 Flux Factors 5.6.4-40
Table 5.6.4-9 Fuel Qualification Table for a PWR Fuel Assembly 5.6.4-41
Table 5.6.4-10 Fuel Qualification Table for 25 PWR Fuel Rods 5.6.4-45
Table 5.6.4-11 Fuel Qualification Table for 9 PWR Fuel Rods 5.6.4-46
Table 5.6.4-12 Fuel Qualification Table for a BWR Fuel Assembly 5.6.4-47
Table 5.6.4-13 Fuel Qualification Table for 25 BWR Fuel Rods 5.6.4-51
Table 5.6.4-14 Fuel Qualification Table for 9 BWR Fuel Rods 5.6.4-57
Table 5.6.4-15 Fuel Qualification Table for MOX Fuel Rods 5.6.4-58
Table 5.6.4-16 Gamma NCT Response Functions 5.6.4-59
Table 5.6.4-17 Neutron NCT Response Functions 5.6.4-59
Table 5.6.4-18 PWR Fuel Assembly Axial Peaking Factors 5.6.4-60
Table 5.6.4-19 BWR Fuel Assembly Axial Peaking Factors 5.6.4-61
Table 5.6.4-20 PWR Fuel Assembly Design Basis Gamma Source Terms 5.6.4-62
Table 5.6.4-21 BWR Fuel Assembly Design Basis Gamma Source Terms 5.6.4-63
Table 5.6.4-22 25 PWR Fuel Rods Design Basis Gamma Source Terms 5.6.4-64
Table 5.6.4-23 25 BWR Fuel Rods Design Basis Gamma Source Terms 5.6.4-65
Table 5.6.4-24 25 MOX Fuel Rods Design Basis Gamma Source Terms 5.6.4-66
Table 5.6.4-25 9 PWR Fuel Rods Design Basis Gamma Source Terms 5.6.4-67
Table 5.6.4-26 9 BWR Fuel Rods Design Basis Gamma Source Terms 5.6.4-68
Table 5.6.4-27 9 MOX Fuel Rods Design Basis Gamma Source Terms 5.6.4-69
Table 5.6.4-28 Design Basis Neutron Sources 5.6.4-70
Table 5.6.4-29 Fuel Dimensions and Densities for MCNP Models 5.6.4-71
Table 5.6.4-30 TN-LC-1FA Basket Model Dimensions 5.6.4-72
Table 5.6.4-31 Composition of Fuel 5.6.4-72
Table 5.6.4-32 NCT Dose Rate Summary (mrem/hr) 5.6.4-73
Table 5.6.4-33 PWR Fuel Assembly NCT Side Surface Dose Rates between Impact Limiters (mrem/hr) 5.6.4-74
Table 5.6.4-34 PWR Fuel Assembly NCT Vehicle Underside Dose Rates (mrem/hr) 5.6.4-75
Table 5.6.4-35 PWR Fuel Assembly NCT Vehicle Side Dose Rates (mrem/hr) 5.6.4-76
Table 5.6.4-36 PWR Fuel Assembly NCT 2 m from Vehicle Side Dose Rates (mrem/hr) 5.6.4-77
Table 5.6.4-37 PWR Fuel Assembly NCT End Dose Rates (mrem/hr) 5.6.4-78
Table 5.6.4-38 25 MOX Rods NCT Side Surface Dose Rates between Impact Limiters (mrem/hr) 5.6.4-79
Table 5.6.4-39 25 MOX Rods NCT Vehicle Underside Dose Rates (mrem/hr) 5.6.4-80
Table 5.6.4-40 25 MOX Rods NCT Vehicle Side Dose Rates (mrem/hr) 5.6.4-81
Table 5.6.4-41 25 MOX Rods NCT 2 m from Vehicle Side Dose Rates (mrem/hr) 5.6.4-82

Table 5.6.4-42 9 EPR MOX Rods NCT Side Surface Dose Rates between Impact Limiters (mrem/hr) *5.6.4-83*
Table 5.6.4-43 9 EPR MOX Rods NCT Vehicle Underside Dose Rates (mrem/hr) *5.6.4-84*
Table 5.6.4-44 9 EPR MOX Rods NCT Vehicle Side Dose Rates (mrem/hr) *5.6.4-85*
Table 5.6.4-45 9 EPR MOX Rods NCT 2 m from Vehicle Side Dose Rates (mrem/hr) *5.6.4-86*
Table 5.6.4-46 9 EPR MOX Rods NCT End Dose Rates (mrem/hr) *5.6.4-87*
Table 5.6.4-47 PWR Fuel Assembly HAC Dose Rates, Fuel Shifted Down (mrem/hr) *5.6.4-88*
Table 5.6.4-48 PWR Fuel Assembly HAC Dose Rates, Fuel Shifted Up (mrem/hr) *5.6.4-89*
Table 5.6.4-49 25 MOX Rods HAC Dose Rates (mrem/hr) *5.6.4-90*
Table 5.6.4-50 Changes in Representative Dose Rates *5.6.4-90a*
Table 5.6.4-51 Differences in MOX Source between BWR and PWR Fuel *5.6.4-90b*
Table 5.6.4-52 Specific Power Conservatism *5.6.4-90c*
Table 5.6.4-53 T-DEPL Calculated Source for the PWR Fuel Assembly *5.6.4-90d*
Table 5.6.4-54 T-DEPL Calculated Source for the BWR Fuel Assembly *5.6.4-90e*

LIST OF FIGURES

Figure 5.6.4-1 TN-LC-1FA PWR Fuel Assembly MCNP Model, y-z View 5.6.4-91
Figure 5.6.4-2 TN-LC-1FA BWR Fuel Assembly MCNP Model, y-z View 5.6.4-92
Figure 5.6.4-3 TN-LC-1FA 25 EPR Rod MCNP Model, y-z View 5.6.4-93
Figure 5.6.4-4 TN-LC-1FA MCNP Model, x-y View through Shear Key 5.6.4-94
Figure 5.6.4-5 TN-LC-1FA MCNP Model, x-y View through Impact Limiter Attachment Blocks 5.6.4-95
Figure 5.6.4-6 TN-LC-1FA NCT Radial Surface Tallies 5.6.4-96
Figure 5.6.4-7 TN-LC-1FA NCT End Surface Tallies 5.6.4-97
Figure 5.6.4-8 TN-LC-1FA HAC 1 m Tallies 5.6.4-98

5.6.4.2 Source Specification

All source terms are developed using the SAS2H module of the SCALE44 code package [2]. Source terms are developed for the following scenarios: (1) 1 PWR fuel assembly, (2) 1 BWR fuel assembly, (3) 25 or 9 PWR fuel rods, (4) 25 or 9 BWR fuel rods, and (5) 25 or 9 MOX fuel rods. The PWR and BWR fuel assembly source terms are developed to bound all PWR and BWR fuel assemblies that may be shipped in the TN-LC package. The list of evaluated fuels are summarized in Table 5.6.4-3 and Table 5.6.4-4 for PWR and BWR fuel assemblies, respectively. The bounding fuel assembly has the highest uranium loading. For PWRs, the bounding fuel assembly type is the B&W 15x15 Mark B10, with 0.490 MTU. For BWRs, the bounding fuel assembly type is the GE 7x7, Version GE1, 2, or 3, with 0.198 MTU. For the bounding fuel assembly types, detailed material masses in each exposure zone are provided in Table 5.6.4-5 and Table 5.6.4-6 for the B&W 15x15 and GE 7x7, respectively.

Proprietary Information Withheld Pursuant to 10 CFR 2.390.

The bounding PWR and BWR fuel rods also have the highest fuel loading. The fuel loading per rod for each of the fuel types is determined in Table 5.6.4-3 and Table 5.6.4-4 for PWR and BWR fuel assemblies, respectively. The same fuel types that are bounding on a fuel assembly basis are also bounding on a fuel rod basis.

SAS2H is used to compute the source terms rather than a more detailed 2-D program, such as TRITON, because the as-modeled fuel assembly designs are simple and may be modeled conservatively in SAS2H. To confirm the adequacy of the SAS2H generated source terms, the design basis NCT source terms for the PWR and BWR fuel assemblies are regenerated using the 2-D TRITON module of the SCALE 6 [7] code package. In both cases, the TRITON generated gamma and neutron source terms are less than the SAS2H generated source terms. The dose rate reduction 2m from the side of the vehicle using the TRITON source terms is approximately 15% and 8% for PWR and BWR source terms, respectively. Therefore, it is conservative to use the SAS2H generated results.

Source terms are also developed for mixed oxide (MOX) rods. **(Proprietary Information Withheld Pursuant to 10 CFR 2.390.)** The uranium and plutonium isotopics used to define the MOX rods in the shielding analysis are listed below.

- U-235/U > 0.5 wt. %.
- Pu-239/ Pu > 40% wt. %.
- Am-241/ $PuO_2 \leq 0.075$ wt. %.
- Pu/Heavy Metal ≤ 7 wt. %.
- Pu-238/Pu-239 ≤ 4 wt. %.

Note, the constraints on the isotopic content of the MOX fuel specified in the bulleted list above are to satisfy decay heat and dose rate restrictions only. There are also constraints due to criticality safety requirements established in an analysis documented in Section 6.10.4. All the constraints on the isotopic content of the MOX fuel to satisfy decay heat, criticality and shielding performance requirements are summarized in Section 1.4.5.

Proprietary Information Withheld Pursuant to 10 CFR 2.390.

The correction factor to the total neutron radiation source employed in the current shielding evaluation to account for the axial burn-up profile variation along an axial extent of BWR and PWR FAs is 1.326 and 1.152 (see notes to Table 5.6.4-19 and Table 5.6.4-18), respectively.

Proprietary Information Withheld Pursuant to 10 CFR 2.390.

Proprietary Information on Pages 5.6.4-9a through 5.6.4-9b
Withheld Pursuant to 10 CFR 2.390.

5.6.4.5 Appendices

5.6.4.5.1 References

1. MCNP5, "MCNP – A General Monte Carlo N-Particle Transport Code, Version 5; Volume II: User's Guide," LA-CP-03-0245, Los Alamos National Laboratory, April 2003.

2. SCALE: A Modular Code System for Performing Standardized Computer Analyses for Licensing Evaluation, Vols. I-III, NUREG/CR-0200, Rev. 4 (ORNL/NUREG/CSD-2/R4), April 1995.

3. NUREG/CR-6801, Recommendations for Addressing Axial Burnup in PWR Burnup Credit Analyses, March 2003.

4. *ORNL/TM-12667, Validation of the SCALE System for PWR Spent Fuel Isotopic Composition Analyses.*

5. *ORNL/TM-13317, An Extension of the Validation of the SCALE (SAS2H) Isotopic Predictions for PWR Spent Fuel.*

6. *NUREG/CR-6798, Isotopic Analysis of High-Burnup PWR Spent Fuel Samples from the Takahama-3 Reactor.*

7. *SCALE: A Modular Code System for Performing Standardized Computer Analyses for Licensing Evaluations, ORNL/TM-2005/39, Version 6, Vols. I-III, January 2009.*

Table 5.6.4-10
Fuel Qualification Table for 25 PWR Fuel Rods

Cooling Time (years)

Burnup, GWD/MTU	Enrichment, wt. % U-235																					
	0.9	1.7	1.9	2.6	2.7	2.8	2.9	3.3	3.7	3.8	3.9	4.0	4.1	4.2	4.3	4.4	4.5	4.6	4.7	4.8	4.9	5.0
9	0.2	0.2	0.2	0.2	0.2	0.2	0.2	0.2	0.2	0.2	0.2	0.2	0.2	0.2	0.2	0.2	0.2	0.2	0.2	0.2	0.2	0.2
31	0.3	0.3	0.3	0.3	0.3	0.3	0.3	0.3	0.3	0.3	0.3	0.3	0.3	0.3	0.3	0.3	0.3	0.3	0.3	0.3	0.3	0.3
35		0.3	0.3	0.3	0.3	0.3	0.3	0.3	0.3	0.3	0.3	0.3	0.3	0.3	0.3	0.3	0.3	0.3	0.3	0.3	0.3	0.3
39			0.3	0.3	0.3	0.3	0.3	0.3	0.3	0.3	0.3	0.3	0.3	0.3	0.3	0.3	0.3	0.3	0.3	0.3	0.3	0.3
52				0.3	0.3	0.3	0.3	0.3	0.3	0.3	0.3	0.3	0.3	0.3	0.3	0.3	0.3	0.3	0.3	0.3	0.3	0.3
53				0.4	0.4	0.3	0.3	0.3	0.3	0.3	0.3	0.3	0.3	0.3	0.3	0.3	0.3	0.3	0.3	0.3	0.3	0.3
54				0.4	0.4	0.4	0.4	0.3	0.3	0.3	0.3	0.3	0.3	0.3	0.3	0.3	0.3	0.3	0.3	0.3	0.3	0.3
55				0.4	0.4	0.4	0.4	0.4	0.4	0.3	0.3	0.3	0.3	0.3	0.3	0.3	0.3	0.3	0.3	0.3	0.3	0.3
56				0.4	0.4	0.4	0.4	0.4	0.4	0.4	0.4	0.4	0.4	0.4	0.3	0.3	0.3	0.3	0.3	0.3	0.3	0.3
57				0.4	0.4	0.4	0.4	0.4	0.4	0.4	0.4	0.4	0.4	0.4	0.4	0.4	0.4	0.4	0.4	0.4	0.3	0.3
62				0.4	0.4	0.4	0.4	0.4	0.4	0.4	0.4	0.4	0.4	0.4	0.4	0.4	0.4	0.4	0.4	0.4	0.4	0.4
63									0.4	0.4	0.4	0.4	0.4	0.4	0.4	0.4	0.4	0.4	0.4	0.4	0.4	0.4
64									0.4	0.4	0.4	0.4	0.4	0.4	0.4	0.4	0.4	0.4	0.4	0.4	0.4	0.4
65									0.4	0.4	0.4	0.4	0.4	0.4	0.4	0.4	0.4	0.4	0.4	0.4	0.4	0.4
66									0.4	0.4	0.4	0.4	0.4	0.4	0.4	0.4	0.4	0.4	0.4	0.4	0.4	0.4
67									0.4	0.4	0.4	0.4	0.4	0.4	0.4	0.4	0.4	0.4	0.4	0.4	0.4	0.4
68									0.5	0.5	0.4	0.4	0.4	0.4	0.4	0.4	0.4	0.4	0.4	0.4	0.4	0.4
69									0.5	0.5	0.5	0.5	0.5	0.5	0.4	0.4	0.4	0.4	0.4	0.4	0.4	0.4
70									0.5	0.5	0.5	0.5	0.5	0.5	0.5	0.5	0.5	0.4	0.4	0.4	0.4	0.4
71									0.5	0.5	0.5	0.5	0.5	0.5	0.5	0.5	0.5	0.5	0.5	0.5	0.5	0.5
72									0.5	0.5	0.5	0.5	0.5	0.5	0.5	0.5	0.5	0.5	0.5	0.5	0.5	0.5
73									0.5	0.5	0.5	0.5	0.5	0.5	0.5	0.5	0.5	0.5	0.5	0.5	0.5	0.5
74									0.5	0.5	0.5	0.5	0.5	0.5	0.5	0.5	0.5	0.5	0.5	0.5	0.5	0.5
75									0.6	0.6	0.5	0.5	0.5	0.5	0.5	0.5	0.5	0.5	0.5	0.5	0.5	0.5
76									0.6	0.6	0.6	0.6	0.5	0.5	0.5	0.5	0.5	0.5	0.5	0.5	0.5	0.5
77									0.6	0.6	0.6	0.6	0.6	0.6	0.6	0.5	0.5	0.5	0.5	0.5	0.5	0.5
78									0.7	0.6	0.6	0.6	0.6	0.6	0.6	0.6	0.6	0.6	0.5	0.5	0.5	0.5
79									0.7	0.7	0.7	0.7	0.6	0.6	0.6	0.6	0.6	0.6	0.6	0.6	0.6	0.5
80									0.7	0.7	0.7	0.7	0.7	0.7	0.6	0.6	0.6	0.6	0.6	0.6	0.6	0.6
81									0.8	0.8	0.7	0.7	0.7	0.7	0.7	0.7	0.7	0.6	0.6	0.6	0.6	0.6
82									0.8	0.8	0.8	0.8	0.7	0.7	0.7	0.7	0.7	0.7	0.7	0.7	0.6	0.6
83									0.9	0.8	0.8	0.8	0.8	0.8	0.8	0.7	0.7	0.7	0.7	0.7	0.7	0.7
84									0.9	0.9	0.9	0.8	0.8	0.8	0.8	0.8	0.8	0.7	0.7	0.7	0.7	0.7
85									1.0	0.9	0.9	0.9	0.9	0.9	0.8	0.8	0.8	0.8	0.8	0.8	0.7	0.7
86									1.0	1.0	1.0	0.9	0.9	0.9	0.9	0.9	0.8	0.8	0.8	0.8	0.8	0.8
87									1.1	1.0	1.0	1.0	1.0	0.9	0.9	0.9	0.9	0.9	0.8	0.8	0.8	0.8
88									1.1	1.1	1.1	1.0	1.0	1.0	1.0	0.9	0.9	0.9	0.9	0.9	0.8	0.8
89									1.2	1.2	1.1	1.1	1.1	1.0	1.0	1.0	1.0	0.9	0.9	0.9	0.9	0.9
90									1.3	1.2	1.2	1.1	1.1	1.1	1.1	1.0	1.0	1.0	1.0	0.9	0.9	0.9

Note: For values not explicitly listed in the table, round burnups up to the first value shown, round enrichments down, and select the cooling time listed. *Maximum pin burnup listed.* Grey areas indicate fuel not analyzed for loading.

Table 5.6.4-11
Fuel Qualification Table for 9 PWR Fuel Rods

Cooling Time (years)

Burnup, GWD/MTU	Enrichment, wt. % U-235																			
	0.9	1.7	1.9	2.6	2.7	3.3	3.7	3.8	3.9	4.0	4.1	4.2	4.3	4.4	4.5	4.6	4.7	4.8	4.9	5.0
31	0.2	0.2	0.2	0.2	0.2	0.2	0.2	0.2	0.2	0.2	0.2	0.2	0.2	0.2	0.2	0.2	0.2	0.2	0.2	0.2
35		0.2	0.2	0.2	0.2	0.2	0.2	0.2	0.2	0.2	0.2	0.2	0.2	0.2	0.2	0.2	0.2	0.2	0.2	0.2
39			0.2	0.2	0.2	0.2	0.2	0.2	0.2	0.2	0.2	0.2	0.2	0.2	0.2	0.2	0.2	0.2	0.2	0.2
51				0.2	0.2	0.2	0.2	0.2	0.2	0.2	0.2	0.2	0.2	0.2	0.2	0.2	0.2	0.2	0.2	0.2
52				0.3	0.2	0.2	0.2	0.2	0.2	0.2	0.2	0.2	0.2	0.2	0.2	0.2	0.2	0.2	0.2	0.2
53				0.3	0.3	0.2	0.2	0.2	0.2	0.2	0.2	0.2	0.2	0.2	0.2	0.2	0.2	0.2	0.2	0.2
54				0.3	0.3	0.3	0.3	0.3	0.2	0.2	0.2	0.2	0.2	0.2	0.2	0.2	0.2	0.2	0.2	0.2
62				0.3	0.3	0.3	0.3	0.3	0.3	0.3	0.3	0.3	0.3	0.3	0.3	0.3	0.3	0.3	0.3	0.3
90							0.3	0.3	0.3	0.3	0.3	0.3	0.3	0.3	0.3	0.3	0.3	0.3	0.3	0.3

Note: For values not explicitly listed in the table, round burnups up to the first value shown, round enrichments down, and select the cooling time listed. *Maximum* pin burnup listed. Grey areas indicate fuel not analyzed for loading.

Table 5.6.4-13
Fuel Qualification Table for 25 BWR Fuel Rods

(Part 6 of 6)

Cooling Time (years)

Burnup, GWD/MTU	Enrichment, wt. % U-235										
	4.0	4.1	4.2	4.3	4.4	4.5	4.6	4.7	4.8	4.9	5.0
63	0.83	0.78	0.78	0.78	0.78	0.78	0.78	0.73	0.73	0.73	0.73
64	0.83	0.83	0.83	0.83	0.83	0.78	0.78	0.78	0.78	0.78	0.78
65	0.88	0.88	0.83	0.83	0.83	0.83	0.83	0.83	0.83	0.78	0.78
66	0.93	0.88	0.88	0.88	0.88	0.88	0.83	0.83	0.83	0.83	0.83
67	0.93	0.93	0.93	0.93	0.88	0.88	0.88	0.88	0.88	0.88	0.83
68	1.00	0.95	0.95	0.95	0.95	0.90	0.90	0.90	0.90	0.90	0.90
69	1.00	1.00	1.00	1.00	0.95	0.95	0.95	0.95	0.95	0.90	0.90
70	1.03	1.03	1.03	1.03	0.98	0.98	0.98	0.98	0.98	0.93	0.93
71	1.08	1.08	1.08	1.03	1.03	1.03	1.03	0.98	0.98	0.98	0.98
72	1.11	1.11	1.11	1.11	1.06	1.06	1.06	1.06	1.01	1.01	1.01
73	1.16	1.16	1.16	1.11	1.11	1.11	1.06	1.06	1.06	1.06	1.06
74	1.21	1.21	1.16	1.16	1.16	1.11	1.11	1.11	1.11	1.06	1.06
75	1.26	1.26	1.21	1.21	1.21	1.16	1.16	1.16	1.11	1.11	1.11
76	1.30	1.30	1.25	1.25	1.25	1.20	1.20	1.20	1.15	1.15	1.15
77	1.36	1.31	1.31	1.31	1.26	1.26	1.26	1.21	1.21	1.21	1.16
78	1.41	1.36	1.36	1.31	1.31	1.31	1.26	1.26	1.26	1.21	1.21
79	1.47	1.42	1.42	1.37	1.37	1.32	1.32	1.32	1.27	1.27	1.27
80	1.49	1.49	1.44	1.44	1.39	1.39	1.34	1.34	1.34	1.29	1.29
81	1.55	1.55	1.50	1.50	1.45	1.45	1.40	1.40	1.35	1.35	1.35
82	1.62	1.62	1.57	1.52	1.52	1.47	1.47	1.42	1.42	1.40	1.40
83	1.68	1.68	1.63	1.60	1.60	1.60	1.50	1.50	1.50	1.50	1.40
84	1.77	1.72	1.70	1.70	1.70	1.60	1.60	1.60	1.50	1.50	1.50
85	1.85	1.80	1.75	1.70	1.70	1.70	1.60	1.60	1.60	1.60	1.50
86	1.91	1.86	1.81	1.81	1.80	1.70	1.70	1.70	1.60	1.60	1.60
87	2.02	1.97	1.92	1.90	1.80	1.80	1.80	1.70	1.70	1.70	1.60
88	2.12	2.07	2.00	2.00	1.90	1.90	1.80	1.80	1.80	1.70	1.70
89	2.18	2.13	2.10	2.10	2.00	2.00	1.90	1.90	1.80	1.80	1.80
90	2.32	2.30	2.20	2.10	2.10	2.00	2.00	1.90	1.90	1.90	1.80

Note: For values not explicitly listed in the table, round burnups up to the first value shown, round enrichments down, and select the cooling time listed. *Maximum* pin burnup listed. Grey areas indicate fuel not analyzed for loading.

Table 5.6.4-14
Fuel Qualification Table for 9 BWR Fuel Rods

Cooling Time (years)

Burnup, GWD/MTU	Enrichment, wt. % U-235																			
	0.9	1.0	1.7	1.9	2.6	3.0	3.7	3.8	3.9	4.0	4.1	4.2	4.3	4.4	4.5	4.6	4.7	4.8	4.9	5.0
12	0.2	0.2	0.2	0.2	0.2	0.2	0.2	0.2	0.2	0.2	0.2	0.2	0.2	0.2	0.2	0.2	0.2	0.2	0.2	0.2
13	0.3	0.2	0.2	0.2	0.2	0.2	0.2	0.2	0.2	0.2	0.2	0.2	0.2	0.2	0.2	0.2	0.2	0.2	0.2	0.2
14	0.3	0.3	0.3	0.3	0.3	0.3	0.3	0.3	0.3	0.3	0.3	0.3	0.3	0.3	0.3	0.3	0.3	0.3	0.3	0.3
31	0.3	0.3	0.3	0.3	0.3	0.3	0.3	0.3	0.3	0.3	0.3	0.3	0.3	0.3	0.3	0.3	0.3	0.3	0.3	0.3
35			0.3	0.3	0.3	0.3	0.3	0.3	0.3	0.3	0.3	0.3	0.3	0.3	0.3	0.3	0.3	0.3	0.3	0.3
39				0.3	0.3	0.3	0.3	0.3	0.3	0.3	0.3	0.3	0.3	0.3	0.3	0.3	0.3	0.3	0.3	0.3
59					0.3	0.3	0.3	0.3	0.3	0.3	0.3	0.3	0.3	0.3	0.3	0.3	0.3	0.3	0.3	0.3
60					0.4	0.3	0.3	0.3	0.3	0.3	0.3	0.3	0.3	0.3	0.3	0.3	0.3	0.3	0.3	0.3
61					0.4	0.4	0.4	0.4	0.4	0.4	0.4	0.4	0.4	0.4	0.4	0.4	0.3	0.3	0.3	0.3
62					0.4	0.4	0.4	0.4	0.4	0.4	0.4	0.4	0.4	0.4	0.4	0.4	0.4	0.4	0.4	0.4
72							0.4	0.4	0.4	0.4	0.4	0.4	0.4	0.4	0.4	0.4	0.4	0.4	0.4	0.4
73							0.5	0.5	0.5	0.5	0.5	0.5	0.5	0.4	0.4	0.4	0.4	0.4	0.4	0.4
78							0.5	0.5	0.5	0.5	0.5	0.5	0.5	0.5	0.5	0.5	0.5	0.5	0.5	0.5
79							0.5	0.5	0.5	0.5	0.5	0.5	0.5	0.5	0.5	0.5	0.5	0.5	0.5	0.5
87							0.5	0.5	0.5	0.5	0.5	0.5	0.5	0.5	0.5	0.5	0.5	0.5	0.5	0.5
88							0.6	0.5	0.5	0.5	0.5	0.5	0.5	0.5	0.5	0.5	0.5	0.5	0.5	0.5
89							0.6	0.6	0.6	0.5	0.5	0.5	0.5	0.5	0.5	0.5	0.5	0.5	0.5	0.5
90							0.7	0.7	0.6	0.6	0.6	0.6	0.6	0.6	0.6	0.6	0.5	0.5	0.5	0.5

Note: For values not explicitly listed in the table, round burnups up to the first value shown, round enrichments down, and select the cooling time listed. *Maximum* pin burnup listed. Grey areas indicate fuel not analyzed for loading.

Table 5.6.4-15
Fuel Qualification Table for MOX Fuel Rods

Cooling Time (years)

Burnup (GWd/MTHM)	MOX 25 pins	MOX 9 pins	Burnup (GWd/MTHM)	MOX 25 pins	MOX 9 pins
6	0.2	0.1	49	1.4	0.2
7	0.2	0.1	50	1.5	0.2
8	0.2	0.1	51	1.6	0.2
9	0.2	0.1	52	1.7	0.2
10	0.2	0.1	53	1.8	0.3
11	0.2	0.1	54	1.9	0.3
12	0.2	0.1	55	2	0.3
13	0.2	0.1	56	2.2	0.3
14	0.2	0.1	57	2.3	0.3
15	0.2	0.2	58	2.4	0.3
16	0.3	0.2	59	2.6	0.3
17	0.3	0.2	60	2.7	0.3
18	0.3	0.2	61	2.9	0.3
19	0.3	0.2	62	3.1	0.4
20	0.3	0.2	63	3.3	0.4
21	0.3	0.2	64	3.6	0.5
22	0.3	0.2	65	3.8	0.5
23	0.4	0.2	66	4.1	0.5
24	0.4	0.2	67	4.4	0.6
25	0.4	0.2	68	4.7	0.6
26	0.5	0.2	69	5.1	0.7
27	0.5	0.2	70	5.4	0.8
28	0.5	0.2	71	5.8	0.8
29	0.5	0.2	72	6.2	0.9
30	0.5	0.2	73	6.6	1
31	0.5	0.2	74	7	1.1
32	0.5	0.2	75	7.4	1.1
33	0.5	0.2	76	7.8	1.2
34	0.5	0.2	77	8.2	1.3
35	0.6	0.2	78	8.7	1.5
36	0.6	0.2	79	9.1	1.6
37	0.6	0.2	80	9.5	1.7
38	0.7	0.2	81	9.9	1.8
39	0.7	0.2	82	10.5	2
40	0.8	0.2	83	10.8	2.1
41	0.9	0.2	84	11.2	2.3
42	0.9	0.2	85	11.6	2.4
43	1	0.2	86	12	2.6
44	1.1	0.2	87	12.4	2.8
45	1.1	0.2	88	12.9	3
46	1.2	0.2	89	13.2	3.2
47	1.3	0.2	90	13.6	3.4
48	1.4	0.2			

Note: For values not explicitly listed in the table, round burnups up to the first value shown and select the cooling time listed. Cooling times listed in years. Pins listed at *maximum* burnup. Grey areas indicate fuel not analyzed for loading.

Table 5.6.4-50
Changes in Representative Dose Rates

Burnup, Enrichment and Cooling Time (BECT) Combinations Radiological Sources Correspond to	***Dose Rate Increases Based on Samples from Various References:***		
	NUREG-6798 [6]	***ORNL-TM-12667 [4]***	***ORNL-TM-13317 [5]***
31 GWD/MTU, 0.9 wt.%, 6.0 years	*15%*	*8%*	*17%*
55 GWD/MTU, 3.8 wt.%, 7.75 years	*16%*	*9%*	*18%*
70 GWD/MTU, 4.3 wt.%, 21.0 years	*18%*	*10%*	*18%*

Table 5.6.4-51
Differences in MOX Source between BWR and PWR Fuel

E_{max} (MeV)	MOX BWR 9 rod (γ/s)	MOX PWR 9 rod (γ/s)	Difference (PWR/BWR)
0.05	2.44E+15	1.21E+15	49.5%
0.1	5.75E+14	2.84E+14	49.4%
0.2	5.30E+14	2.61E+14	49.2%
0.3	1.47E+14	7.28E+13	49.4%
0.4	1.15E+14	5.65E+13	49.1%
0.6	8.78E+14	4.61E+14	52.5%
0.8	1.19E+15	6.26E+14	52.5%
1	2.82E+14	1.53E+14	54.3%
1.33	9.59E+13	5.91E+13	61.6%
1.66	3.92E+13	2.26E+13	57.7%
2	4.04E+12	1.99E+12	49.3%
2.5	1.09E+13	5.24E+12	48.3%
3	3.23E+11	1.60E+11	49.6%
4	4.02E+10	1.99E+10	49.5%
5	6.45E+07	3.64E+07	56.4%
6.5	2.59E+07	1.46E+07	56.4%
8	5.08E+06	2.86E+06	56.3%
10	1.08E+06	6.08E+05	56.3%
Total Gamma (γ/s)	6.32E+15	3.21E+15	50.8%
Total Neutron (n/s)	2.06E+09	1.13E+09	54.9%

Table 5.6.4-52
Specific Power Conservatism

Assembly Type	***PWR representative Assembly***			***BWR representative Assembly***			
Burnup, GWD/MTU	*45*	*55*	*62*	*45*	*55*	*65*	*70*
Enrichment, wt.%	*2.7*	*3.2*	*3.4*	*2.6*	*2.6*	*2.6*	*3.7*
Neutrons, %	*<0.5*	*1.5*	*3.0*	*2.0*	*3.5*	*5.0*	*6.0*
Gamma,%	*1.0*	*4.0*	*7.0*	*3.5*	*6.5*	*10.5*	*11.0*

Table 5.6.4-53
T-DEPL Calculated Source for the PWR Fuel Assembly

E_{max} (MeV)	Bottom Nozzle (γ/s)	In-Core (γ/s)	Plenum (γ/s)	Top Nozzle (γ/s)
0.05	8.82E+11	2.62E+15	8.60E+11	4.43E+11
0.10	3.67E+10	5.37E+14	7.97E+10	2.49E+10
0.20	2.08E+10	4.44E+14	2.70E+10	6.05E+09
0.30	1.29E+09	1.25E+14	1.51E+09	3.00E+08
0.40	3.41E+09	8.75E+13	3.10E+09	3.92E+08
0.60	6.38E+10	9.75E+14	4.16E+10	2.58E+07
0.80	3.44E+10	2.97E+15	2.72E+10	9.28E+08
1.00	1.30E+11	4.21E+14	2.80E+10	7.40E+10
1.33	1.05E+13	2.23E+14	2.31E+13	7.27E+12
1.66	2.95E+12	6.57E+13	6.53E+12	2.05E+12
2.00	1.88E+03	1.57E+12	4.02E+03	1.24E+03
2.50	7.06E+07	3.52E+12	1.56E+08	4.91E+07
3.00	6.04E+04	1.10E+11	1.33E+05	4.19E+04
4.00	9.00E-06	1.01E+10	4.60E-05	7.41E-06
5.00	4.09E-36	1.04E+07	2.05E-36	0.00E+00
6.50	1.18E-36	4.18E+06	5.90E-37	0.00E+00
8.00	1.50E-37	8.20E+05	7.50E-38	0.00E+00
10.00	2.00E-38	1.74E+05	1.00E-38	0.00E+00
Total gamma (γ/s)	1.46E+13	8.47E+15	3.07E+13	9.87E+12
Total neutron (n/s)	2.98E+08			

Table 5.6.4-54
T-DEPL Calculated Source for the BWR Fuel Assembly

E_{max} (MeV)	Bottom Nozzle (γ/s)	In-Core (γ/s)	Plenum (γ/s)	Top Nozzle (γ/s)
0.05	7.71E+11	5.79E+15	8.28E+11	3.41E+11
0.10	1.63E+10	1.32E+15	9.03E+09	1.32E+10
0.20	6.97E+09	1.34E+15	1.58E+10	5.01E+09
0.30	7.84E+08	3.36E+14	2.57E+09	5.31E+08
0.40	6.33E+09	2.65E+14	2.97E+10	3.78E+09
0.60	3.01E+10	1.39E+15	7.48E+10	2.05E+10
0.80	1.27E+11	2.65E+15	6.53E+11	7.55E+10
1.00	1.10E+12	4.07E+14	3.30E+11	3.60E+11
1.33	4.33E+12	1.56E+14	1.44E+12	3.59E+12
1.66	1.22E+12	6.17E+13	4.06E+11	1.01E+12
2.00	2.63E+08	7.59E+12	1.11E+08	1.96E+08
2.50	3.02E+07	2.96E+13	1.45E+07	2.48E+07
3.00	2.57E+04	4.97E+11	1.22E+04	2.12E+04
4.00	9.07E-07	4.45E+10	9.87E-13	4.99E-06
5.00	0.00E+00	2.80E+06	2.36E-37	0.00E+00
6.50	0.00E+00	1.12E+06	6.79E-38	0.00E+00
8.00	0.00E+00	2.21E+05	8.64E-39	0.00E+00
10.00	0.00E+00	4.68E+04	1.15E-39	0.00E+00
Total gamma (γ/s)	7.61E+12	1.38E+16	3.79E+12	5.43E+12
Total neutron (n/s)	8.01E+07			

6.10.1.3 General Considerations

6.10.1.3.1 Model Configuration

The fuel, basket, and packaging are modeled explicitly in the MCNP5 V1.4 computer program [1]. The waste package consists of several components. The outer containment is the TN-LC cask which is modeled in the radial direction as concentric layers of stainless steel and lead. The top and bottom of the cask is composed of layered stainless steel and lead. Before shipping MTR fuel, the TN-LC cask will be outfitted with the TN-LC-MTR basket. This basket is comprised of three components: outer aluminum rails, a stainless steel weldment, and three sets of fuel buckets. Each bucket features three compartments for MTR fuel. Between four and six fuel buckets are stacked along the length of the cask. Therefore, the total cask capacity is between 36 and 54 MTR fuel elements. Each bucket cavity is intended to hold one MTR fuel element.

Figure 6.10.1-2 shows a planar view of the TN-LC-MTR cask loaded with MTR fuel elements. The cask is surrounded by a 12 in. layer of full-density water to provide reflection.

In both the NCT and HAC models, water is modeled inside the package at the density that maximizes reactivity. Because the cask is designed for wet loading, water drains freely inside the basket, and preferential flooding scenarios are not credible. However, the cavity could be partially flooded. Because the baskets drain freely, if the TN-LC cavity is partially flooded, the only credible scenario is that some fuel would be submerged in water, and the remaining fuel would remain unsubmerged. Therefore, any partial flooding scenarios would result in unmoderated fuel. It is demonstrated that MTR fuels have very low reactivity in the absence of moderation. Therefore, any partial flooding would uncover fuel and decrease the reactivity. It is demonstrated explicitly in Section 6.10.2.4 for HEU NRU fuel that a partially flooded cavity results in lower reactivities, and MTR fuel will behave in a similar manner. For these reasons, cases are not developed for partial and/or preferential flooding. Water is always modeled at the same density in all basket regions of the model.

Effect of Manufacturing Tolerances on Reactivity:

The manufacturing tolerances of the basket components are modeled in order to maximize the reactivity. In these calculations, the HFBR fuel element is used as a representative fuel element as the HFBR fuel element is the most reactive fuel element listed in Table 6.10.1-2 and Table 6.10.1-3, as demonstrated in Section 6.10.1.9.3.

The tolerances for the TN-LC, basket, and bucket are given in accordance with ASME Y14.5M-1994 [2] with the exception of components manufactured from stock material. For decimal values quoted to the hundredth of an inch, the tolerances are ±0.05 in. For decimal values quoted to the thousand of an inch, the tolerances are ±0.015 in. Angles are quoted to within ±1 degree.

For stock materials, tolerances are given by ASTM A480 [6]. The TN-LC-MTR bucket contains three sizes of stock plate with the tolerances given in Table 6.10.1-6. The tolerance values are taken from Tables A2.13 and A2.17 of ASTM A480. Maximum values are used to define the largest possible range and produce the most conservative results.

For the fuel bucket, the thickness of the stainless steel plates is decreased according to the values in Table 6.10.1-6. The fuel bucket compartment plates are thinned on both sides. The plates that comprise the side walls of the buckets are also thinned. This reduces neutron absorption in the stainless steel and increases reactivity. Bucket dimensions are summarized in Table 6.10.1-7.

Proprietary Information Withheld Pursuant to 10 CFR 2.390.0

Proprietary Information Withheld Pursuant to 10 CFR 2.390. Increasing the thickness of the outer plates causes increased reflection and produces a higher calculated k_{eff}. Altering the

LIST OF FIGURES

Figure 6.10.2-1 MCNP NRU/NRX Fuel Element Models 6.10.2-30
Figure 6.10.2-2 MCNP TN-LC-NRUX Model, y-z View 6.10.2-31
Figure 6.10.2-3 MCNP TN-LC-NRUX Model, x-y View 6.10.2-32
Figure 6.10.2-4 MCNP TN-LC-NRUX Single Package Model with Tolerances 6.10.2-33
Figure 6.10.2-5 MCNP TN-LC-NRUX Array Model 6.10.2-34
Figure 6.10.2-6 Partially Filled Cavity 6.10.2-35

6.10.2.3 General Considerations

6.10.2.3.1 Model Configuration

The fuel, basket, and packaging are modeled explicitly in the MCNP computer program [1]. The packaging is conservatively modeled without the neutron shield and impact limiters in both the NCT and HAC models. The key nominal dimensions are provided in Table 6.10.2-4 for the cask and Table 6.10.2-5 for the TN-LC-NRUX basket. The TN-LC cask and TN-LC-NRUX basket dimensions are obtained from the drawings in Chapter 1. The overall model geometry is illustrated in Figure 6.10.2-2. A view showing the basket is illustrated in Figure 6.10.2-3.

The cask body is modeled with nominal dimensions because the tolerances on the cask body dimensions would have little effect on the system reactivity. However, key basket dimensions are modeled considering tolerances in order to maximize the reactivity. The tolerance study is described in more detail in Section 6.10.2.4.

Several items are neglected for simplicity, including the tube cap, lid spacer plate, and lid spacer blocks. The bottom of the basket, as well as the bottom spacer, are also neglected. These items have little effect on the reactivity. Because the bottom spacer and basket bottom are not modeled, the active fuel length may contact the bottom of the cask in the models which maximizes neutron reflection from the bottom end of the cask.

Only the active fuel regions of the NRU or NRX elements are modeled, and it is assumed that any flow tubes are removed. The NRU and NRX fuel element dimensions are given in Table 6.10.2-2 and Table 6.10.2-3, respectively. The majority of the models are for NRU fuel only because it is demonstrated that NRU fuel is more reactive than NRX fuel.

In both the NCT and HAC models, water is modeled inside the package at the density that maximizes reactivity. *In the fully-flooded models,* water is always modeled at the same density in all basket regions of the model. Above the basket but inside the cavity, water is modeled at full density to maximize neutron reflection. All single package models are reflected with 12 in. of water.

Because the cask is designed for wet loading, water drains freely inside the basket, and *preferential flooding scenarios are not credible. However, the cavity could be partially flooded. Because the baskets drain freely, if the TN-LC cavity is partially flooded, the only credible scenario is that some fuel would be submerged in water, and the remaining fuel would remain unsubmerged. Therefore, any partial flooding scenarios would result in less moderation for the fuel. It is demonstrated that NRU/NRX fuels have very low reactivity in the absence of moderation. Therefore, any partial flooding would uncover fuel and decrease the reactivity. The effect of partial flooding is demonstrated explicitly.*

Under HAC, it is assumed that the fuel, which is loaded as undamaged, may become damaged. The fuel would not be damaged under NCT, but, to be conservative and simplify the modeling, fuel damage is also modeled under NCT. For modeling purposes, it is assumed that the fuel rod pitch may either contract until the rods touch or expand in a uniform manner until constrained by the basket tubes. Applying this penalizing damage assumption to every fuel element bounds all credible accident damage scenarios. Both minimum and maximum pitch HAC models are illustrated in Figure 6.10.2-3.

For the NCT array, an array of 3 packages is modeled to justify a CSI = 100. Water of variable density is placed between the packages. No HAC array cases are developed.

In Case NB6, Case NB5 is used as the parent case, and the 0.25-in. side guide plates (guide plate A) are modeled only at the maximum thickness of 0.25+0.085 = 0.335 in. since the results from Case NB5 imply that the reactivity may increase slightly due to increased reflection from the steel surrounding the basket tube assemblies. The reactivity increases by ~3 mk for this case compared to the parent case. Because this is the most reactive case, Figure 6.10.2-4 shows the model geometry for Case NB6. The input file for this case is also included in Section 6.10.2.9.2.

In Case NB7, Case NB6 is used as the parent case, and the 0.375-in. side guide plates are modeled at the maximum thickness per ASTM A 480 of 0.375+0.09 = 0.465 to increase reflection. However, reactivity decreases by 1 mk, indicating the change is within the statistical variation of the calculation. Because the tolerance changes have little effect with increasing distance from the fuel, additional tolerance studies on the basket shell and cask are not performed.

In Case NB8, Case NB6 is used as the parent case, and the active fuel is shifted up 30 cm so that a layer of water exists between the bottom of the active fuel and the end of the cask. The reactivity change is within the uncertainty of the calculation.

In Cases NB20 through NB23, Case NB6 is used as the parent case, and it is assumed that the cavity is partially flooded so that the lower half of the active fuel is moderated with full-density water, while the voids above this height is filled with water of density 0, 0.25, 0.5, and 0.75 g/cm^3. The geometry is shown in Figure 6.10.2-6. As expected, uncovering the fuel is less reactive than the fully flooded condition.

In Cases NB9 through NB12, Case NB6 is used as the parent case, and the density of water inside the basket region is reduced. The water density above the basket region is conservatively set at 1.0 g/cm^3 to maximize reflection. Reactivity drops quickly with reduced water density, indicating that the system is most reactive with full-water moderation.

Therefore, Case NB6 is the most reactive, with k_s = 0.87191. This result is less than the USL of 0.9227.

6.10.2.4.2 Results

The single package results are summarized in Table 6.10.2-8 and Table 6.10.2-9. The most reactive configurations are listed in boldface.

Table 6.10.2-9
Single Package Results, Tolerance and Moderation Study

Proprietary Information Withheld Pursuant to 10 CFR 2.390.

Pitch (cm)	Water Density (g/cm^3)	k_{eff}	σ	k_s ($k_{eff}+2\sigma$)
1.650	1.0	0.85441	0.00094	0.85629
1.650	1.0	0.86509	0.00114	0.86737
1.650	1.0	0.86276	0.00099	0.86474
1.650	1.0	0.86305	0.00091	0.86487
1.650	1.0	0.86626	0.00109	0.86844
1.650	**1.0**	**0.86991**	**0.00100**	**0.87191**
1.650	1.0	0.86841	0.00103	0.87047
1.650	1.0	0.86971	0.00097	0.87165
1.650	0.25	0.49884	0.00089	0.50062
1.650	0.5	0.69583	0.00108	0.69799
1.650	0.75	0.80678	0.00109	0.80896
1.650	0.9	0.85075	0.00106	0.85287
Cavity Half-filled with Water				
Pitch (cm)	*Water Density (g/cm^3)*	*k_{eff}*	*σ*	*k_s ($k_{eff}+2\sigma$)*
1.650	*0*	*0.86199*	*0.00094*	*0.86387*
1.650	*0.25*	*0.86151*	*0.00108*	*0.86367*
1.650	*0.5*	*0.86071*	*0.00108*	*0.86287*
1.650	*0.75*	*0.86154*	*0.00107*	*0.86368*

Table 6.10.2-10
TN-LC-NRUX NCT Array Results

Proprietary Information Withheld Pursuant to 10 CFR 2.390.

Water Density Between Packages (g/cm^3)	Water Density Inside Packages (g/cm^3)	k_{eff}	σ	k_s ($k_{eff}+2\sigma$)
0	**1.0**	**0.87264**	**0.00068**	**0.87400**
0.25	1.0	0.87194	0.00067	0.87328
0.5	1.0	0.87137	0.00075	0.87287
0.75	1.0	0.87157	0.00075	0.87307
1.0	1.0	0.87250	0.00071	0.87392
0	0.75	0.81432	0.00071	0.81574
0	0.9	0.85424	0.00072	0.85568

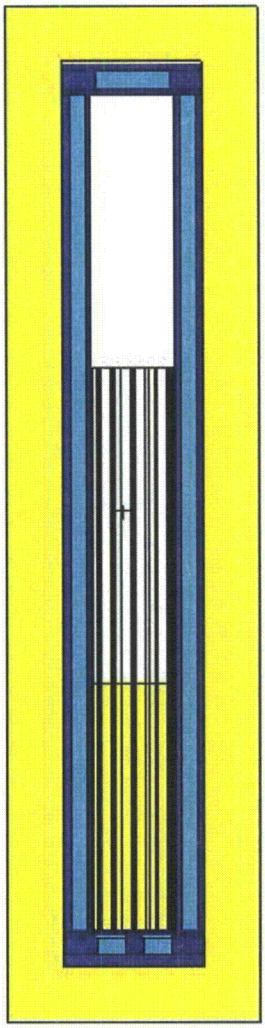

Figure 6.10.2-6
Partially Filled Cavity

6.10.3.3 General Considerations

6.10.3.3.1 Model Configuration

The fuel, basket, and packaging are modeled explicitly in the MCNP5 V1.4 computer program [1]. The TN-LC package model is a simplified representation of the cask and baskets. The body of the casks is represented by coaxial cylinders of steel and lead, with no effort to model minor details of the design since they have a negligible effect on the reactivity calculation. The impact limiters at the ends of the cask and the neutron shield have also been omitted. The entire cask is surrounded in the model by a reflective region of water that is 12 in. thick.

The model of the cask is shown in Figure 6.10.3-2. The dimensions of the cask that were used to construct the model are given in Table 6.10.3-4. The cask contains five baskets that hold the TRIGA fuel. The remaining space in the cask is occupied by a steel spacer which is not included in the model for simplicity. The length of the spacer in the Chapter 1 drawings is 23.50 in. The model is based on a spacer that is 1.25 in. shorter, but this should have a negligible effect on the results of these calculations. Only the short TN-LC-TRIGA basket design, with the dimensions labeled "option 1," is modeled since the long TN-LC-TRIGA basket is used for FFCR assemblies which are less reactive than standard fuel assemblies, as discussed in Section 6.10.3.2.

The model of the basket is also simplified, and only the key features of the basket that are relevant to criticality analysis are included. Thus, the lifting lugs, the steel inserts, and the fasteners are not modeled. The model of the poison plates includes 1 in. × 1 in. drainage holes at the bottom of the plates which were present in an earlier version of the design but do not appear in the final drawings. Thus, the model conservatively underestimates the amount of poison that is in the basket.

Since the fuel assemblies are held in fairly small compartments, without much room to move during an accident, the baskets and fuel are assumed to be undamaged in all calculations performed for this analysis under both normal conditions of transport (NCT) and hypothetical accident conditions (HAC). Although the cask is designed to be sealed to prevent the entrance of water into the cavity and to remain leak tight under accident conditions, all of the calculations assume that water is present inside the cask, and the density of this water is allowed to vary to ensure that the calculation that maximizes reactivity is performed and used for this analysis. The drainage holes in the basket (although they are not completely represented in the MCNP model) allow water to flow throughout the inner cavity of the cask. Thus, *preferential flooding is not credible, and* the calculations here assume that the density of water is the same everywhere inside the cask. While it is possible that the cask could be partially filled with water, with some fuel assemblies submerged and others uncovered, this scenario was not modeled because it is less reactive (due to less moderation) than the case in which all fuel assemblies are submerged. *It is demonstrated that the reactivity of TRIGA fuels reduces in the absence of moderation. It is demonstrated explicitly in Section 6.10.2.4 for HEU NRU fuel that a partially flooded cavity results in lower reactivities, and TRIGA fuel will behave in a similar manner. For these reasons, cases are not developed for partial and/or preferential flooding.*

6.10.3.3.2 Material Properties

The composition of the TRIGA fuel is presented in Table 6.10.3-3. The stainless steel components, including the cladding of some types of TRIGA fuel assemblies, the basket, and parts of the cask, are modeled as SS304 using the standard composition provided in the SCALE

material library [2] (presented in Table 6.10.3-5), which is the standard for criticality analysis. Although the TN-LC design uses XM-19 stainless steel for the outer steel parts of the cask,

LIST OF FIGURES

Figure 6.10.4-1 *1FA Basket with All Functional Components* *6.10.4-50*
Figure 6.10.4-2 *PWR Compartment Components* *6.10.4-51*
Figure 6.10.4-3 *BWR Compartment Sleeve and Hold-Down Ring* *6.10.4-52*
Figure 6.10.4-4 *25 Pin Can and Fuel Rod Tubes* *6.10.4-53*
Figure 6.10.4-5 *Radial and Axial Cross Sections of the 1FA Basket KENO Model* *6.10.4-54*
Figure 6.10.4-6 *TN-LC 1FA Basket KENO Model* *6.10.4-55*
Figure 6.10.4-7 *BWR and PWR Fuel Models* *6.10.4-56*
Figure 6.10.4-8 *Array of Casks for NCT Analysis* *6.10.4-57*
Figure 6.10.4-9 *Damaged Fuel Models* *6.10.4-58*
Figure 6.10.4-10 *25 Pin Can Model with PWR Fuel* *6.10.4-59*
Figure 6.10.4-11 *Assembly Positioning* *6.10.4-60*
Figure 6.10.4-12 *PRA Locations for PWR Fuel Requiring 5 PRAs* *6.10.4-61*
Figure 6.10.4-13 *Possible PRA Configuration for WE 14x14 and WE 15x15 Class Assemblies – NCT and HAC* *6.10.4-62*
Figure 6.10.4-14 *BWR Modeling Cases to Assess Hold Down Ring Effects* *6.10.4-63*
Figure 6.10.4-15 *PRA Configuration for BW 15x15, BW 17x17 and WE 17x17 Class Fuel Assemblies – NCT and HAC* *6.10.4-64*
Figure 6.10.4-16 *KENO Model of the Most Reactive Case with Poison Plate Bolt Holes* *6.10.4-65*

poison plates remains the same regardless of whether a PWR assembly, BWR assembly, or individual pins are transported.

Also shown in Figure 6.10.4.2 are stainless steel bolts that bore through the poison plates. These bolts attach the aluminum rails to the basket frames and pass through the poison plates. In Section 6.10.4.4.1 the effect of these stainless steel holes is evaluated by modifying the system with the most reactive fuel and configuration.

Additionally, Poison Rod Assemblies (PRAs) are required while transporting PWR fuel assemblies in order to ensure that the maximum reactivity is subcritical and below the Upper Subcritical Limit (USL). The minimum required B_4C content of the absorber rods in the PRAs is 40 percent theoretical density (TD) (75 percent credit is taken in the criticality analysis, or 30 percent TD). The minimum required B_4C content of the absorber rods is only 30 percent (in the KENO input) because assuming a higher B_4C content is not expected to reduce the reactivity of the system since the absorber rods are already "black" to the neutrons in the system. Note that the absorber rods are also referred to as PRAs in this Appendix.

The BWR fuel assembly compartment is surrounded by the PWR compartment and the 25 pin can is placed in the BWR compartment. Additional reactivity control is not necessary for the BWR and 25 pin can transportation.

6.10.4.1.2 Summary Table of Criticality Evaluation

The upper subcritical limit (USL) for ensuring that the package is acceptably subcritical as determined in Section 6.10.4.8 is:

$$USL = 0.9420$$

The package is considered to be acceptably subcritical if the computed k_{safe} (k_s), which is defined as $k_{effective}$ (k_{eff}) plus twice the statistical uncertainty (σ), is less than or equal to the USL, or:

$$k_s = k_{eff} + 2\sigma \leq USL$$

The USL is determined on the basis of a benchmark analysis and incorporates the combined effects of code computational bias, the uncertainty in the bias based on computational uncertainties, and an administrative margin. The results of the benchmark analysis indicate that the USL is adequate to ensure subcriticality of the package.

The package design is shown to meet the requirements of 10 CFR 71.55(b). No credit is taken for fuel burnup; in other words, the fuel rods are modeled as fresh fuel, which ensures that a highly conservative k_s is obtained. The package is evaluated under Normal Conditions of Transport (NCT) and Hypothetical Accident Conditions (HAC) in accordance with the requirements of 10 CFR 71.55 and 10 CFR 71.59. In all single package evaluations, water is modeled in all cavities with the most reactive density for both NCT and HAC conditions. Close full reflection of the package is achieved using 12 feet of water.

In the NCT array models, a close-packed array of three packages is utilized. The entire array is reflected with 12 feet of water. No HAC array models are developed. Therefore, the HAC array result is the same as the single package result.

The maximum results of the criticality calculations are summarized in Table 6.10.4-1. The maximum calculated k_s is *0.9366*, which occurs for HAC with a PWR fuel assembly. The maximum reactivity is below the USL of 0.9420.

6.10.4.1.3 Criticality Safety Index

No HAC array models are developed (2N=1). Therefore, per 10CFR71.59, N=0.5, and the criticality safety index (CSI) is 50/N = 100. In the NCT array cases, 5N=2.5, so that 3 packages are modeled.

6.10.4.3 General Considerations

6.10.4.3.1 Model Configuration

The cask model comprises the fuel, basket, and packaging, which are modeled explicitly in SCALE [1]. The packaging is conservatively modeled without the neutron shield and impact limiters in both the NCT and HAC conditions. The length of the cask modeled covers the active length of the fuel and 12 feet of water is modeled in the axial directions as well as the sides of the cask. A KENO model of the cask without fuel is shown in Figure 6.10.4-5. The figure on the left shows the radial cross section of the cask with the 25 pin can. In the same figure, the axial cross section is also presented on the right.

A more detailed view of the KENO model is shown in Figure 6.10.4-6. In the figure, all the compartments are shown to provide an overall view of the compartments relative to one another. The cask model is based on materials and dimensions shown in the drawings in Chapter 1. The dimensions of the components labeled in Figure 6.10.4-6 are listed in the accompanying Table 6.10.4-6.

In the simulation models, only the lengths of the compartments/components that cover the active length of the fuels to be transported are modeled.

In both the NCT and HAC models, water is modeled inside the package at the density that maximizes reactivity. Because the cask is designed for wet loading, water drains freely inside the basket, and preferential flooding scenarios are not credible. However, the cavity could be partially flooded. Because the baskets drain freely, if the TN-LC cavity is partially flooded, the only credible scenario is that some fuel would be submerged in water, and the remaining fuel would remain unsubmerged. Therefore, any partial flooding scenarios would result in unmoderated fuel. LWR fuels have very low reactivity in the absence of moderation. Therefore, any partial flooding would uncover fuel and decrease the reactivity. For these reasons, cases are not developed for partial and/or preferential flooding.

Normal Conditions of Transport Fuel Models:

The intact fuel models constructed are used for the NCT analysis. The NCT analysis calls for simulation of single package transport and an array of packages. For BWR and PWR fuels, the assemblies are modeled, centered in their respective compartments with the fuel rods also centered in each lattice cell. Water is modeled in the compartment cavity and fuel gap with Zircalloy as the cladding material. The fuel parameters used are presented in Table 6.10.4-2 and Table 6.10.4-3. The PWR and BWR fuel models for NCT single package analysis are shown in Figure 6.10.4-7. The model on the left represents the most reactive BWR fuel assembly for the 10x10 assemblies, while the model on the right represents the most reactive PWR fuel assembly in NCT.

In Figure 6.10.4-8, a model of the three array package used for NCT analysis is shown. The figure shows that some space exists between the casks by the virtue of the arrangement of the casks. The three casks are surrounded by 12 feet of water in all directions, while the space between the casks is modeled with various moderator densities to determine the most reactive external moderator density for the configuration shown.

Hypothetical Accident Condition Fuel Models:

The analytical results reported in Chapter A.2, Appendix A.2.13.1 demonstrate that the cask containment boundary and basket structure do not experience any significant distortion under hypothetical accident conditions. Therefore, the basket and cask geometry remain intact in HAC.

This analysis addresses potential fuel damage scenarios under HAC of transportation. The type and extent of fuel rod damage under HAC can be broken down into several categories. The worst case gross damage from a cask-drop accident is assumed to be either a single-ended or double-ended rod shear with fresh water intrusion. The bent or bowed fuel rod cases assume that the fuel is intact but not in its nominal fuel rod pitch. It is possible that the fuel rods may be crushed

CE 16x16 Class Assemblies:

The most reactive CE 16x16 assembly is the CE 16x16 System 80 fuel assembly as shown in Table 6.10.4-8. The number of PRAs required is 5, each at a minimum diameter of 1.02 cm. The maximum allowable U-235 enrichment is 5.00 weight percent. The configuration of PRA location is as shown in Figure 6.10.4-12.

BW 17x17 Class Assemblies:

In the case of B&W 17x17 Mark C, a PRA diameter of 0.76 cm or a linear density of 0.343 g/cm is required. The maximum allowable enrichment is 5.00 weight percent U-235. The PRA Configuration is as illustrated in Figure 6.10.4-15.

For each class, the result is shown in Table 6.10.4-21 with HAC scenario. As a resultant, the PRA requirement under all conditions of transport is as summarized in Table 6.10.4-26. This table contains the number of PRAs necessary for each assembly class, maximum enrichment allowed, the linear density of each PRA before the 75% credit is applied for analysis, or the actual minimum 40% TD required, and the minimum diameter of each PRA. Note that in Table 6.10.4-21; only PRA Configuration 1 is evaluated, since it has been shown that both Configurations 1 and 2 are acceptable in Table 6.10.4-19.

Under HAC, the PRA configuration is not expected to change. All rotationally symmetric configurations of the absorber rods are also acceptable.

Proprietary Information Withheld Pursuant to 10 CFR 2.390.

As the results in Table 6.10.4-17 demonstrate, BWR fuels will remain subcritical and under the USL for HAC. For the transportation of 25 individual fuel rods, HAC is not evaluated. This is due to the fact that the reactivity of the system is bounded by PWR fuel assembly transportation by more than 0.30 in Δk for NCT, and any postulated HAC is also bounded by PWR fuel rod pitch expansion analysis performed. These scenarios have been explored for PWR and BWR fuels to show that the 25 fuel rods are bounded.

6.10.4.4.2 Results

The results for single package transport are presented in Table 6.10.4-22. In this table, taking the most reactive fuel under NCT, the B&W 15x15 Mark B11 fuel assembly from Table 6.10.4-9 (Case ID P_B011), eight PRAs are added to the system. Additionally, the most reactive CE 16x16 and CE 15x15 fuel assemblies are selected and evaluated with five PRAs and one PRA, respectively, to demonstrate that they remain subcritical and under the USL. The remaining cases presented in this table are reproduced with their original Case IDs.

The most reactive configuration results from the PWR fuel assembly under HAC. In HAC, it has been shown that the WE 14x14 class assemblies are the most reactive. However, the CE 15x15 Assembly Class accepts only 1 PRA and would result in a higher k_{eff}. The CE 16x16 Assembly Class with five PRAs is added for completeness in this result, although, without control components, the WE 14x14 Assembly Class remains the most reactive. For BWR fuel, the Allis Chalmers - LaCrosse assemblies are the most reactive.

6.10.4.5 Evaluation of Package Arrays under Normal Conditions of Transport

6.10.4.5.1 Configuration

Consistent with the PWR NCT results in Table 6.10.4-8, B&W 15x15 Mark B11 fuel is used in the PWR NCT array calculations. For the package arrays under NCT, only PWR and BWR fuel assembly transport was considered because transport of 25 fuel rods will be bounded by the assembly transport conditions. Since CSI is 100, an array of three casks is modeled, as shown in Figure 6.10.4-8, and the gap between them is filled with water or air. The water density was varied between 0.01 and 100 percent. The PWR results are presented in Table 6.10.4-23 without PRAs. Because PRAs are not included in this step, the results exceed the USL. The BWR fuel, NCT array configuration is similar to that of PWR fuels. Consistent with the BWR NCT results in Table 6.10.4-15, the most reactive BWR assembly of all types, Allis Chalmers – LaCrosse, is selected as the design basis BWR fuel.

6.10.4.5.2 Results

The results show that for an external moderator density (EMD) or density of water located between the casks of 0.01 percent, the most reactive configuration under NCT exists. This configuration will be subcritical and under the USL with five PRAs located in the prescribed locations of the CE 16x16 assembly class, one (1) PRA for the CE 15x15 class, and eight (8) PRAs for the remaining fuel classes. The resulting PWR reactivity for the NCT array with PRAs is presented in Table 6.10.4-24. For BWR fuel, the most reactive fuel assembly, the Allis Chalmers LaCrosse fuel assembly, is used to perform the 3-array NCT analysis. As shown in Table 6.10.4-25, the system remains subcritical.

Table 6.10.4-1
Summary of Criticality Evaluation

Proprietary Information Withheld Pursuant to 10 CFR 2.390.

Description	k_{eff}	USL
Normal Conditions of Transport: PWR fuel		
Single Package Maximum	0.8895	0.9420
3 Package Array Maximum	0.9047	0.9420
Normal Conditions of Transport: BWR fuel		
Single Package Maximum	0.7806	0.9420
3 Package Maximum	0.8202	0.9420
Hypothetical Accident Conditions: PWR fuel		
Single Package Maximum	*0.9366*	0.9420
Infinite Array Maximum	*0.9366*	0.9420
Hypothetical Accident Conditions: BWR fuel		
Single Package Maximum	0.8118	0.9420
Infinite Array Maximum	0.8118	0.9420
Normal Conditions of Transport:25 Pin Can		
Single Package PWR	0.3782	0.9420
Single Package BWR	0.3865	0.9420
Single Package MOX	0.5210	0.9420
Single Package EPR	0.3616	0.9420

Table 6.10.4-20
Evaluation of Effects due to PRA Clad Variation, Single Package

Case ID	Description	k_{eff}	1σ	k_s
Proprietary Information Withheld Pursuant to 10 CFR 2.390.	BW 15x15 Fuel Assembly – Single Package NCT, 5 PRAs			
	Case 1 - PRA Clad: solid zirc	0.9110	0.0008	0.9126
	Case 2 - PRA Clad: zirc-with gap	0.9111	0.0010	0.9131
	Case 3 - PRA Clad: ss304-with gap	0.9128	0.0009	0.9146
	CE 15x15 Palisade Fuel Assembly HAC, 1 PRA			
	Case 1 - PRA Clad: solid zirc	0.9295	0.0008	0.9311
	Case 2 - PRA Clad: zirc-with gap	0.9294	0.0008	0.9310
	Case 3 - PRA Clad: ss304-with gap	0.9270	0.0009	0.9288
	Exxon/ANP 15x15 CE Fuel Assembly HAC, 1 PRA			
	Case 1 - PRA Clad: solid zirc	0.9235	0.0008	0.9251
	Case 2 - PRA Clad: zirc-with gap	0.9231	0.0009	0.9249
	Case 3 - PRA Clad: ss304-with gap	0.9254	0.0010	0.9274
	WE 14x14 Fuel Assembly HAC, 6 PRAs			
	Case 1 - PRA Clad: solid zirc	0.9316	0.0009	0.9334
	Case 2 - PRA Clad: zirc-with gap	0.9353	0.0010	0.9373
	Case 3 - PRA Clad: ss304-with gap	0.9350	0.0008	0.9366

Table 6.10.4-21
Design Basis PRA Configuration for Various PWR Assemblies, HAC Single Package

Case ID	Description	k_{keno}	1σ	k_{eff}
Proprietary Information Withheld Pursuant to 10 CFR 2.390.	BW 15x15, 8 PRAs	0.8914	0.0010	0.8934
	CE 15x15, 1 PRA	0.9331	0.0010	0.9351
	CE 16x16, 5 PRAs	0.9231	0.0009	0.9249
	Framatome, CE, 14x14, 5 PRAs	0.9243	0.0009	0.9261
	BW 17x17, 8 PRAs	0.9225	0.0008	0.9241
	Framatome, MK BW 17x17, 8 PRAs	0.9127	0.0009	0.9145
	WE 15x15, 8 PRAs	0.9119	0.0009	0.9137
	WE 17x17, 8 PRAs	0.9168	0.0009	0.9186
	CE 15x15, 1 PRA-Poison Plate Bolt Holes	*0.9348*	*0.009*	*0.9366*

Table 6.10.4-22
NCT and HAC Results for Single Package Transport

Case ID	Description	k_{eff}	1σ	k_s
Proprietary Information Withheld Pursuant to 10 CFR 2.390.	**Normal Conditions of Transport: PWR fuel**			
	Single Package Maximum, 8 PRAs	0.8596	0.0008	0.8612
	Single Package Maximum, 1 PRA	0.8875	0.0010	0.8895
	Single Package Maximum, 5 PRAs	0.8724	0.0009	0.8742
	Normal Conditions of Transport: BWR fuel			
	Single Package Maximum	0.7788	0.0009	0.7806
	Hypothetical Accident Conditions: PWR fuel			
	Single Package Maximum	*0.9348*	*0.0009*	*0.9366*
	Hypothetical Accident Conditions: BWR fuel			
	Single Package Maximum	0.8099	0.0009	0.8118
	Normal Conditions of Transport: 25 Pin Can			
	Single Package Maximum	0.5194	0.0008	0.5210

Table 6.10.4-23
NCT Package Array Results at Varying External Moderator Density – PWR Fuels (no PRAs)

Case ID	Description	k_{keno}	1σ	k_{eff}
Proprietary Information Withheld Pursuant to 10 CFR 2.390.	AIR	1.0172	0.0009	1.0190
	0.01% EMD	**1.0177**	**0.0009**	**1.0195**
	10% EMD	1.0116	0.0009	1.0133
	20% EMD	1.0092	0.0010	1.0112
	30% EMD	1.0092	0.0009	1.0110
	40% EMD	1.0079	0.0010	1.0098
	50% EMD	1.0073	0.0010	1.0093
	60% EMD	1.0077	0.0009	1.0095
	70% EMD	1.0063	0.0009	1.0080
	80% EMD	1.0061	0.0009	1.0079
	90% EMD	1.0044	0.0009	1.0063
	100% EMD	1.0049	0.0009	1.0067

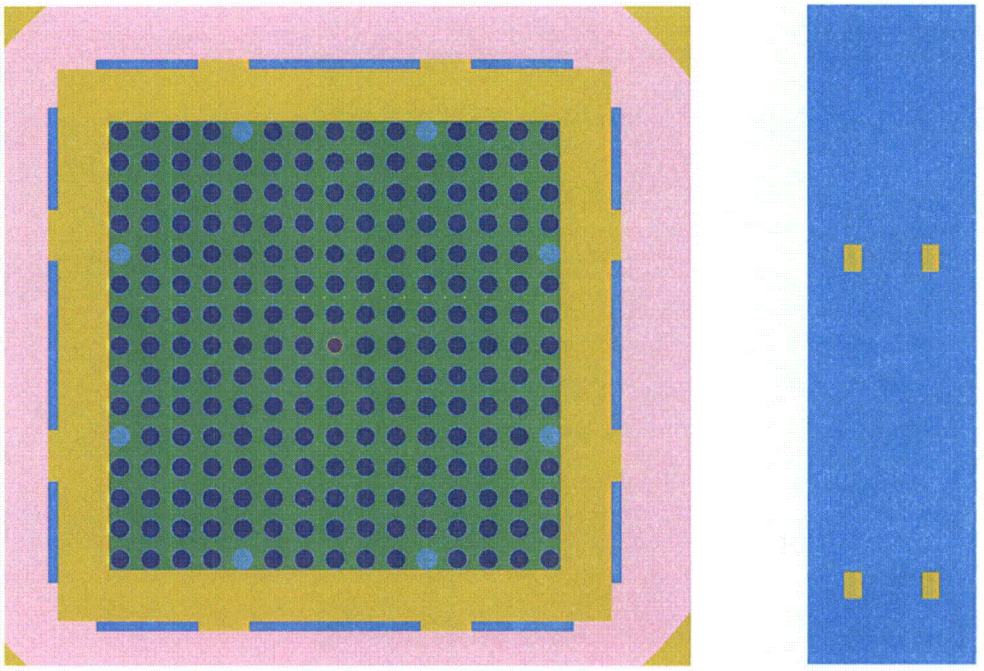

Figure 6.10.4-16
KENO Model of the Most Reactive Case with Poison Plate Bolt Holes

PROPRIETARY AND SECURITY RELATED INFORMATION WITHHELD UNDER 10 CFR 2.390

REVISION	DESCRIPTION	DATE
1	REVISED PER RSI COMMENTS	08/15/11
0	FIRST ISSUE	05/31/11

ALL DIMENSIONS ARE NOMINAL UNLESS A SPECIFIC TOLERANCE IS INDICATED WITH THE DRAWING DIMENSION

DIMENSIONS ARE IN INCHES AND DEGREES UNLESS OTHERWISE SPECIFIED. DIMENSIONING IN ACCORDANCE WITH ASME Y14.5M-1994.

INTERPRET WELD SYMBOLS PER ANSI / AWS 2.4

TRANSNUCLEAR
AN AREVA COMPANY

SAFETY ANALYSIS REPORT

TN-LC CASK ASSEMBLY

DRAWING NO.	SCALE	SHEET
65200-71-01	NONE	1 OF 11

PROPRIETARY AND SECURITY RELATED INFORMATION WITHHELD UNDER 10 CFR 2.390

PROPRIETARY AND SECURITY RELATED INFORMATION WITHHELD UNDER 10 CFR 2.390

PROPRIETARY AND SECURITY RELATED INFORMATION WITHHELD UNDER 10 CFR 2.390

PROPRIETARY AND SECURITY RELATED INFORMATION WITHHELD UNDER 10 CFR 2.390

PROPRIETARY AND SECURITY RELATED INFORMATION WITHHELD UNDER 10 CFR 2.390

PROPRIETARY AND SECURITY RELATED INFORMATION WITHHELD UNDER 10 CFR 2.390

PROPRIETARY AND SECURITY RELATED INFORMATION WITHHELD UNDER 10 CFR 2.390

PROPRIETARY AND SECURITY RELATED INFORMATION WITHHELD UNDER 10 CFR 2.390

PROPRIETARY AND SECURITY RELATED INFORMATION WITHHELD UNDER 10 CFR 2.390

PROPRIETARY AND SECURITY RELATED INFORMATION WITHHELD UNDER 10 CFR 2.390

PROPRIETARY AND SECURITY RELATED INFORMATION WITHHELD UNDER 10 CFR 2.390

REVISION	DESCRIPTION	DATE
1	REVISED PER RSI COMMENTS	08/15/11
0	FIRST ISSUE	05/31/11

ALL DIMENSIONS ARE NOMINAL UNLESS A SPECIFIC TOLERANCE IS INDICATED WITH THE DRAWING DIMENSION

DIMENSIONS ARE IN INCHES AND DEGREES UNLESS OTHERWISE SPECIFIED. DIMENSIONING IN ACCORDANCE WITH ASME Y14.5M-1994.

INTERPRET WELD SYMBOLS PER ANSI / AWS 2.4

TRANSNUCLEAR
AN AREVA COMPANY

SAFETY ANALYSIS REPORT

TN-LC
IMPACT LIMITER ASSEMBLY

DRAWING NO.	SCALE	SHEET
65200-71-20	NONE	1 OF 3

PROPRIETARY AND SECURITY RELATED INFORMATION WITHHELD UNDER 10 CFR 2.390

PROPRIETARY AND SECURITY RELATED INFORMATION WITHHELD UNDER 10 CFR 2.390

PROPRIETARY AND SECURITY RELATED INFORMATION WITHHELD UNDER 10 CFR 2.390

REVISION	DESCRIPTION	DATE
1	REVISED PER RSI COMMENTS	08/15/11
0	FIRST ISSUE	05/31/11

ALL DIMENSIONS ARE NOMINAL UNLESS A SPECIFIC TOLERANCE IS INDICATED WITH THE DRAWING DIMENSION

DIMENSIONS ARE IN INCHES AND DEGREES UNLESS OTHERWISE SPECIFIED. DIMENSIONING IN ACCORDANCE WITH ASME Y14.5M-1994.

INTERPRET WELD SYMBOLS PER ANSI / AWS 2.4

TRANSNUCLEAR
AN AREVA COMPANY

SAFETY ANALYSIS REPORT
TN-LC-NRUX BASKET
BASKET ASSEMBLY

DRAWING NO.	SCALE	SHEET
65200-71-40	NONE	1 OF 5

PROPRIETARY AND SECURITY RELATED INFORMATION WITHHELD UNDER 10 CFR 2.390

PROPRIETARY AND SECURITY RELATED INFORMATION WITHHELD UNDER 10 CFR 2.390

PROPRIETARY AND SECURITY RELATED INFORMATION WITHHELD UNDER 10 CFR 2.390

PROPRIETARY AND SECURITY RELATED INFORMATION WITHHELD UNDER 10 CFR 2.390

PROPRIETARY AND SECURITY RELATED INFORMATION WITHHELD UNDER 10 CFR 2.390

REVISION	DESCRIPTION	DATE
1	REVISED PER RSI COMMENTS	08/15/11
0	FIRST ISSUE	05/31/11

ALL DIMENSIONS ARE NOMINAL UNLESS A SPECIFIC TOLERANCE IS INDICATED WITH THE DRAWING DIMENSION

DIMENSIONS ARE IN INCHES AND DEGREES UNLESS OTHERWISE SPECIFIED. DIMENSIONING IN ACCORDANCE WITH ASME Y14.5M-1994.

INTERPRET WELD SYMBOLS PER ANSI / AWS 2.4

TRANSNUCLEAR
AN AREVA COMPANY

SAFETY ANALYSIS REPORT
TN-LC-NRUX BASKET
BASKET TUBE ASSEMBLY

DRAWING NO.	SCALE	SHEET
65200-71-50	NONE	1 OF 5

PROPRIETARY AND SECURITY RELATED INFORMATION WITHHELD UNDER 10 CFR 2.390

PROPRIETARY AND SECURITY RELATED INFORMATION WITHHELD UNDER 10 CFR 2.390

PROPRIETARY AND SECURITY RELATED INFORMATION WITHHELD UNDER 10 CFR 2.390

PROPRIETARY AND SECURITY RELATED INFORMATION WITHHELD UNDER 10 CFR 2.390

PROPRIETARY AND SECURITY RELATED INFORMATION WITHHELD UNDER 10 CFR 2.390

REVISION	DESCRIPTION	DATE
1	REVISED PER RSI COMMENTS	08/15/11
0	FIRST ISSUE	05/31/11

ALL DIMENSIONS ARE NOMINAL UNLESS A SPECIFIC TOLERANCE IS INDICATED WITH THE DRAWING DIMENSION

DIMENSIONS ARE IN INCHES AND DEGREES UNLESS OTHERWISE SPECIFIED. DIMENSIONING IN ACCORDANCE WITH ASME Y14.5M-1994.

INTERPRET WELD SYMBOLS PER AWS / AWS 2.4

TRANSNUCLEAR
AN AREVA COMPANY

SAFETY ANALYSIS REPORT
TN-LC-MTR BASKET
GENERAL ASSEMBLY

DRAWING NO.	SCALE	SHEET
65200-71-80	NONE	1 OF 4

PROPRIETARY AND SECURITY RELATED INFORMATION WITHHELD UNDER 10 CFR 2.390

PROPRIETARY AND SECURITY RELATED INFORMATION WITHHELD UNDER 10 CFR 2.390

PROPRIETARY AND SECURITY RELATED INFORMATION WITHHELD UNDER 10 CFR 2.390

DRAWING NO.	SHEET	REVISION
65200-71-60	4 OF 4	1

PROPRIETARY AND SECURITY RELATED INFORMATION WITHHELD UNDER 10 CFR 2.390

REVISION	DESCRIPTION	DATE
1	REVISED PER RSI COMMENTS	08/15/11
0	FIRST ISSUE	05/31/11

ALL DIMENSIONS ARE NOMINAL UNLESS A SPECIFIC TOLERANCE IS INDICATED WITH THE DRAWING DIMENSION

DIMENSIONS ARE IN INCHES AND DEGREES UNLESS OTHERWISE SPECIFIED. DIMENSIONING IN ACCORDANCE WITH ASME Y14.5M–1994.

INTERPRET WELD SYMBOLS PER AWS / ANSI 2.4

TRANSNUCLEAR
AN AREVA COMPANY

SAFETY ANALYSIS REPORT
TN-LC-MTR BASKET
FUEL BUCKET

DRAWING NO.	SCALE	SHEET
65200-71-70	NONE	1 OF 2

PROPRIETARY AND SECURITY RELATED INFORMATION WITHHELD UNDER 10 CFR 2.390

DRAWING NO. 65200-71-80 SHEET 1 OF 5

PROPRIETARY AND SECURITY RELATED INFORMATION WITHHELD UNDER 10 CFR 2.390

REVISION	DESCRIPTION	DATE
1	REVISED PER RSI COMMENTS	08/15/11
0	FIRST ISSUE	05/31/11

ALL DIMENSIONS ARE NOMINAL UNLESS A SPECIFIC TOLERANCE IS INDICATED WITH THE DRAWING DIMENSION

DIMENSIONS ARE IN INCHES AND DEGREES UNLESS OTHERWISE SPECIFIED. DIMENSIONING IN ACCORDANCE WITH ASME Y14.5M-1994.

INTERPRET WELD SYMBOLS PER ANSI / AWS 2.4

TRANSNUCLEAR
AN AREVA COMPANY

SAFETY ANALYSIS REPORT

TN-LC-TRIGA BASKET

DRAWING NO.	SCALE	SHEET
65200-71-80	NONE	1 OF 5

PROPRIETARY AND SECURITY RELATED INFORMATION WITHHELD UNDER 10 CFR 2.390

PROPRIETARY AND SECURITY RELATED INFORMATION WITHHELD UNDER 10 CFR 2.390

PROPRIETARY AND SECURITY RELATED INFORMATION WITHHELD UNDER 10 CFR 2.390

PROPRIETARY AND SECURITY RELATED INFORMATION WITHHELD UNDER 10 CFR 2.390

PROPRIETARY AND SECURITY RELATED INFORMATION WITHHELD UNDER 10 CFR 2.390

REVISION	DESCRIPTION	DATE
1	REVISED PER RSI COMMENTS	08/15/11
0	FIRST ISSUE	05/31/11

ALL DIMENSIONS ARE NOMINAL UNLESS A SPECIFIC TOLERANCE IS INDICATED WITH THE DRAWING DIMENSION

DIMENSIONS ARE IN INCHES AND DEGREES UNLESS OTHERWISE SPECIFIED. DIMENSIONING IN ACCORDANCE WITH ASME Y14.5M-1994.

INTERPRET WELD SYMBOLS PER ANSI / AWS 2.4

TRANSNUCLEAR
AN AREVA COMPANY

SAFETY ANALYSIS REPORT

TN-LC-1FA BASKET

DRAWING NO.	SCALE	SHEET
65200-71-90	NONE	1 OF 5

PROPRIETARY AND SECURITY RELATED INFORMATION WITHHELD UNDER 10 CFR 2.390

PROPRIETARY AND SECURITY RELATED INFORMATION WITHHELD UNDER 10 CFR 2.390

PROPRIETARY AND SECURITY RELATED INFORMATION WITHHELD UNDER 10 CFR 2.390

PROPRIETARY AND SECURITY RELATED INFORMATION WITHHELD UNDER 10 CFR 2.390

PROPRIETARY AND SECURITY RELATED INFORMATION WITHHELD UNDER 10 CFR 2.390

REVISION	DESCRIPTION	DATE
1	REVISED PER RSI COMMENTS	08/15/11
0	FIRST ISSUE	05/31/11

ALL DIMENSIONS ARE NOMINAL UNLESS A SPECIFIC TOLERANCE IS INDICATED WITH THE DRAWING DIMENSION

DIMENSIONS ARE IN INCHES AND DEGREES UNLESS OTHERWISE SPECIFIED. DIMENSIONING IN ACCORDANCE WITH ASME Y14.5M-1994.

INTERPRET WELD SYMBOLS PER ANSI / AWS 2.4

TRANSNUCLEAR
AN AREVA COMPANY

SAFETY ANALYSIS REPORT
TN-LC-1FA BWR
SLEEVE AND
HOLD-DOWN RING

DRAWING NO.	SCALE	SHEET
65200-71-98	NONE	1 OF 2

PROPRIETARY AND SECURITY RELATED INFORMATION WITHHELD UNDER 10 CFR 2.390

PROPRIETARY AND SECURITY RELATED INFORMATION WITHHELD UNDER 10 CFR 2.390

REVISION	DESCRIPTION	DATE
1	REVISED PER RSI COMMENTS	08/15/11
0	FIRST ISSUE	05/31/11

ALL DIMENSIONS ARE NOMINAL UNLESS A SPECIFIC TOLERANCE IS INDICATED WITH THE DRAWING DIMENSION

DIMENSIONS ARE IN INCHES AND DEGREES UNLESS OTHERWISE SPECIFIED. DIMENSIONING IN ACCORDANCE WITH ASME Y14.5M-1994.

INTERPRET WELD SYMBOLS PER ANSI / AWS 2.4

TRANSNUCLEAR
AN AREVA COMPANY

SAFETY ANALYSIS REPORT
TN-LC-1FA
25 PIN CAN BASKET

DRAWING NO.	SCALE	SHEET
65200-71-102	NONE	1 OF 5

PROPRIETARY AND SECURITY RELATED INFORMATION WITHHELD UNDER 10 CFR 2.390

PROPRIETARY AND SECURITY RELATED INFORMATION WITHHELD UNDER 10 CFR 2.390

PROPRIETARY AND SECURITY RELATED INFORMATION WITHHELD UNDER 10 CFR 2.390

PROPRIETARY AND SECURITY RELATED INFORMATION WITHHELD UNDER 10 CFR 2.390

DRAWING NO.	SHEET	REVISION
65200-71-102	5 OF 5	1

Enclosure 7 to TN E-31368

List of References Associated with RSI Responses

List of References
Response to Request for Supplemental Information
TN-LC Transportation Package Application
(Docket No. 71-9358; TAC No. L24543)

1) References in response to RSI-9:

   a. TN Letter to USNRC, E-18578, "TN-32 Cask Thermal Testing – Docket 72-1021", dated December 1, 2000.

2) References in response to RSI-10:

   a. TN-LC SAR, Chapter 3, Reference [15]:
   Updated Final Safety Analysis Report for NUHOMS® HD Horizontal Modular Storage System for Irradiated Nuclear Fuel, Rev. 2, including Amendment 1, Section 4.8.6 and related pages.

   b. TN-LC SAR, Chapter 3, Reference [21]:
   Safety Analysis Report for NUHOMS®-MP197 Transport Packaging, including application for Revision to CoC No. 9302, Docket No. 71-9302, dated April 14, 2009, plus supplemental submittals on June 22, 2009, April 20, 2010, July 15, 2010, and March 29, 2011, Section 3.4.1.1 and Appendix A, Section A.3.6.7.4 and related pages.

   c. TN-LC SAR, Chapter 3, Reference [25]:
   Updated Final Safety Analysis Report for the Standardized NUHOMS® Horizontal Modular Storage System for Irradiated Nuclear Fuel, NUH-003, Revision 11, Appendix J, Section J.4.4, Appendix M, Sections M.4.2, M.4.4.4, and M.4.8, Appendix P, Sections P.4.2 and P.4.8, Appendix T, Sections T.4.2 and T.4.8, and related pages.

   d. TN-LC SAR, Chapter 3, Reference [35]:
   Safety Analysis Report for the Standardized NUHOMS® Horizontal Modular Storage System for Irradiated Nuclear Fuel, Application for Amendment 13, Docket 72-1004, Appendix Y, Section Y.4.9 and Appendix Z, Section Z.4.9 and related pages.

File No # 4.6.4 / 1
Record # 3

TRANSNUCLEAR, INC.

E-18578
December 1, 2000

Ms. Mary Jane Ross-Lee
Spent Fuel Licensing Section
Spent Fuel Project Office
Office of Nuclear Material Safety and Safeguards
US Nuclear Regulatory Commission
Washington, D.C. 20555-0001

Subject: TN-32 Cask Thermal Testing
Docket 72-1021

Dear Ms. Ross-Lee:

In accordance with Section 9 of Certificate of Compliance No. 1021 for the TN-32 Dry Storage Cask, each agent and/or subcontractor authorized by Transnuclear to complete final assembly of the TN-32 cask body is required to verify the heat transfer performance of a single cask. This test is to be performed prior to the first loading of any cask assembled by that agent and/or subcontractor with a heat load equal to or greater than 23.7 kilowatts.

Transnuclear, Inc. is currently fabricating TN-32 casks at Ranor in Westminster, MA and Precision Components Corporation in York, PA. Thermal tests were performed at both of these facilities by an outside test organization, National Technical Systems, of Acton MA under subcontract to Transnuclear. NTS Report No. 36322-00N Rev. 0 documents the test of a TN-32 cask fabricated at Precision Components Corp. NTS Report No. 62119-01N Rev. 0 documents the test performed on a TN-32 cask fabricated at Ranor.

Heat dissipation for the TN-32 cask to the ambient occurs three-dimensionally with a significant portion of the design heat load of 32.7 kW being radially dissipated through the neutron shield region of the cask body. The remaining heat load is conducted in the axial direction along the cask body shell components. The radial heat transfer performance is dependent on the degree of physical contact between adjacent cask shell components which is typically controlled by the fabrication process. The thermal testing was performed at the two fabrication facilities to measure the effective thermal conductivity of a cask in the radial direction over an approximately 10.5-ft exposed length within the neutron shield region. These measured thermal conductivities were used as thermal input into the ANSYS model used to perform the SAR normal thermal analysis. The temperature distribution computed for each case is then evaluated against the SAR reported values.

FOUR SKYLINE DRIVE, HAWTHORNE, NEW YORK 10532
Phone: 914-347-2345 • Fax: 914-347-2346

The first thermal test was performed at Precision Components Corporation (PCC). The cask selected was in a semi-finished condition with the cask cavity aluminum sprayed, and the basket rails installed. The aluminum spray created a surface that prohibited attaching the thermocouples directly to the cavity wall. Rather, these thermocouples were attached to the peripheral insert attachment bolts. This method results in additional thermal resistance through the cask body and conservative results. As described in the test report, the resulting temperature distribution varied axially but the data obtained was still adequate to determine the effective radial conductivity of the cask body.

The second test was performed at Ranor. This test incorporated several lessons learned from the test conducted at PCC, resulting in a more accurate thermal test. A cask was selected for testing that was not aluminum sprayed and did not have the peripheral inserts installed. The thermocouples were then directly attached to the cask cavity wall to yield more easily interpretable results. Additional insulation was added to the cask cavity to ensure that the heat transfer remained in the radial direction during the thermal test. In addition, the heater assembly placed within the cask cavity was modified to provide a more even distribution of heat. The improvements in the testing approach resulted in a fairly uniform temperature distribution as presented in the test report.

Evaluation of the Measured Cask Body Radial Conductivities

As stated in the test report, the measured thermal conductivity for the PCC test was 5.62 Btu/hr-ft-°F for an average temperature difference of 66.4 °F across the cask body without considering the extra thermal resistance of the rail bolts. A calculation was made to determine the thermal resistance introduced by the rail bolt and its impact on the measured temperatures. It was considered in the calculation that the heat flux entering the bolt cap flows through the bolt threads to the cask body. According to the bolt type (1-8 UNC-2A), a nominal air gap of 0.00123 inches was considered between the internal and external threads. The inserted length of the bolt into the cask body is 0.196 inches. The result is a thermal resistance of 1.323 °F/(Btu/hr) for the rail bolt, which causes a temperature difference of 5.6 °F across the bolt in the thermal test conditions at PCC.

Subtracting the temperature difference caused by the rail bolt (5.6 °F) from the average temperature difference calculated in the test report (66.4°F) gives a temperature difference of 60.8 °F across the cask body. Recalculation of the effective radial conductivity considering the new resultant temperature difference gives an effective conductivity of 6.139 Btu/hr-ft-°F.

To demonstrate that the TN-32 casks can dissipate the design heat load of 32.7 kW without exceeding the allowable temperature limits for any cask component or the fuel, the normal thermal analysis (Section 4.4 of the TN-32 SAR) was re-performed with the measured cask body radial conductivity. The three-dimensional thermal model of Section 4.4.1 of the TN-32 SAR was updated with the measured conductivity. Elements forming the cask body along the neutron shield length were given the measured conductivity in the radial direction. The axial conductivities were unchanged from the SAR analysis. All other modeling details, including

boundary conditions, modeling dimensions, and the remaining material properties remain unchanged from the normal storage thermal analysis.

The following are the maximum temperatures calculated for normal storage conditions at the design heat load of 32.7 kW using the measured conductivity.

PCC Test

Component	Calculated Maximum Temperature	SAR Temperature	Allowable Range
(---)	(°F)	(°F)	(°F)
Seals (Lid and Port Cover)	251	256	-40 to 536
Lid	258	263	**
Basket Plates	532	527***	**
Fuel Cladding	571	565***	622 max

** The components perform their intended safety function within the operating range.
*** Previous thermal analysis presented in approved TSAR Rev. 9A showed that the maximum basket temperature was 531°F and the maximum fuel cladding temperature was 595°F. The structural analysis of the basket is based on a maximum temperature of 531°F. The temperature difference of 1°F would not significantly affect the structural analysis results. The thermal analysis of the Rev. 9A TSAR was based on a heat load of 27.1 kW. The thermal analysis presented in Rev. 0 of the FSAR is based on a heat load of 32.7 kW. Through a refined thermal analysis, we were able to demonstrate that the temperatures of the Rev. 9A TSAR were not exceeded, despite the increase in heat load.

The thermal evaluation presented above concludes the thermal performance of the cask tested at PCC is very close to the theoretical performance reported in the SAR. The basket and fuel cladding maximum temperatures are slightly higher than the values presented in the SAR, while the cask body temperatures are slightly lower than the values presented in the SAR. This temperature distribution is within the measurement uncertainty of the test.

The measured thermal conductivity for the Ranor test was 10.27 Btu/hr-ft-°F as stated in the test report. The same approach as described above was chosen to demonstrate that the fabricated TN-32 cask dissipate the design heat load of 32.7 kW without exceeding the allowable temperature limits for any cask component.

The following are the maximum temperatures calculated for normal storage conditions at the design heat load of 32.7 kW using the measured conductivity.

RANOR Test

Component	Calculated Maximum Temperature	SAR Temperature	Allowable Range
(---)	(°F)	(°F)	(°F)
Seals (Lid and Port Cover)	240	256	-40 to 536
Lid	246	263	**
Basket Plates	512	527	**
Fuel Cladding	551	565	622 max

** The components perform their intended safety function within the operating range.

The Ranor test demonstrated that the cask thermal performance exceeded the theoretical performance reported in the SAR. Temperatures were at least 14 °F lower than the values presented in the SAR.

The manufacturing process used by the two fabricators, PCC and Ranor, are very similar. The results of the Ranor test were more precise due to improvements in the test process. Both the PCC and Ranor tests demonstrate that the TN-32 cask performs in accordance with the SAR evaluation. The temperature distribution in each cask with a 32.7 kW heat load demonstrates that all allowable cask component and fuel temperature limits are not exceeded.

Therefore it is concluded that casks manufactured by both fabricators meet the thermal requirements specified in the TN-32 SAR.

If you have any questions regarding this submittal, please feel free to contact me.

Sincerely,

Tara J. Neider
Vice President

cc: NRC Document Control Desk
Keith Waldrop, Duke
Lisa Shell, Virginia Power
Eric Meils, Wisconsin Electric
Project 1066

4.2 Summary of Thermal Properties of Materials

The analyses use interpolated values when appropriate for intermediate temperatures where the temperature dependency of a specific parameter is deemed significant. The interpolation assumes a linear relationship between the reported values.

1. Homogenized PWR Fuel with Helium Backfill[1]

Temp	Transverse conductivity in Helium
(°F)	(Btu/hr-in-°F)
137	0.0188
231	0.0221
327	0.0258
423	0.0304
520	0.0350
617	0.0406
715	0.0468
813	0.0542
1010	0.0684

Temp	Axial Conductivity
(°F)	(Btu/hr-in-°F)
212	0.0576
392	0.0606
572	0.0644
752	0.0695
932	0.0763
1112	0.0852

Temp	$C_{p,\,eff}$
(°F)	(Btu/lbm-°F)
80	0.0593
260	0.0654
692	0.0726
1502	0.0779

ρ_{eff}
(lbm/in^3)
0.1248

2. PWR Fuel with Air Backfill at low pressures for vacuum drying conditions

Temp	Transverse Conductivity for Vacuum Conditions
(°F)	(Btu/hr-in-°F)
188	0.0079
270	0.0099
355	0.0126
444	0.0157
535	0.0197
629	0.0242
723	0.0300
819	0.0363

3. Helium [5]

Temperature		Conductivity	
(K)	(°F)	(W/m-K)	(Btu/hr-in-°F)
200	-100	0.1151	0.0055
250	-10	0.1338	0.0064
300	80	0.1500	0.0072
400	260	0.1800	0.0087
500	440	0.2110	0.0102
600	620	0.2470	0.0119
800	980	0.3070	0.0148
1000	1340	0.3630	0.0175

Density and specific heat of helium is set to zero for transient runs.

[1] See Section 4.8 for calculation of the effective fuel properties

4.8 Effective Fuel Properties

4.8.1 Discussion

The NUHOMS®-32PTH DSC finite element models simulate the effective thermal properties of the fuel with a homogenized material occupying the volume within the basket where the fuel assemblies are stored. Effective values for density, specific heat, and conductivity are determined for this homogenized material for use in the finite element models.

The 32PTH DSC is capable of handling a variety of spent PWR fuel assemblies. In order to determine conservative thermal properties of the homogenized fuel assembly, all of the PWR fuel assemblyies types to be stored in the 32PTH DSC are studied. WE and MK BW fuel assemblies are considered in one category with active fuel length of 144". The lowest effective thermal conductivity, density, and specific heat of these studied fuel assembly groupies are selected to apply in the finite element model. Use of these properties would conservatively predict bounding maximum temperatures for the components of the NUHOMS®-32PTH DSC. The effective fuel properties for CE 14x14 assembly are considered separately since CE 14x14 assembly has a shorter active fuel length.

The characteristics of the fuel assemblies to be stored in the 32PTH DSC are listed in Table 4-12.

4.8.2 Summary of Material Properties

1. UO2, Fuel Pellets

Conductivity and specific heat for fuel pellets are taken from [30] and listed below.

Temperature (°C)	k (cal/s-cm-°C) [30]	Temperature (°F)	k* (Btu/hr-in-°F)
25	0.025	77	0.503
100	0.021	212	0.423
200	0.018	392	0.362
300	0.015	572	0.302
500	0.0132	932	0.266
700	0.0123	1292	0.248
800	0.0124	1472	0.250

Temperature (°C)	C_p (cal/g-°C) [30]	Temperature (°F)	C_p (Btu/lbm-°F)
0	0.056	32	0.056
100	0.063	212	0.063
200	0.0675	392	0.068
400	0.0722	752	0.072
1200	0.079	2192	0.079

* *See Section 4.8.6 for effect of irradiation on thermal conductivity of UO_2*

The density of fuel pellets (UO_2) is 10.96 g/cc = 0.396 lbm/in^3 [30].

2. Zircaloy-4, Cladding

Table B-2.I of Reference [31] lists measured and calculated values of thermal conductivity for zircaloy-4 at various temperatures. The measured values used in this calculation are listed below.

Temperature (K)	k (W/m-K) [31]	Temperature (°F)	k (Btu/hr-in-°F)
373.2	13.6	212	0.655
473.2	14.3	392	0.689
573.2	15.2	572	0.732
673.2	16.4	752	0.790
773.2	18.0	932	0.867
873.2	20.1	1112	0.968

Table B-1.1 of [31] lists specific heat values for Zircaloy as a function of temperature.

Temperature (K)	C_p (J/kg-K) [31]	Temperature (°F)	C_p (Btu/lbm-°F)
300	281	80	0.067
400	302	260	0.072
640	331	692	0.079
1090	375	1502	0.090

The density of Zircaloy is 6.56 g/cm3 = 0.237 lbm/in3, as defined in [30].

Table B-3.11 of [31] lists the measured emissivity values for fuel cladding. For ease of calculation a temperature independent emissivity of 0.8 is set for zircaloy4 in this calculation.

$\varepsilon zirc = 0.80$

3. Helium

Temperature (K)	Conductivity [5] (W/m-k)	Temperature (°F)	Conductivity (Btu/hr-in-°F)
200	0.1151	-100	0.0055
250	0.1338	-10	0.0064
300	0.150	80	0.0072
400	0.180	260	0.0087
500	0.211	440	0.0102
600	0.247	620	0.0119
800	0.307	980	0.0148
1000	0.363	1340	0.0175

4. Air at low pressure (0.1 bar)

Temperature (K)	Conductivity [5] (W/m-k)	Temperature (°F)	Conductivity (Btu/hr-in-°F)
200	0.0180	-100	0.0009
300	0.0263	80	0.0013
400	0.0336	260	0.0016
500	0.0403	440	0.0019
600	0.0466	620	0.0022
800	0.0577	980	0.0028
1000	0.0681	1340	0.0033

The air conductivity at low pressure is used to calculate the effective transverse conductivity for vacuum drying conditions. Air is not allowed for blowdown operations. Only helium *is allowed. For conservatism, air conductivity is utilized in the calculational models (for 14 hours) for vacuum drying and transfer cask backfill operations.*

5. Stainless Steel SA-240, Type 304

A stainless steel emissivity of 0.3, a value lower than the measured values from Reference [14] is used in the analysis for conservatism.

4.8.3 Effective Fuel Conductivity

4.8.3.1 Transverse Effective Conductivity

The purpose of the effective conductivity in the transverse direction of a fuel assembly is to relate the temperature drop of a homogeneous heat generating square to the temperature drop across an actual assembly cross section for a given heat load. This relationship is established by the following equation obtained from Reference [32]:

$$k_{eff} = \frac{Q}{4L_a(T_c - T_o)}(0.29468)$$

where:

k_{eff} = Effective thermal conductivity (Btu/hr-in.-°F)
Q = Assembly head generation (Btu/hr)
Q_{react} = Reaction solution retrieved from quarter model (Btu/hr)

$Q = 4 \times Q_{react} \times L_a$ for WE and MK BW assemblies with quarter symmetric models

$Q = Q_{react} \times L_a$ for CE 14x14 assembly with full-scale model

Q_{react} = Reaction solution retrieved from the ANSYS model (Btu/hr-in)
L_a = Assembly active length (in.)
T_o = Maximum temperature (°F)
T_s = Surface temperature (°F)

Discrete finite element models of the fuel assemblies to be stored in the NUHOMS®-32PTH DSC are developed using the ANSYS computer code [16]. These two-dimensional models simulate heat transfer by radiation and conduction and include the geometry of the fuel rods and fuel pellets. Helium or air properties are used as the fill gas in the fuel assembly. A fuel

assembly decay heat load of 0.8 kW[9] is used for heat generation. An active length of 144" is assumed for WE and MK BW assemblies. The active fuel length of CE 14x14 assembly is considered to be 137".

The finite element models are used to calculate the maximum radial temperature difference with isothermal boundary conditions. All components are modeled using 2-D PLANE55 thermal solid elements. LINK32 elements are placed on the exteriors of the fuel assembly components to set up the creation of the radiation super-element. The compartment wall is modeled using LINK32 elements and used only to set up the surrounding surface for the creation of the radiation matrix super-element using the /AUX12 processor in ANSYS. All LINK32 elements are unselected prior to solution of the thermal problem. The thermal properties used in the model are described in Section 4.8.2, and the fuel assembly geometries are shown in Table 4-12. A typical ANSYS finite element model of fuel assemblies is shown in Figure 4-40 for fuel assemblies WE 17x17 and CE 14x14.

Several computational runs were made for each model using isothermal boundary temperatures ranging from 100 to 1000°F. In determining the temperature dependent effective conductivities of the fuel assemblies an average temperature, equal to $(T_o + T_s)/2$, is used for the fuel temperature. The transverse effective conductivity is calculated in helium for storage and transfer conditions. For vacuum drying conditions, the conductivity of helium is replaced by air conductivity at low pressure. The vacuum drying of the DSC generally does not reduce the pressure sufficiently to reduce the thermal conductivity of the water vapor and air in the DSC cavity [33]. Therefore, air conductivity at low pressures is assumed for the backfill gas for vacuum drying conditions and the effect of water vapor conductivity is neglected.

4.8.3.2 Axial Effective Conductivity

The backfill gas, fuel pellets, and zircaloy behave like resistors in parallel. However, due to the small conductivity of the fill gas and the axial gaps between fuel pellets, credit is only taken for the zircaloy in the determination of the axial effective conductivities.

$$kaxial = \frac{cladding\ area}{4a^2} \times cladding\ conductivity$$

with a = half of compartment width = 8.7"/2 = 4.35"

4.8.4 Effective Fuel Density and Specific Heat

Volume average density and weight average specific heat are calculated to determine the effective density and specific heat for each fuel assembly type separately. The equations to determine the effective density and specific heat are shown below.

$$\rho_{eff} = \frac{\sum \rho_i V_i}{V_{assembly}} = \frac{\rho_{UO2}\ V_{UO2} + \rho_{Zr4}\ V_{Zr4}}{4a^2 L_a}$$

$$C_{p,eff} = \frac{\sum \rho_i V_i C_{Pi}}{\sum \rho_i V_i} = \frac{\rho_{UO2}\ V_{UO2}\ C_{P,UO2} + \rho_{Zr4}\ V_{Zr4}\ C_{P,Zr4}}{\rho_{UO2}\ V_{UO2} + \rho_{Zr4}\ V_{Zr4}}$$

[9] 0.8 kW is the maximum decay heat load for the fuel assemblies in the center of the basket.

4.8.5 Conclusion

The effective transverse conductivity values are plotted in Figure 4-41. Among WE and MK BW assemblies, fuel type WEO 17x17 has the lowest conductivity for the range of 100 to 700°F under helium atmosphere. For temperatures higher than 700°F, fuel assembly MK BW 17x17 has the lowest transverse conductivity. To bound the transverse effective conductivity, the lowest effective conductivity value in each temperature range is selected to apply in the thermal analysis. The effective transverse conductivity of CE 14x14 is used separately in a DSC model with 137" active fuel length.

The calculated transverse effective conductivities for vacuum drying conditions are plotted in Figure 4-42. As Figure 4-42 shows, fuel assembly MK BW 17x17 has the lowest conductivity for vacuum drying conditions, which are used in thermal analysis for vacuum conditions.

The axial effective conductivity for each fuel type is calculated using the equation from Section 4.8.3.2. The resultant values are listed in Table 4-13 and plotted in Figure 4-43. The lowest axial effective conductivity belongs to fuel type WE 15x15 among WE and MK BW assemblies. This value is used in all DSC models except for the DSC model containing CE 14x14 fuel assemblies. analysis. The latest model uses the CE 14x14 axial conductivity shown separately in Figure 4-43.

Effective density of each fuel type is calculated using the corresponding equation from Section 4.8.4. Since using the lowest density results in the highest cladding temperature for accident conditions, the density of fuel assembly WEO 17x17 is the bounding density. The calculated effective density values are listed in Table 4-13.

Effective specific heat values are calculated as a function of temperature using the corresponding equation from Section 4.8.4. Properties of fuel pellets and fuel cladding from Section 4.8.2 are linearly interpolated for this purpose. The lowest specific heat belongs to the fuel type WE 15x15 (and WES 15x15). Since the lowest specific heat results in the highest cladding temperature for transient calculations, specific heat of fuel type WE 15x15 (and WES 15x15) is selected for thermal analysis as the bounding property. The calculated effective specific heat values are listed in Table 4-13.

Since CE 14x14 fuel assembly is analyzed only for steady state transfer conditions, the effective density and the effective specific heat are not calculated for this fuel type.

The bounding effective fuel properties used in the finite element models for WE and MK BW assemblies are listed in Section 4.2.

4.8.6 Effect of Irradiation on UO_2 Thermal Conductivity

Based on Ronchi study [37], UO_2 thermal conductivity of irradiated UO_2 with ~62 GWd/t and irradiation temperature $T_{irr} \geq 1300K$ drops significantly (more that 50%) compared to un-irradiated UO_2. The thermal conductivity values of UO_2 in Section 4.8.2 [30] are compared to the values obtained from [37] study in the figure below.

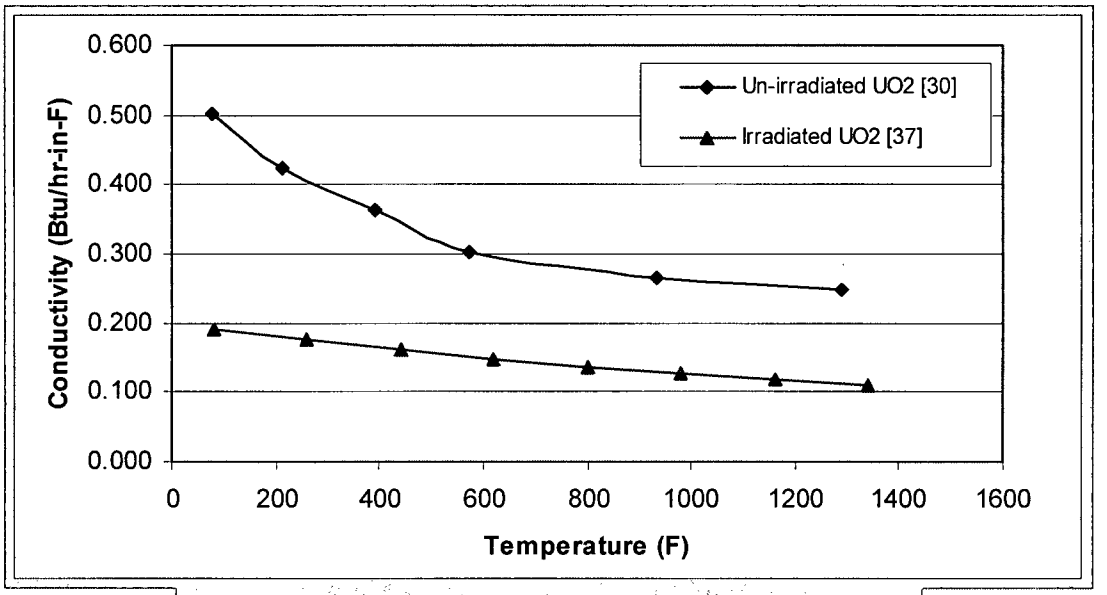

Irradiated and Un-irradiated UO_2 Thermal Conductivity

The comparison shows that the [30] values in the fuel assembly temperature range of interest are higher by approximately a factor of two compared to values obtained from Ronchi study [37].

Using irradiated UO_2 conductivity decreases the effective conductivity of fuel assembly in transverse direction. Note that as discussed in Section 4.8.3.2, axial effective thermal conductivity of fuel assembly is calculated based on the fuel cladding material only and does not include the UO_2 fuel pellet thermal conductivity. Therefore, the axial effective conductivity of fuel assembly is not impacted.

A sensitivity analysis is performed to determine the impact of the irradiated UO_2 conductivity on the maximum fuel cladding temperatures. A sensitivity analysis includes two steps. In the first step, the transverse effective conductivity for fuel assemblies with irradiated and un-irradiated UO_2 conductivities are calculated based on the methodology described in Section 4.8.3.1.

In the second step, the calculated fuel assembly effective conductivities from the first step are used in the 32PTH DSC model from Section 4.3.1.3 to determine the maximum fuel cladding temperature. Normal transfer conditions for 32PTH DSC in OS187H transfer cask with heat load zoning configuration 1 at 115°F ambient is selected for this analysis.

The transverse effective conductivity for fuel assemblies calculated based on irradiated [37] and un-irradiated [30] UO_2 thermal conductivities are compared in the figure below. The transverse

effective conductivity for fuel assemblies used in the evaluation based on UO_2 properties used in the ANSYS model for fuel assembly effective conductivity calculation documented in the Section 4.2 (1) is also added to the figure below for reference.

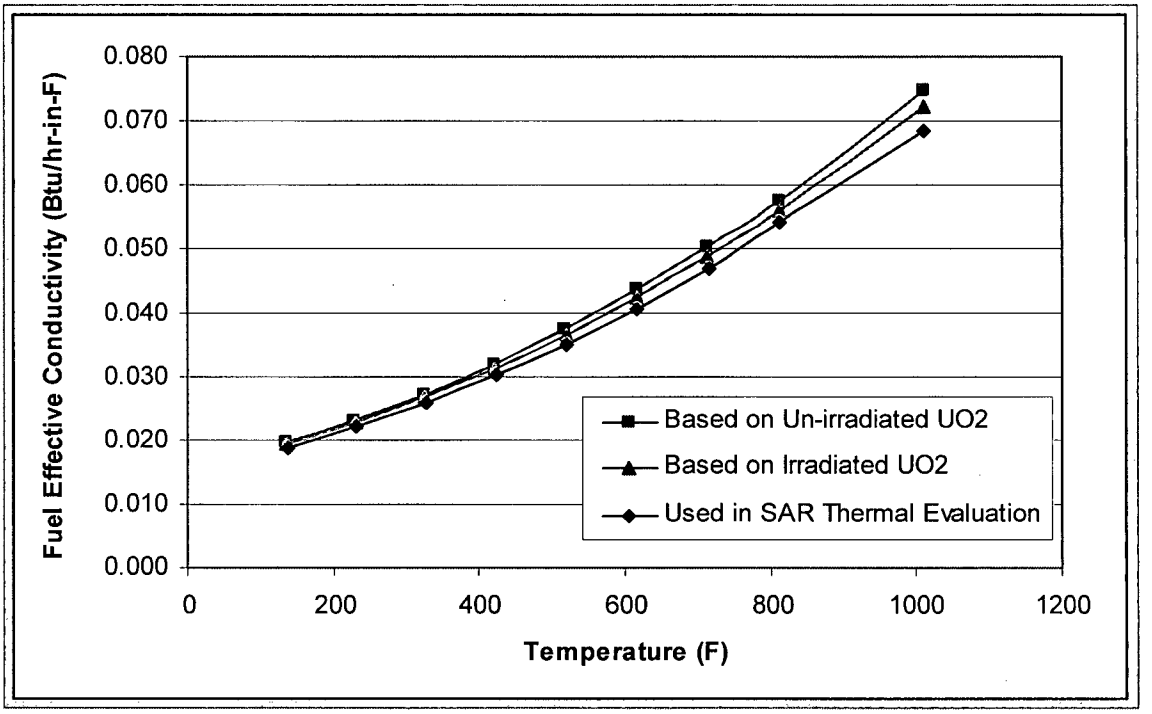

Transverse Effective Conductivity for Fuel Assembly

As seen in the figure above, the fuel assembly effective thermal conductivity calculated with irradiated UO_2 conductivity is approximately 3% lower than the one calculated with un-irradiated UO_2 conductivity at the fuel cladding temperature of 700°F. The results of the sensitivity runs for the maximum fuel cladding temperature calculation using the DSC model from Section 4.3.1.3 are summarized in the table below.

Maximum Component Temperatures - Sensitivity Analysis
(32PTH DSC in OS187H, HLZC #1, 115 °F Ambient)

Component	*(1)*	*(2)*
Fuel Cladding	*716*	*717*
Fuel Compartment	*691*	*692*
Basket Al Plates	*691*	*691*
Basket Rails	*560*	*560*
DSC Shell	*475*	*475*

Notes:
(1) Effective conductivity for fuel assembly is based on un-irradiated UO_2 conductivity as shown in Section 4.2, subsection 1.

(2) Effective conductivity for fuel assembly is based on irradiated UO_2 conductivity values from Ronchi study [37].

The sensitivity analysis results show that values for both cases are comparable to those shown in Table 4-1, 2nd Part for Config. # 1. It also shows that the maximum fuel cladding temperature changes by approximately 1°F (0.14%) which is negligible. These results show that the fuel cladding temperatures are not sensitive to change in UO_2 thermal conductivity due to irradiation. Therefore, use of UO_2 fuel pellets conductivity from [30] is reasonable for irradiated UO_2.

4.8.6.1 UO_2 Thermal Conductivity used in ANSYS Fuel Assembly Model

The ANSYS model described in Section 4.8.3.1 erroneously but conservatively used UO_2 conductivity values which are lower than those shown in Section 4.8.2 (1). A comparison of these values is shown in the table below.

UO_2 Thermal Conductivity

Section 4.8 (1)		*Used in ANSYS model described in Section 4.8.3.1*	
Temperature (°F)	*k (Btu/hr-in-°F)*	*Temperature (°F)*	*k (Btu/hr-in-°F)*
77	*0.503*	*32*	*0.056*
212	*0.423*	*212*	*0.063*
392	*0.362*	*392*	*0.068*
572	*0.302*	*752*	*0.072*
932	*0.266*		
1292	*0.248*		
1472	*0.250*		

As seen from the table above, the UO_2 conductivity values used in the ANSYS model are at least 30% lower than the values obtained from Ronchi study [37]. Use of lower UO_2 thermal conductivity values in the ANSYS model of the fuel assembly results in conservatively lower values of effective thermal conductivity for fuel assembly. This in turn results in higher calculated fuel cladding and DSC component temperatures which are conservative. The transverse effective thermal conductivity for fuel assembly used in the thermal analysis is compared to the corresponding values from sensitivity analysis in the second figure in Section 4.8.6.

Since the effective thermal conductivity for fuel assembly used in thermal analyses of this SAR is lower than the effective thermal conductivity for fuel assembly with irradiated UO_2, the calculated maximum component temperatures are conservative and the difference in irradiated and un-irradiated UO_2 fuel pellet thermal conductivity values does not affect thermal analysis results reported in this SAR.

4.15 References

1. Cogema Logistics, Personnel Communication.
2. USNRC, SFPO, Interim Staff Guidance – 11, Rev. 3, "Cladding Considerations for the Transportation and Storage of Spent Fuel."
3. Perry, R. H., Chilton, C. H., "Chemical Engineers' Handbook," 5th Edition, 1973.
4. USDOE, "Topical Report on Actinide-Only Burnup Credit for PWR Spent Nuclear Fuel Packages," Department of Energy, Report No. DOE / RW0472, Rev. 2, 1998.
5. Rohsenow, W. M., Hartnett, J. P., Ganic, E. N. , "Handbook of Heat Transfer Fundamentals," 2nd Edition, 1985.
6. ASME Boiler and Pressure Vessel Code, Section II, Part D, "Material Properties," 1998 and 2000 addenda.
7. Issard, Herve, "ACL Progress on Boralyn Development," Cogema Logistics presented in "Transnuclear Group Technical Exchange Meeting," October 11, 2002.
8. Final Documentation Package TN-68, P.O. # EP-2001-022, Section G, "Thermal Conductivity Measurements of Borated Aluminum Specimens," Rev. 0.
9. AAR Brooks & Perkins Advanced Structures Division, "Boral® The Neutron Absorber – Product Performance," Report 624.
10. Zoldners, N. G., "Thermal Properties of Concrete under Sustained Elevated Temperatures," ACI Publications, Paper SP 25-1, American Concrete Institute, Detroit, MI, 1970.
11. Cavanaugh, Kevin, "Guide to Thermal Properties of Concrete and Masonry Systems," Reported by ACI Committee 122, Report # ACI 122R-02, American Concrete Institute, Detroit, MI, 2002.
12. Bentz, D. P., "A Computer Model to Predict the Surface Temperature and Time-of-wetness of Concrete Pavements and Bridge Decks," Report # NISTIR 6551, National Institute of Standards and Technology, 2000.
13. Siegel, Robert, Howell, R. H., "Thermal Radiation Heat Transfer," 4th Edition, 2002.
14. Azzazy Technology Inc., "Emissivity Measurements of 304 Stainless Steel," Report Number ATI-2000-09-601, 2000.
15. Kreith, Frank, "Principles of Heat Transfer," 3rd Edition, 1973.
16. ANSYS Computer Code and User's Manuals, Rev. 6.0.
17. USNRC, Code of Federal Regulations, Part 71, "Packaging and Transportation of Radioactive Material," 2003.
18. "ASHRAE Handbook Fundamentals," 4th Edition, 1983.
19. Updated Final Safety Analysis Report, Standardized NUHOMS® Horizontal Modular Storage System for Irradiated Nuclear Fuel, Rev. 9, Feb. 2006.
20. Viebrock, J. M., Douglas, H. M., "Domestic Light Water Reactor Fuel Design Evolution," Vol. III, Nuclear Assurance Corporation, 1981.
21. American Concrete Institute, "Code Requirements for Nuclear Safety Related Concrete Structures (ACI 349-97) and Commentary (ACI 349R-97)," 1997.
22. USNRC, SFPO, NUREG-1536, "Standard Review Plan for Dry Cask Storage Systems - Final Report," 1997.
23. Gregory, J. J., Mata, R., Keltner, N. R., "Thermal Measurements in a Series of Long Pool Fires," SANDIA Report, SAND 85-0196, TTC-0659, 1987.
24. Parker O-Ring Handbook, 5700, Y2000 Edition, 1999.

25. Transnuclear, Inc., "Thermal Testing of the NUHOMS® Horizontal Storage Module, Model HSM-H," Doc. No. E-21625, Rev. 1.
26. Chun, R., Witte, M., Schwartz, M., "Dynamic Impact Effects on Spent Fuel Assemblies," Lawrence Livermore National Laboratory, Report UCID-21246, 1987.
27. Young, W. C., "Roark's Formulas for Stress and Strain," 6th Edition, 1989.
28. Plannel, et al., "Extended Fuel Burnup Demonstration Program – Topical Report – Transport Considerations for Transnuclear Casks," DOE/ET 34014-11, TN-E4226, Transnuclear, Inc. 1983.
29. Brookmire, et al., "Storage of Burnable Poison Rod Assemblies and Thimble Plug Devices in Dry Storage Casks Surry ISFSI," NE-1162, Rev. 0, 1998.
30. Oak Ridge National Laboratory, RSIC Computer Code Collection, "SCALE, A Modular Code System for Performing Standardized Computer Analysis for Licensing Evaluation for Workstations and Personal Computers," NUREG/CR-0200, Rev. 6, ORNL/NUREG/CSD-2/V3/R6.
31. USNRC, SFPO, NUREG/CR-0497, "A Handbook of Materials Properties for Use in the Analysis of Light Water Reactor Fuel Rod Behavior," MATPRO - Version 11, EG&G Idaho, Inc., TREE-1280, 1979.
32. SANDIA Report, SAND90-2406, "A Method for Determining the Spent Fuel Contribution to Transport Cask Containment Requirements," 1992.
33. Diament, R.M.E., "Thermal and Acoustic Insulation," 1986.
34. Kreith, Frank, "The CRC Handbook of Thermal Engineering," 2000.
35. "ASHRAE Handbook, Fundamentals," – SI Edition, 1997.
36. I.E. Idelchik, "Handbook of Hydraulic Resistance," 3rd Edition, 1994.
37. *C. Ronchi, M. Sheindlin, D. Staicu, M. Kinoshita, Effect of burn-up on the thermal conductivity of uranium dioxide up to 1000.000 MWd t^{-1}, Journal of Nuclear Materials, 327 (2004), 58 – 76.*

Table 4-1
Maximum Component Temperatures during Transfer Operations at 115°F ambient

Component	Maximum Temperature 34.8 kW (°F)	Allowable Maximum Temperature (°F)
DSC shell	475	
Cask inner shell	340	
Lead gamma shielding	337	621 [3]
Cask structural shell	280	
Neutron shield panel	263	
Cask lid inner plate*	275	
Cask lid outer plate	217	
Solid neutron shield	265	300 [1]
Cask lid seal †	240	400 [24]
Bottom plate seal ‡	255	400 [24]
Liquid neutron shield (Bulk temperature) §	265	286.9 **
Liquid neutron shield (Maximum temperature)	275	

	Maximum Temperature (°F) 34.8 kW						Allowable Max. Temp. (°F)
Basket Type	Type I				Type II		
Component	**Conf. # 1**	**Conf. # 2**	**Conf. # 3**	**Conf. # 4**	††	‡‡	
Fuel cladding	719	705	700	715	723	727	752 [2]
Fuel compartment	693	667	673	689	697	700	
Basket Al plates	692	666	672	688	696	699	
Basket rails	561	559	559	558	561	565	

	Maximum Temperature (°F) 33.8 kW for CE 14x14 Fuel Assembly		Allowable Max. Temp. (°F)
Basket Type	Type I		
Component	**Configuration # 6**	**Configuration # 7**	
Fuel cladding	717	712	752 [2]
Fuel compartment	689	685	
Basket Al plates	689	684	
Basket rails	555	552	
DSC Shell	467	467	

* Temperatures of cask lid, solid neutron absorber, and seals are from the transfer cask sub-models.
† Maximum temperature of cask body at seal location
‡ Maximum temperature of ram access ring at seal location
§ Bulk temperature is the volumetric average temperature of the elements in shielding segments 8 and 9, see Figure 4-2.
** 286.9°F is the saturated water temperature at 40 psig.
†† Conf. #1 with Al-1100 for rail inserts and back-plates
‡‡ Conf. #1 with Al-6061 for rail inserts and back-plates

Table 4-12
Characteristics of Fuel Assemblies

Fuel Type	WE & WES 15x15	WE & WEV 17x17	MK BW 17x17	WEO 17x17	CE 14x14
Active fuel length	142-144	144	144	144	137
Pellet OD	0.3649-0.3669	0.3225	0.3195	0.3088	0.3765
Rod OD	0.422	0.374	0.374	0.360	0.440
Clad wall thickness	0.0243	0.0225	0.0240	0.0225	0.028
Rod pitch	0.563	0.496	0.496	0.496	0.580
No. of fuel rods	204	264	264	264	176
No. of Guide/Instrument tubes	21	25	25	25	5
Guide tube OD	0.484-0.545	0.429-0.482	0.482	0.429-0.482	1.115
Guide tube wall thickness	0.015	0.016	0.016	0.016	0.04
Instrument tube OD	0.545	0.474-0.545	0.482	0.474-0.545	---
Instrument tube wall thickness	0.015	0.015-.016	0.016	0.015-.016	---

All Dimensions are in inches

Table 4-13
Effective Fuel Properties

Transverse Effective Fuel Conductivity in Helium

Fuel Type	WE & WES 15x15			WE 17x17		
T_o (°F)	T_c (°F)	T_{avg} (°F)	k (Btu/hr-in-°F)	T_c (°F)	T_{avg} (°F)	k (Btu/hr-in-°F)
100	172	136	0.0194	171	136	0.0194
200	261	231	0.0230	261	231	0.0226
300	352	326	0.0269	352	326	0.0266
400	445	423	0.0311	445	423	0.0307
500	538	519	0.0368	539	520	0.0354
600	633	617	0.0424	633	617	0.0418
700	729	714	0.0490	729	715	0.0476
800	825	813	0.0560	825	813	0.0552
1000	1019	1010	0.0737	1019	1010	0.0727
Q_{react} (Btu/hr-in)	4.751			4.685		
Q (Btu/hr) / kW	2699 / 0.8			2699 / 0.8		

Fuel Type	MK BW 17x17			WEO 17x17		
T_o (°F)	T_c (°F)	T_{avg} (°F)	k (Btu/hr-in-°F)	T_c (°F)	T_{avg} (°F)	k (Btu/hr-in-°F)
100	170	135	0.0197	173	137	0.0189
200	260	230	0.0230	262	231	0.0223
300	352	326	0.0266	353	327	0.0260
400	445	423	0.0307	445	423	0.0307
500	539	520	0.0354	539	520	0.0354
600	633	617	0.0418	633	617	0.0418
700	729	715	0.0476	729	715	0.0476
800	825	813	0.0552	825	813	0.0552
1000	1020	1010	0.0690	1019	1010	0.0727
Q_{react} (Btu/hr-in)	4.685			4.685		
Q (Btu/hr) / kW	2699 / 0.8			2699 / 0.8		

Transverse Effective Fuel Conductivity for Vacuum Conditions

Fuel Type	WE & WES 15x15			WE 17x17		
T_o (°F)	T_c (°F)	T_{avg} (°F)	k (Btu/hr-in-°F)	T_c (°F)	T_{avg} (°F)	k (Btu/hr-in-°F)
100	272	186	0.0081	275	188	0.0079
200	336	268	0.0103	340	270	0.0099
300	408	354	0.0130	411	356	0.0124
400	486	443	0.0163	489	445	0.0155
500	569	535	0.0203	572	536	0.0192
600	656	628	0.0250	658	629	0.0238
700	746	723	0.0304	748	724	0.0288
800	838	819	0.0368	839	820	0.0354
Q_{react} (Btu/hr-in)	4.685			4.685		
Q (Btu/hr) / kW	2699 / 0.8			2699 / 0.8		

Fuel Type	MK BW 17x17			WEO 17x17		
T_o (°F)	T_c (°F)	T_{avg} (°F)	k (Btu/hr-in-°F)	T_c (°F)	T_{avg} (°F)	k (Btu/hr-in-°F)
100	276	188	0.0078	275	188	0.0079
200	340	270	0.0099	339	270	0.0099
300	412	356	0.0123	410	355	0.0126
400	490	445	0.0153	488	444	0.0157
500	572	536	0.0192	570	535	0.0197
600	659	630	0.0234	657	629	0.0242
700	748	724	0.0288	746	723	0.0300
800	840	820	0.0345	838	819	0.0363
Q_{react} (Btu/hr-in)	4.685			4.685		
Q (Btu/hr) / kW	2699 / 0.8			2699 / 0.8		

Table 4-13 – Continued
Effective Fuel Properties

Axial Effective Fuel Conductivity in Helium or Vacuum

Fuel type	WE & WES 15x15	WE & WEV 17x17	MK BW 17x17	WEO 17x17
No of fuel rods	204	264	264	264
OD fuel rod (in)	0.422	0.374	0.374	0.360
Clad thickness (in)	0.0243	0.0225	0.0240	0.0225
No of guides tubes	20	24	24	24
OD guide tubes (in)	0.484	0.429	0.482	0.429
Wall thickness (in)	0.015	0.016	0.016	0.016
No of Instrument tubes	1	1	1	1
OD Instrument tube (in)	0.545	0.474	0.482	0.474
Wall thickness (in)	0.015	0.015	0.016	0.015

Fuel type	WE & WES 15x15	WE & WEV 17x17	MK BW 17x17	WEO 17x17
Cladding area (in^2)	6.66	7.08	7.55	6.82
Compartment area (in^2)	75.69	75.69	75.69	75.69
Temperature	k-axial	k-axial	k-axial	k-axial
(°F)	(Btu/hr-in-°F)	(Btu/hr-in-°F)	(Btu/hr-in-°F)	(Btu/hr-in-°F)
212	0.0576	0.0612	0.0653	0.0590
392	0.0606	0.0644	0.0687	0.0620
572	0.0644	0.0685	0.0730	0.0659
752	0.0695	0.0739	0.0788	0.0711
932	0.0763	0.0811	0.0865	0.0781
1112	0.0852	0.0905	0.0966	0.0872

Table 4-13 – Continued
Effective Fuel Properties

Effective Fuel Density

Fuel Type	WE & WES 15x15	WE 17x17	MK BW 17x17	WEO 17x17
No of fuel rods	204	264	264	264
OD fuel rod (in)	0.422	0.374	0.374	0.360
Clad thickness (in)	0.0243	0.0225	0.0240	0.0225
No of guides tubes	20	24	24	24
OD guide tubes (in)	0.484	0.429	0.482	0.429
Wall thickness (in)	0.015	0.016	0.016	0.016
No of Instrument tubes	1	1	1	1
OD Instrument tube (in)	0.545	0.474	0.482	0.474
Wall thickness (in)	0.015	0.015	0.016	0.015
Active fuel length (in)	142	144	144	144
Pellet OD (in)	0.3649	0.3225	0.3195	0.3088
Fuel Type	**WE & WES 15x15**	**WE 17x17**	**MK BW 17x17**	**WEO 17x17**
Cladding area (in^2)	6.66	7.08	7.55	6.82
Cladding volume (in^3)	946	1019	1088	982
Pellet area (in^2)	21.33	21.57	21.17	19.77
UO_2 volume (in^3)	3029	3105	3048	2847
ρ eff (lbm/in^3)	0.1325	0.1350	0.1344	0.1248

Effective Specific Heat of Fuel

Fuel Type	WE & WES 15x15	WE 17x17	MK BW 17x17	WEO 17x17
No of fuel rods	204	264	264	264
OD fuel rod (in)	0.422	0.374	0.374	0.360
Clad thickness (in)	0.0243	0.0225	0.0240	0.0225
No of guides tubes	20	24	24	24
OD guide tubes (in)	0.484	0.429	0.482	0.429
Wall thickness (in)	0.015	0.016	0.016	0.016
No of Instrument tubes	1	1	1	1
OD Instrument tube (in)	0.545	0.474	0.482	0.474
Wall thickness (in)	0.015	0.015	0.016	0.015
Active fuel length (in)	142	144	144	144
Pellet OD (in)	0.3649	0.3225	0.3195	0.3088
	WE & WES 15x15	**WE 17x17**	**MK BW 17x17**	**WEO 17x17**
Cladding area (in^2)	6.66	7.08	7.55	6.82
Cladding volume (in^3)	946	1019	1088	982
Pellet area (in^2)	21.33	21.57	21.17	19.77
UO_2 volume (in^3)	3029	3105	3048	2847
Temperature	Cp eff	Cp eff	Cp eff	Cp eff
(°F)	(Btu/lbm-°F)	(Btu/lbm-°F)	(Btu/lbm-°F)	(Btu/lbm-°F)
80	0.0593	0.0594	0.0595	0.0594
260	0.0654	0.0655	0.0656	0.0656
692	0.0726	0.0727	0.0728	0.0727
1502	0.0779	0.0780	0.0782	0.0781

Table 4-13 – Concluded
Effective Fuel Properties for CE 14x14

Transverse Effective Fuel Conductivity in Helium

Fuel Type			**CE 14x14**	
T_o (°F)	T_c (°F)	T_{avg} (°F)	Q_{react} (Btu/hr-in)	k (Btu/hr-in-°F)
100	181	140	19.968	0.0182
225	291	258	19.969	0.0222
350	404	377	19.969	0.0271
475	519	497	19.970	0.0331
600	637	618	19.970	0.0402
725	755	740	19.970	0.0483
850	875	863	19.970	0.0577

Axial Effective Conductivity

Fuel type	**CE 14x14**
No of fuel rods	176
OD fuel rod (in)	0.440
Clad thickness (in)	0.028
No of guide tubes	5
OD guide tubes (in)	1.115
Wall thickness (in)	0.04
No of instrument tubes	---
OD instrument tube (in)	---
Wall thickness (in)	---
Fuel type	**CE 14x14**
Cladding area (in^2)	7.05
Compartment area (in^2)	75.69
Temperature	k-axial
(°F)	(Btu/hr-in-°F)
212	0.0610
392	0.0642
572	0.0682
752	0.0736
932	0.0808

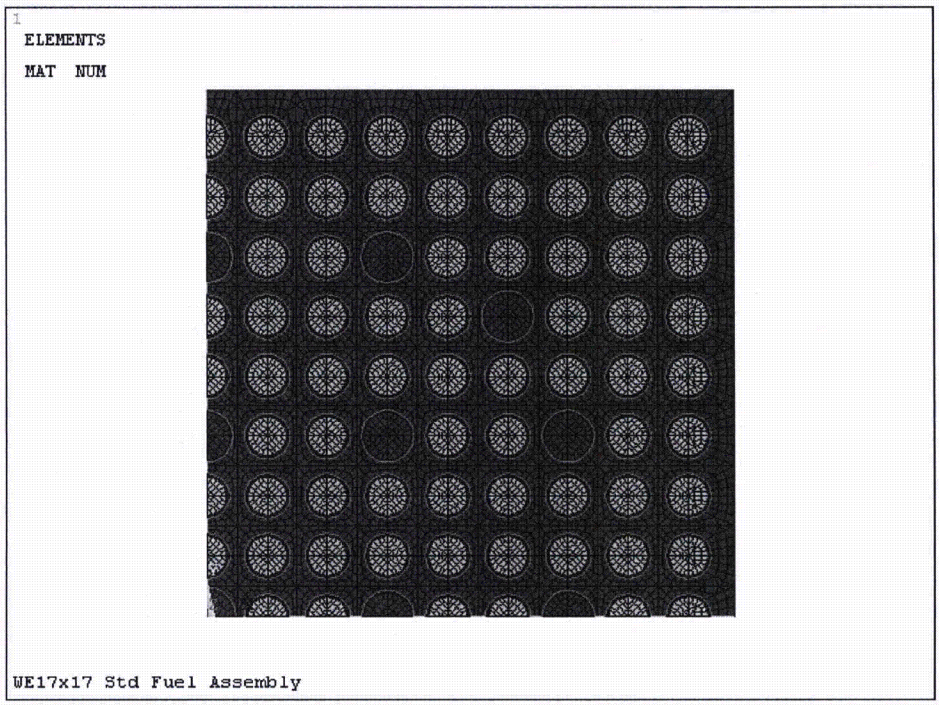

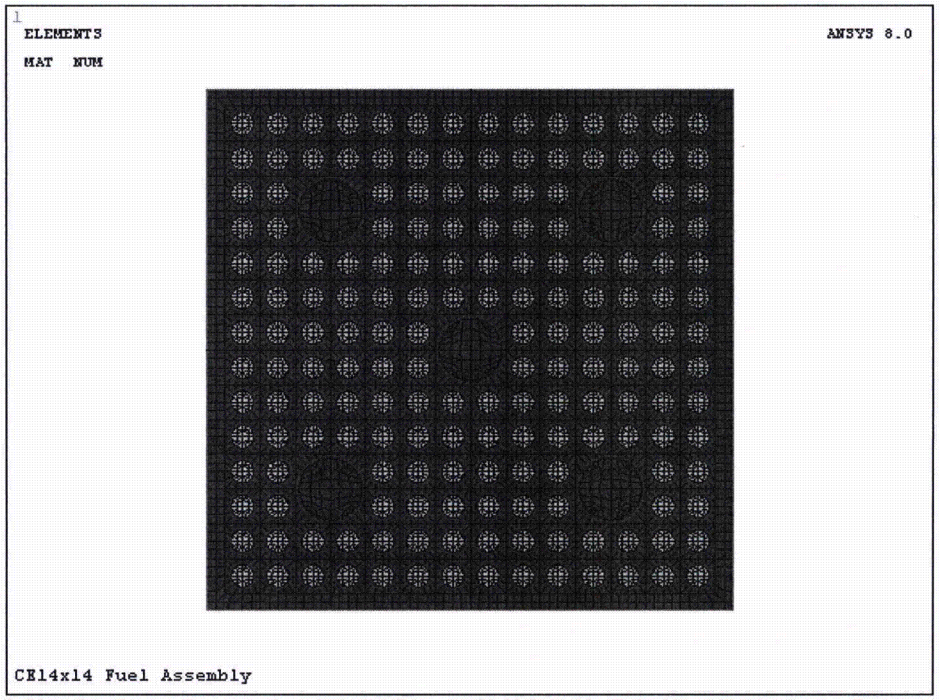

Figure 4-40
Finite Element Model of Fuel Assemblies

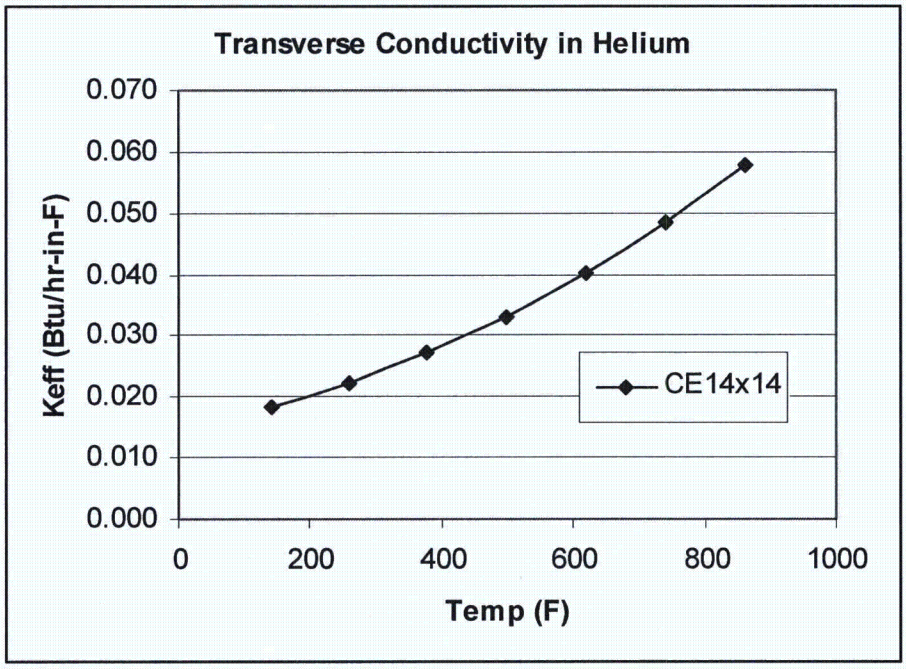

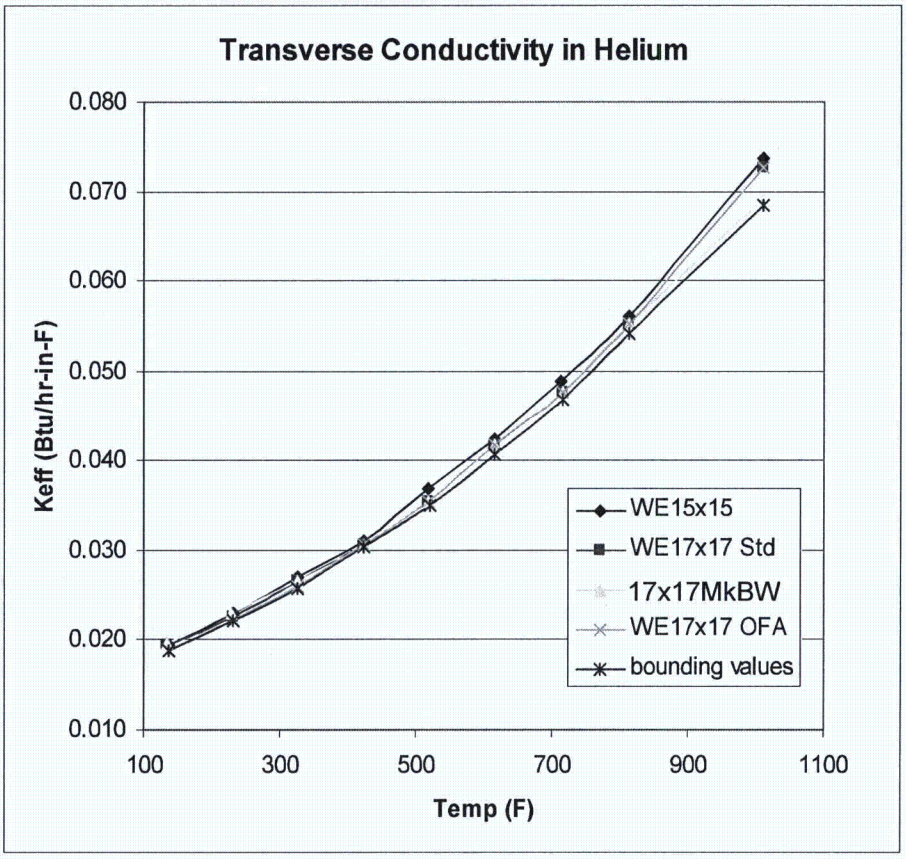

Figure 4-41
Effective Transverse Fuel Conductivity in Helium

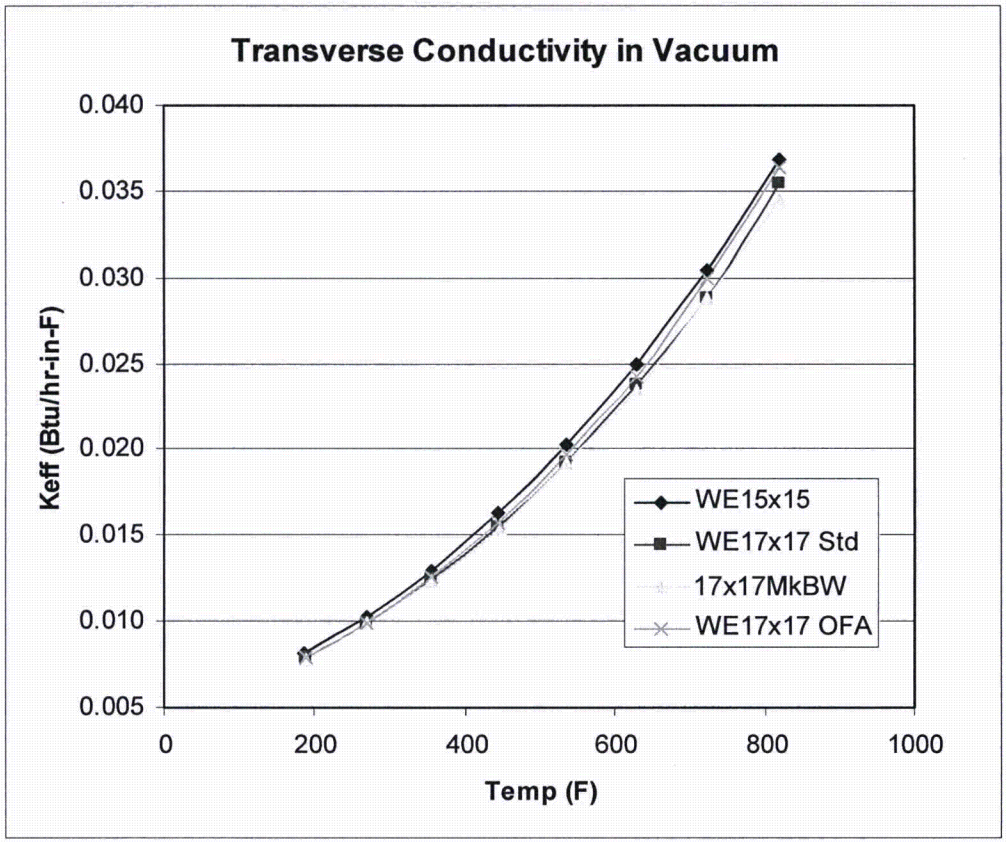

Figure 4-42
Effective Transverse Fuel Conductivity for Vacuum Conditions

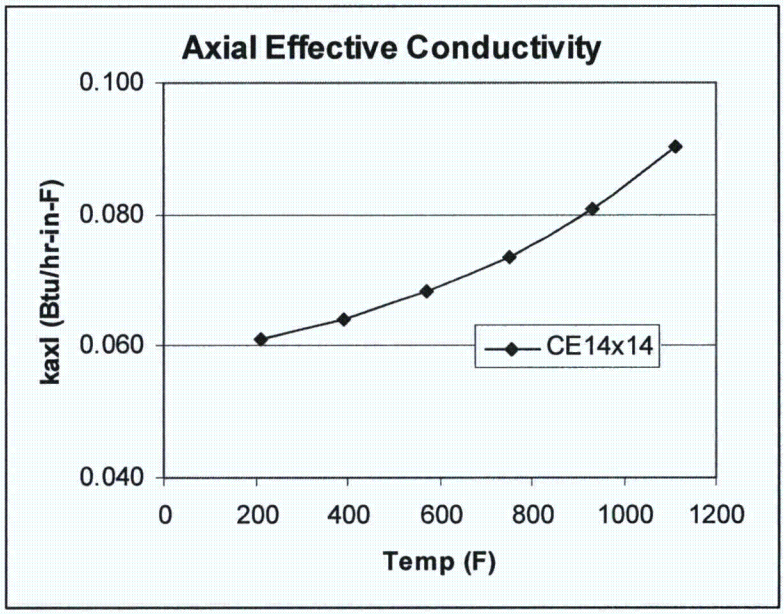

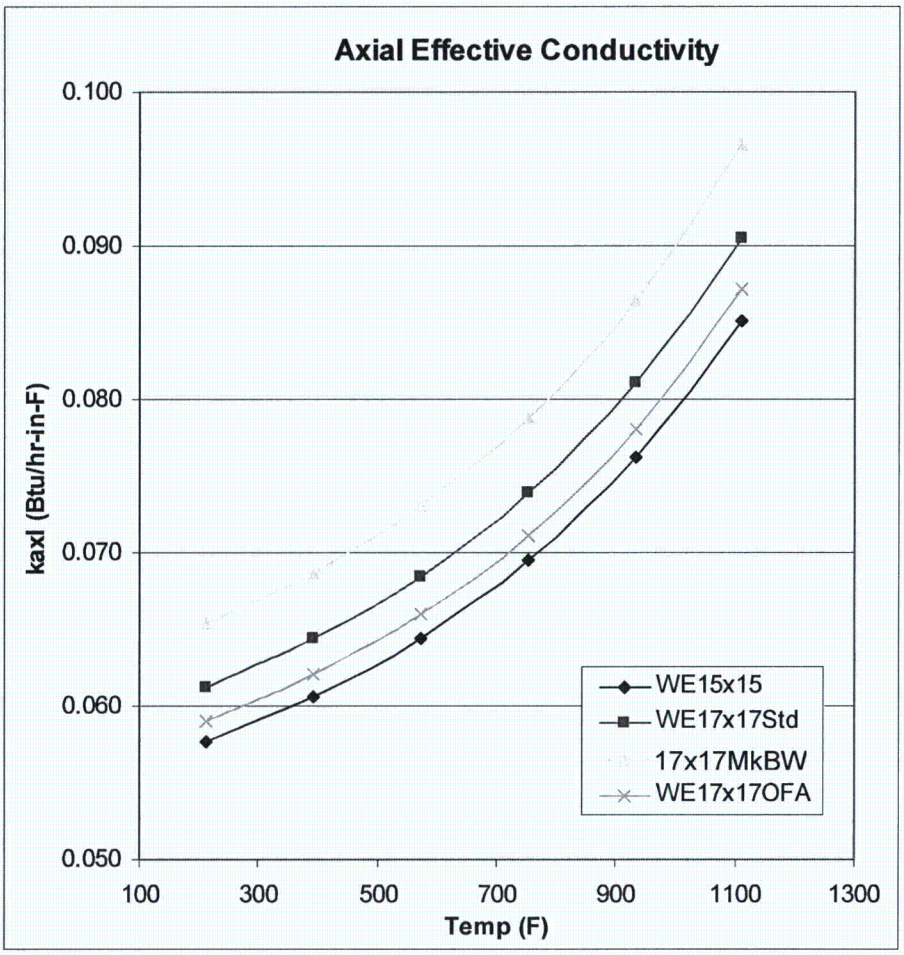

Figure 4-43
Effective Axial Fuel Conductivity

3.4 Thermal Evaluation for Normal Conditions of Transport

The normal conditions of transport are used for determination of the maximum fuel cladding temperature, NUHOMS®-MP197 component temperatures, confinement pressures and thermal stresses. These steady state environmental conditions correspond to the maximum daily averaged ambient temperature of 100 °F and the 10CFR Part 71.71(c) insolation averaged over a 24 hour period.

3.4.1 Thermal Models

The finite element models are developed using the ANSYS computer code [10]. ANSYS is a comprehensive thermal, structural, and fluid flow analysis package. It is a finite element analysis code capable of solving steady-state and transient thermal analysis problems in one, two, and three dimensions. Heat transfer via a combination of conduction, radiation, and convection can be modeled by ANSYS. The three-dimensional geometry of the packaging was modeled. Solid entities were modeled by SOLID70 three-dimensional thermal elements. SURF152 surface effect elements were used for the application of the solar heat load.

Two finite element models are used for the normal conditions of transport evaluation:

- A cask body model to determine temperature distributions within the cask body, impact limiters, and thermal shield.

- A basket model to determine temperature distributions within the DSC and it's contents. This model also includes the helium gap between the DSC and the cask cavity inner surfaces.

The interior nodes of the cask body model line up with the exterior nodes of the basket model. The analysis is performed by first running the cask body model. The temperatures on the inner cavity surfaces are then applied as a boundary condition to the exterior nodes of the basket model. This approach allowed the modeling of sufficient detail within the packaging while keeping the overall size of the individual models reasonable.

3.4.1.1 Cask Body Model

To determine component temperatures within the cask body during normal conditions of transport, a finite element model of the cask body is developed. The three-dimensional model represents a 90° symmetric section of the packaging and includes the geometry and material properties of the impact limiters, thermal shield, the cask body, lead, neutron shielding (resin in aluminum containers), and outer shell.

The neutron shielding consists of 60 long slender resin-filled aluminum containers placed between the cask body and outer stainless steel shell. The aluminum containers are confined between the cask body and outer shell, and butt against the adjacent shells. For conservatism, an air gap of 0.01 in. at thermal equilibrium is assumed to be present between the resin boxes and adjacent shells. Radiation across these gaps is conservatively neglected. The redwood and balsa

within the impact limiters are modeled as an isotropic material containing bounding material properties as described in Section 3.2 for wood.

The finite element plot of the cask body model is shown in Figure 3-1.

Generally, good surface contact is expected between adjacent components. However, to bound the heat conductance uncertainty between adjacent components, the following gaps at thermal equilibrium are assumed:

- 0.0100" radial gaps between resin boxes and adjacent shells
- 0.0300" radial gap between lead and cask body
- 0.0600" radial gap between cask lid and cask body
- 0.0625" axial gap between cask lid and cask body
- 0.0600" radial and axial gaps between ram plate and cask body
- 0.0625" axial gap between rear impact limiter and thermal shield
- 0.0625" axial gap between thermal shield and cask body
- 0.1250" axial gap between front impact limiter and cask body
- 0.0625" axial gap between thermal shield and impact limiter

All heat transfer across the gaps is by gaseous conduction. Other modes of heat transfer are neglected.

Heat Dissipation

Heat is dissipated from the surface of the packaging by a combination of radiation and natural convection.

Heat dissipation by natural convection is described by the following equations for the average Nusselt number [11]:

$$\overline{N}_{u_L} = \overline{H}_c \frac{L}{k} = 0.13(Gr_L Pr)^{1/3} \quad \text{for } Pr\,Gr_L > 10^9 \qquad \text{(Horizontal cylinders and vertical surfaces)}$$

$$\overline{N}_{u_L} = \overline{H}_c \frac{L}{k} = 0.59(Gr_L Pr)^{1/4} \quad \text{for } 10^4 < Pr\,Gr_L < 10^9 \qquad \text{(vertical surfaces)}$$

where,

Gr_L = Grashof number = $\rho^2 g\beta(T_s-T_a)L^3/\mu^2$
ρ = density, lb/ft^3
g = acceleration due to gravity, ft/sec^2
β = temperature coefficient of volume expansion, 1/R
μ = absolute viscosity, lb/ft-sec
L = characteristic length, ft
Pr = Prandtl number
H_c = natural convection coefficient

R_{in} = inner radius of lead cavity @ 70°F= 36.50"
R_{out} = outer radius of lead cavity @ 70°F = 39.75"
L_{cavity} = length of lead cavity @ 70°F = 195.75"

$R_{in,\,620} = (R_{in})(1+(\alpha_{CS})(\Delta T)) = (36.50)[1+(7.44E\text{-}6)(550)] = 36.6494"$

$R_{out,\,620} = (R_{out})(1+(\alpha_{CS})(\Delta T)) = (39.75)[1+(7.44E\text{-}6)(550)] = 39.9127"$

$L_{cavity,\,620} = (L_{cavity})(1+(\alpha_{CS})(\Delta T)) = (195.75)[1+(7.44E\text{-}6)(550)] = 196.5510"$

$V_{cavity} = V_{lead} = (\pi)(R_{out,620}^2 - R_{in,620}^2)(L_{cavity,\,620}) = 154{,}274.9\ in^3$

$M_{lead} = (V_{lead})(\rho_{lead}) = (154{,}274.9\ in^3)(0.3978\ lbm/in^3) = 61{,}363.6\ lbm$

Determination of Lead Gap

α_{CS} = 7.02 x 10^{-6} in/in-°F @ 360°F (via linear interpolation from expansion coefficients table, above)

$\alpha_{lead,\,620}$ = 20.39 x 10^{-6} in/in-°F @ 620°F (from expansion coefficients table, above)

$\alpha_{lead,\,360}$ = 17.83 x 10^{-6} in/in-°F @ 360°F (via linear interpolation from expansion coefficients table, above)

ρ_{lead} = 0.4037 lbm/in^3 at 360°F, via linear interpolation from lead density table, above)

$R_{in,\,cs,\,360} = (R_{in})(1+(\alpha_{CS})(\Delta T)) = (36.50)[1+(7.02E\text{-}6)(290)] = 36.5743"$

$R_{out,\,cs,\,360} = (R_{out})(1+(\alpha_{CS})(\Delta T)) = (39.75)[1+(7.02E\text{-}6)(290)] = 39.8309"$

$L_{lead,\,360} = (L_{cavity,\,620})/(1+(\alpha_{lead,620})(620-70))*(1+(\alpha_{lead,620})(360-70)) =$

$(196.5510) / [1+(20.39E\text{-}6)(550)] * [1+(17.83E\text{-}6)(290)] = 195.3764"$

$V_{lead,\,360} = M_{lead} / \rho_{lead} = 61{,}363.6 / 0.4037 = 152{,}004.6\ in^3$

Since $R_{in,cs,360} = R_{in,lead,360}$, then :

$V_{lead,360} = (\pi)(R_{out,\,lead,360}^2 - R_{in,\,ss,\,360}^2)(L_{lead,\,360})$

It gives:

$R_{out,lead,360} = 39.8162"$

Air gap = $R_{out,cs,360} - R_{out,\,lead,360} = 39.8309 - 39.8162 = 0.0147"$

The assumed air gap of 0.025" is larger than the above calculated gap. Therefore, using a gap of 0.025" is conservative to maximize the DSC shell temperature.

A.3.6.7.2 Gap between Finned Aluminum Shell and Cask Shield Shell

An air gap of 0.01" is considered in the model between the cask shield shell (SA-516-70) and the finned aluminum shell (Al 6061) for the MP197HB cask with over 26 kW

heat load. The following calculation shows that the modeled gap of 0.01" is adequate to bound the existing contact resistance between these two shells.

Yovanovich suggests the following approach in [38] to calculate the thermal contact conductance.

$$h_j = h_c + h_g \qquad \text{(A.1)}$$

h_j = total thermal contact conductance (m^2-K/W)
h_c = contact conductance (m^2-K/W)
h_g = gap conductance (m^2-K/W)

The thermal contact resistance is:

$$R_j = 1/h_j \qquad \text{(A.2)}$$

The contact conductance, h_c, is given in [38] by:

$$h_c = 1.25\, k_s \frac{m}{\sigma}\left(\frac{P}{H_c}\right)^{0.95} \qquad \text{(A.3)}$$

Where

$k_s = 2\,k_1\,k_2\,/(k_1 + k_2)$ Harmonic mean thermal conductivity of interface (W/m-K)

$m = \sqrt{m_1^{\,2} + m_2^{\,2}}$ Effective mean absolute asperity slope of interface

$\sigma = \sqrt{\sigma_1^{\,2} + \sigma_2^{\,2}}$ Effective RMS surface roughness of contacting asperities (m)

P = Contact pressure (MPa)
H_c = Microhardness of the softer of the two contacting solids (MPa) = $H_{C,Al}$ in this evaluation

The mean absolute asperity slope for each plate can be approximated by the following correlation from [38]:

$$m_i = 0.125\left(\sigma_i \times 10^{-6}\right)^{0.402} \quad \text{for } 0.216\,\mu m \le \sigma \le 9.6\,\mu m \qquad \text{(A.4)}$$

As seen in equation (A.3), the contact conductance, h_c, depends heavily on the contact pressure, P. Assuming a very small contact pressure of 10^{-6} psi, gives a negligible contact conductance, h_c and eliminates this term in calculation of the total thermal contact conductance in equation (A.1).

A contact pressure of 10^{-6} psi is equivalent to having no friction between the two shells, which is very conservative.

Due to elimination of h_c in equation (A.1), the conductivities of the contacting plates are not required for this calculation.

The gap conductance, h_g, is given in [38] by:

$$h_g = k_g\,/(Y + M) \qquad \text{(A.5)}$$

Where
k_g = thermal conductivity of the gap substance (W/m-K)

Y = effective gap thickness (m)
M = gas parameter (m)

Based on [38], the effective gap thickness, Y, shown in the figure below, can be calculated as follows:

$$Y = 1.53\,\sigma\,(P / H_c)^{-0.097} \qquad \text{for } 10^{-5} < P/H_c < 2\text{x}10^{-2} \qquad \text{(A.6)}$$

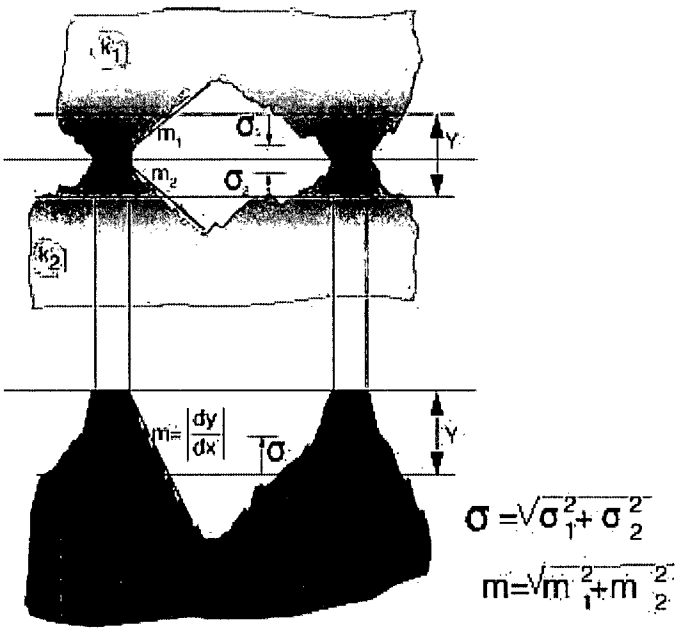

Conforming Rough Surfaces [38]

The gas parameter M accounts for the rarefaction effects at high temperatures and low gas pressure. This gas-surface parameter depends on the thermal accommodation coefficients, the ratio of specific heats, the Prandtl number, and the molecular mean free-path of the gas. This complex gas-surface parameter depends on gas pressure and temperature according to the following relationship:

$$M = M_0 \frac{T}{T_0} \frac{P_{g,0}}{P_g} \qquad \text{(A.7)}$$

Where M_0 denotes the gas parameter value at the reference values of gas temperature and pressure, T_0 and $P_{g,0}$, respectively. T and P_g are temperature and pressure of the contact gas. The gas parameter for air is 0.373x10-6 m at 50°C and 1 atm, as reported in [38].

An operating temperature of 200°F (378K) is considered for T and k_g in equations (A.5) and (A.7). The assumed operating temperature is well below the cask shield shell and the finned aluminum shell temperatures in Table A.3–11 and is therefore conservative.

A pressure of 1 atm is considered for air between the two shells.

Based on data in Section A.3.2.1, material # 16, the air conductivity is 0.0015 Btu/hr-in-°F or 0.031 W/m-K at 200°F.

The following data is considered for roughness and hardness of the shells.

Surface Properties for Aluminum and Stainless Steel Plates

Material	Roughness (μm)	Hardness	Microhardness (1) (MPa)
Aluminum	0.2 to 6.3 [39]	25 to 95 Brinell 500kg [40]	440 to 1079
SA 203, Gr. E	0.2 to 6.3 [39]	(2)	---

Notes:
(1) For conversion of roughness units see reference [42]
(2) Based on [38], the hardness of the softer plate, aluminum here, is taken for evaluation.

Surface roughness is mainly determined by the production method. The roughness values in the above table correspond to average values for cold rolling / drawing process.

The contact resistances are calculated based on the average roughness and hardness are listed below.

σ_{Al} = 3.25 μm, $H_{c,Al}$ = 760 MPa
σ_{CS} = 3.25 μm

The calculated contact resistance between cask shield shell and finned aluminum shell is 2.7E-3 m^2-K/W as listed in the following table.

Contact Resistances between Shield Shell and Finned Aluminum Shell

Contact Type	Al / SA203
σ (μm)	4.60E-06
P (MPa)	6.891E-09
H_c (MPa)	760
P_g (atm)	1.0
T (K)	378
k_g (W/m-K)	0.031
P/H_c	9.073E-12
Y (μm)	8.283E-05
M (μm)	4.361E-07
h_c (W/m^2-K)	0.00
h_g (W/m^2-K)	374
h_j (W/m^2-K)	374
R_j (m^2-K/W)	2.7E-03

The equivalent thermal resistance for the air gaps across the shells considered in the MP197HB is:

$$R_{j,\mathrm{model}} = \frac{\Delta x_{gap}}{k_g} \qquad \text{(A.8)}$$

Δx_{gap} = 0.01" = 2.54E-4 m

$$R_{j,model} = \frac{2.54E-4}{0.031} = 8.2E-3 \text{ m}^2\text{-K/W}$$

The above thermal resistance considered in the model ($R_{j,model}$) is about three times larger than the calculated contact resistances (R_j) between cask shield shell and finned aluminum shell. This indicates that the air gap of 0.01" considered in the model is more than adequate to bound the contact resistance between the cask shield shell and the finned aluminum shell.

A.3.6.7.3 Gap between Basket Outer Surface and DSC Shell Inner Surface in the 69BTH DSC Model

Based on the drawings in Chapter A.1, Appendix A.1.4.10, a nominal diametrical cold gap of 0.40" is considered between the basket and the canister shell for the 69BTH DSC. The nominal canister inner diameter (ID) of the 69BTH DSC is 68.75". The nominal basket outer diameter (OD) is then 68.35".

To calculate the minimum gap, the average temperatures for the basket, aluminum rails, and DSC shell at the hottest cross section for NCT at 100°F ambient are required to calculate the thermal expansion at thermal equilibrium. These temperatures are retrieved from the 69BTH DSC/basket model described in Section A.3.3.1.4. These average temperatures are listed in the following table.

Average Temperatures at Hottest Cross Section for 69BTH Basket

Component	HLZC#1, 26kW NCT at 100°F T_{avg} (°F)	HLZC#4, 32kW NCT at 100°F T_{avg} (°F)
Basket (compartments & wrap plates only)	547	547
Al Rail @ 0 degree	472	504
Al Rail @ 180 degree	398	421
DSC Shell	388	408

The hot dimensions of the basket OD and DSC ID are calculated as follows.

The outer diameter of the hot basket is:

$$OD_{B,hot} = OD_B + [L_{SS,B} \times \alpha_{SS,B} (T_{avg,B} - T_{ref})] + L_{Rail} \times [\alpha_{Al,0} (T_{avg,R0} - T_{ref}) + \alpha_{Al,180} (T_{avg,R180} - T_{ref})]$$

Where:

$OD_{B,hot}$ = hot OD of the basket

OD_B = nominal cold OD of the basket
= 68.75" – 0.40" = 68.35"

$L_{SS,B}$ = width of basket at 0-180 direction
= 9 × compartment width +
9 × 2 × compartment plate +
6 × Al/Poison within nine-compartment blocks +
2 × Al/Poison between nine-compartment blocks +
6 × wrap plate

$= 9 \times 6 + 9 \times 2 \times 0.165 + 6 \times 0.25 + 2 \times 0.375 + 6 \times 0.105 = 59.85$"

L_{Al} = width of aluminum rail = $(OD_B - L_{SS,B})/2 = 4.25$"

$\alpha_{SS,B}$ = Average stainless steel axial coefficient of thermal expansion (interpolated using data in [10], in/in-°F)

α_{Al} = Average aluminum coefficient of thermal expansion (interpolated using data in [10], in/in-°F)

$T_{avg,B}$ = Average basket temperature at the hottest cross section, see table above, (°F)

$T_{avg,R0}$ = Average Al rail temperature at the hottest cross section at 0 degree orientation, see table above, (°F)

$T_{avg,R180}$ = Average Al rail temperature at the hottest cross section at 180 degree orientation, see table above, (°F)

T_{ref} = reference temperature for stainless steel and aluminum alloys = 70°F [10]

The inner diameter of the hot DSC shell is:

$ID_{DSC,hot} = ID_{DSC} [1 + \alpha_{SS,DSC} (T_{avg,DSC} - T_{ref})]$

Where:

$ID_{DSC,hot}$ = Hot ID of DSC shell

ID_{DSC} = Cold ID of DSC shell = 68.75"

$\alpha_{SS,DSC}$ = Average stainless steel axial coefficient of thermal expansion (interpolated using data in [10], in/in-°F)

$T_{avg,DSC}$ = Average DSC shell temperature at hottest cross section, see above table, (°F)

T_{ref} = Reference temperature for low alloy steel = 70°F [10]

The diametrical hot gap between the basket and cask inner shell is:

$G_{hot} = ID_{DSC,hot} - OD_{B,hot}$

The diametrical hot gap at the hottest cross section is calculated for 26kW (HLZC#1) and 32 kW ((HLZC#4) heat loads in the 69BTH basket to bound the problem. The calculated hot gaps are listed below.

Diametrical Hot Gaps for 69BTH Basket

26kW, HLZC # 1					
	Cold dimension	Temp	$\alpha x10^{-6}$ (1)	ΔL	Hot dimension
	(in)	(°F)	(in/in/°F)	(in)	(in)
Basket width	59.85	547	9.747	0.278	60.128
Large rail @ 0°	4.25	472	13.844	0.024	4.274
Large rail @ 180°	4.25	398	13.592	0.019	4.269
Basket OD	68.35				68.671
DSC ID	68.75	388	9.464	0.207	68.957
Gap	0.4				**0.286**

32kW, HLZC # 4					
	Cold dimension	Temp	$\alpha x10^{-6}$ (1)	ΔL	Hot dimension
	(in)	(°F)	(in/in/°F)	(in)	(in)
Basket width	59.85	547	9.747	0.278	60.128
Large rail @ 0°	4.25	504	13.916	0.026	4.276
Large rail @ 180°	4.25	421	13.684	0.020	4.270
Basket OD	68.35				68.674
DSC ID	68.75	408	9.516	0.221	68.971
Gap	0.4				**0.297**

Note:
(1) The average thermal expansion coefficient is calculated by interpolation using data in [10].

A uniform diametrical hot gap of 0.30" is considered in the model between the basket and the DSC shell for the 69BTH DSC. This assumption is conservative since the hot gaps shown in the above table are smaller than the assumed gap of 0.3".

A.3.6.7.4 Contact Resistance across Paired Aluminum and Poison Plates in 69BTH Basket

The 0.01" gaps considered on both sides of the paired aluminum and poison plates account for all the thermal resistance across the paired plates. Dividing the thermal resistance into three separate resistances would only change the temperature distribution between the two paired plates without changing the overall thermal resistance. The temperature distribution among the paired aluminum and poison plates are of no particular significance.

The following calculation shows that the modeled gaps (0.01") on both sides of the paired aluminum and poison plates are adequate to bound the existing contact resistances.

According to the basket configuration, three contact resistances are recognizable for the paired aluminum/poison plates sandwiched between the fuel compartments or wrap plates:

a) contact resistance between the aluminum plate and the stainless steel fuel compartment or wrap plates

b) contact resistance between the aluminum plate and the poison plate

c) contact resistance between the poison plate and the stainless steel fuel compartment or wrap plate

These contact resistances are shown schematically in the following figure.

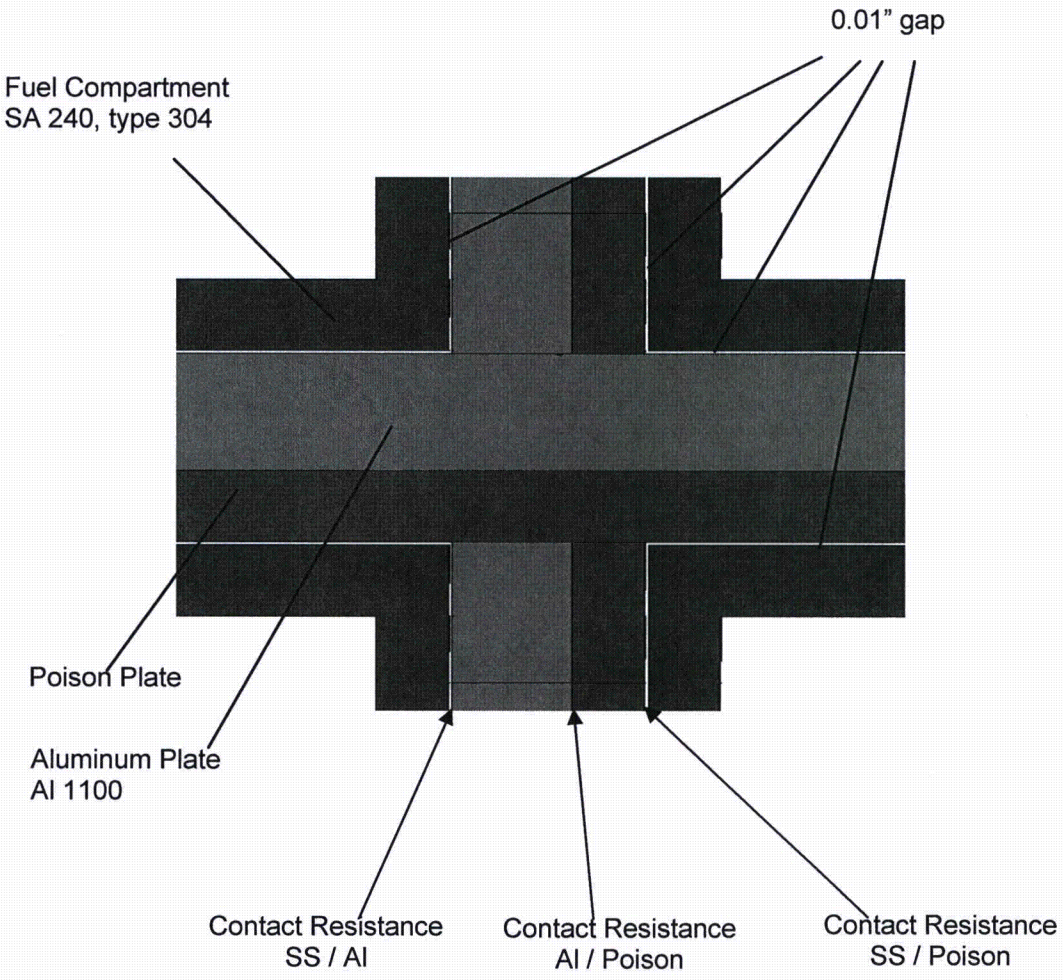

Location of Contact Resistances

The contact resistances between the components shown in the above figure are calculated using the same methodology as the one described in Section A.3.6.7.2.

The gas parameter for helium is 2.05×10^{-6} m at 50°C and 1 atm, as reported in reference [38].

The thermal contact resistance is:

$R_j = 1/h_j$

Based on the location of the contact resistances shown in the above figure, the total thermal contact resistance for the paired plates is:

$$R_{j,plates} = R_{j,SS-Al} + R_{j,Al-Poison} + R_{j,poison-SS}$$

$R_{j,ss\text{-}Al}$ = contact resistance between stainless steel and aluminum plates
$R_{j,Al\text{-}Poison}$ = contact resistance between aluminum and poison plates
$R_{j,Poison\text{-}SSl}$ = contact resistance between poison and stainless steel plates

An operating temperature of 400°F (204°C) is considered for conductivity of helium. The assumed operating temperature is well below the average basket temperature at the hottest cross section shown in Section A.3.6.7.3 and is therefore conservative.

A moderate gas pressure (Pg) of 5 psig (1.34 abs atm), lower than the normal operating pressures listed in Table A.3–23, is considered to evaluate the contact resistances.

Based on data in Section A.3.2.1, material # 15, the helium conductivity is 9.84E-3 Btu/hr-in-°F or 0.204 W/m-K at 400°F. The following data is considered for roughness and hardness of the plates.

Surface Properties for Aluminum and Stainless Steel Plates

Material	Roughness (μm)	Hardness	Microhardness [1] (MPa)
Aluminum 1100/ Poison Plate	0.2 to 6.3 [39]	25 to 95 Brinell 500kg [40]	440 to 1079
SA 240, type 304	0.2 to 6.3 [39]	92 Rockwell B [41], Table 2	1960 to 2000

Note: [1] For conversion of roughness units see reference [42]

Surface roughness is mainly determined by the production method. The roughness values in the above table correspond to average values for cold rolling / drawing process. The hardness values are collected for aluminum alloys 6063 and 6061, which are the closest to aluminum alloy 1100.

The contact resistances calculated based on the average roughness and hardness are:

σ_{Al} = 3.25 μm, $H_{c,Al}$ = 760 MPa
σ_{poison} = 3.25 μm, $H_{c,poison}$ = 760 MPa
σ_{SS} = 3.25 μm, $H_{c,SS}$ = 1980 MPa

The calculated contact resistances are listed in the following table.

Contact Resistances between Plates in 69BTH Basket

Contact Type	Al / Poison	SS / Al or SS/ Poison
σ (m)	4.60E-06	4.60E-06
P (MPa)	6.891E-09	6.891E-09
H_c (MPa)	760	760
P_g (atm)	1.34	1.34
T (K)	478	478
k_g (W/m-K)	0.204	0.204
P/H_c	9.073E-12	9.073E-12
Y (m)	8.283E-05	8.283E-05
M (m)	2.262E-06	2.262E-06
h_c (W/m^2-K)	0.00	0.00
h_g (W/m^2-K)	2402	2402
h_j (W/m^2-K)	2402	2402
R_j (m^2-K/W)	4.164E-04	4.164E-04

The total thermal contact resistance across the plates is:

$$R_{j,total} = 3 \times 4.164E-4 = 1.249E-3 \text{ m}^2\text{-K/W}$$

The equivalent thermal resistance for the helium gaps across the plates considered in the 69BTH basket model is:

Δx_{He} = 2 × 0.01" = 0.02" = 5.08E-4 m (total gap thickness across plates)

$$R_{j,model} = \frac{\Delta x_{He}}{k_g}$$

$$R_{j,model} = \frac{5.08E-4}{0.204} = 2.486E-3 \text{ m}^2\text{-K/W}$$

The total thermal resistance considered in the model ($R_{j,model}$) is about two times larger than the calculated contact resistances for the paired plates ($R_{j,total}$). This shows that the gaps considered in the model are more than adequate to bound the contact resistances and the other uncertainties, such as thickness tolerances, surface finishing, etc., involved in fabrication of the basket.

If the poison plate is paired with multiple aluminum plates, the total thermal contact resistance across the plates depends on the number of aluminum plates as follows.

$$R_{j,multiple} = R_{j,SS-Al} + (m-1)R_{j,Al-Al} + R_{j,Al-Poison} + R_{j,poison-SS}$$

m = number of aluminum plates used to pair with poison plate

According to the table of the contact resistances, the contact resistances between Al/SS, Al/Al, and Al/poison plates are equal if the contact pressure nears zero. The total thermal resistance for multiple aluminum plates is therefore:

$$R_{j,multiple} = (n+1)R_{j,Al-Al}$$

n = number of multiple aluminum plates including poison plate

The maximum number of multiple aluminum plates that can be used in 69BTH basket can be calculated by setting $R_{j,multiple}$ in the above equation equal to the total thermal resistance considered in the model, $R_{j,model}$.

$$n_{max} = \frac{R_{j,model}}{R_{j,Al-Al}} - 1$$

$$n_{max} = \frac{2.486E-3}{4.164E-4} - 1 = 4.97$$

This shows that at least four plates, three aluminum plates and one poison plate can be paired together in 69BTH basket without affecting the thermal performance evaluated in this calculation.

A.3.6.8 Sensitivity Study for Effects of Fire Emissivity

A fire emissivity (ε_f) of 0.9 was considered in Section A.3.4.2 to calculate the fire radiation heat transfer coefficient ($h_{r,fire}$). Assuming conservatively, the fire as a black body, an emissivity of 1.0 can be considered for the fire. The effect of this assumption is enveloped for the MP197HB TC in a sensitivity analysis in this section considering the maximum heat load of 32 kW with the external fins installed on the shield shell. The only change is the increase of the fire emissivity (ε_f) from 0.9 to 1.0 in the input file for running the finned TC under HAC. The maximum component temperatures from the sensitivity run with ε_f=1.0 are shown in the following table.

Maximum Component Temperatures for ε_f = 1.0

DSC type	69BTH DSC, with 32 kW heat load, Finned MP197HB TC, ε_f = 1.0			
Component	Time (hr)	T_{max} (°F)	T_∞ (°F)[2]	Limit (°F)
DSC shell	7.0	512	[3]	---
DSC shell at mid-length[1]	7.0	512	[3]	---
Cask inner shell	1.9	497	400	---
Gamma shield	0.5	571	399	621 [5]
Outer shell	0.5	720	382	---
Shield shell	0.5	1440	335	---
Cask lid	13.0	315	309	---
Cask bottom plate	1.0	416	383	---
Cask lid seal	10.0	323	314	400 [18, 19]
Vent & test seal at top	13.0	313	308	400 [18, 19]
Ram plate seal	1.9	380	377	400 [18, 19]
Test seal at bottom	13.0	382	377	400 [18, 19]
Drain port seal at bottom	10.0	388	381	400 [18, 19]
Helium in TC cavity	4.0	389	380	---

Notes:

[1] This value is the maximum DSC shell temperature in the region where the fuel assemblies have the maximum peaking factor.

[2] These values are retrieved from the transient model at 27.0 hrs after the end of the fire accident. Based on the time-temperature histories for the original TC model shown in Figure A.3-40 through Figure A.3-42, the steady state temperatures are bounded by these temperatures.

[3] Due to the adiabatic boundary conditions considered conservatively for the steady state cool-down runs (described in Section A.3.4.2), the maximum DSC shell temperature at the end of the transient run remains bounded by the steady state temperature of 537°F reported for the 69BTH DSC with 32kW heat load in Table A.3-17.

J.4 Thermal Evaluation

J.4.1 Discussion

The fuel qualification tables for the PWR fuel were adjusted for the inclusion of BPRAs, which generate a small amount of heat during transfer and storage in the NUHOMS® system. No recalculation of any thermal analysis was necessary to qualify the BPRAs as discussed in the following subsections. However, the pressure analysis is amended to analyze the BPRAs, which add gas during normal, off-normal, and accident conditions. The pressure analysis assumes intact BPRAs are loaded into the DSC. Failed BPRAs loaded in the DSC will have less available gas for release, therefore reducing the internal DSC pressures as compared to the case with intact BPRAs.

J.4.2 Summary of Thermal Properties of Materials

The only thermal property potentially affected by the addition of BPRAs is the effective conductivity of the fuel assemblies used in the thermal analysis. The effect of the addition of BPRAs will slightly increase the effective conductivity due to the addition of conduction paths and surface area available for radiation; however, no credit is taken for their presence.

J.4.3 Technical Specifications of Components

Refer to Section J.5 for the type of BPRA assemblies being considered. The BPRA assemblies generate a maximum 8 watts per BPRA of heat during transfer and storage operations in the NUHOMS® system, as calculated in Section J.5 of this appendix.

J.4.4 Thermal Evaluation for Normal and Off-Normal Conditions

Decay Heat

The addition of the BPRA components adds a small amount of decay heat to the fuel assemblies, which needs to be addressed. The maximum heat generation of the BPRA components is calculated to be 8 watts, as described in Section J.5.2. A new fuel qualification table (Table *1-2c of Fuel Specification 1.2.1*) has been added to address the addition of the heat generated by the BPRAs. The same methodology as presented in Chapter 8 of the SAR is used. The total decay heat of each assembly is taken to be that generated by the fuel plus the decay heat generated by the BPRAs. The criteria for fuel cladding temperature limit remains the same, but the allowable decay heat from the fueled rods in an assembly is reduced by 8 watts to accommodate the BPRAs. Therefore, the results from Chapter 8 of the SAR for normal and off-normal conditions remain valid for the maximum design basis decay heat of 1 kW per assembly, including the BPRA contribution.

Pressure Evaluation

The BPRAs generate Helium gas during reactor operation. Therefore, an evaluation of the impact on the existing DSC internal pressure calculations was performed. The B&W BPRA initially contains 22.3 lbs. of an aluminum oxide (Al_2O_3) composite. This composite contains 4 w/o Boron, of which 18.16 w/o is B-10. If, conservatively, 100% of the B-10 is assumed to react to generate Helium, this corresponds to the amount of Helium generation calculated below. There are 10 grams per mole of B-10 [J-8].

$$n_{B\text{-}10} = 22.3\,lbs \cdot 453.6\frac{g}{lbs} \cdot 0.04 \cdot 0.1816 \cdot \frac{1\,gmole}{10\,g} \cdot = 7.35\,gmoles$$

Conservatively, 30% of this Helium gas is assumed to be released into the BPRA rod void volume and is available for release into the DSC cavity in the case of BPRA rod rupture. Therefore, the total number of gas moles that are generated and released into the BPRA rod void volume is 24*7.35*0.3 = 52.9 gmoles. In addition, the BPRA rods are prepressurized with helium to one atmosphere. The void volume in each BPRA rod is 3.55 in^3. Assuming there are 24 BPRAs per DSC with 16 rods each, the total number of initial fill gas (Helium) moles is calculated below.

$$n_{He} = \frac{(14.7\,psia)(6894.8\,Pa/psi)(24 \cdot 16 \cdot 3.55\,in^3)(1.6387 \times 10^{-5}\,m^3/in^3)}{(8.314\,J/g\,mol \cdot K)(293.15\,K)} \cdot \frac{kg/m \cdot s^2}{Pa} \cdot \frac{J}{kg \cdot m^2/s^2}$$

$$= 0.93\,g\,moles$$

Therefore, the total number of gas moles per 24 B&W BPRAs is 52.9 + 0.93 = 53.8 gmoles.

For the Westinghouse 17x17 BPRA the total Helium released into the BPRA rodlet void volume is 2e-4 lb-moles, or 0.0907 gmoles per rodlet. The total Helium gas generated and released for 24 BPRA assemblies assuming the maximum 24 rodlets per BPRA assembly is 24*24*0.0907 = 52.2 gmoles. Thus, the B&W 15x15 BPRAs bound the WE 17x17 BPRAs for the DSC internal pressure calculations.

For normal and off-normal conditions, 1% and 10% release of the Helium gas from the BPRAs into the DSC cavity is assumed similar to the fuel assembly rods, as shown in Table J.4–1.

Thermal Expansion

As described in FSAR section 8.1.1.3B, adequate space is provided in the 24P standard DSC cavity between the basket assembly and the shield plug assemblies for free thermal expansion. To verify that for the 24P long cavity DSC adequate provision for free axial

J.14 References

J-1 "Characteristics of Potential Repository Wastes," DOE/RW-0184/R1," Office of Civilian Radioactive Waste Management, July 1992.

J-2 "ORIGEN2.1 – Isotope Generation and Depletion Code – Matrix Exponential Method," CCC-371, Oak Ridge National Laboratory, RSIC Computer Code Collection, File Number QA040.208.0002, August 1991.

J-3 Ludwig, S.B., and J.P. Renier, "Standard- and Extended-Burnup PWR and BWR Reactor Models for the ORIGEN2 Computer Code," ORNL/TM-11018 Oak Ridge National Laboratory, December 1989.

J-4 Oak Ridge National Laboratory, RSIC Computer Code Collection, "SCALE: A Modular Code System for Performing Standardized Computer Analysis for Licensing Evaluations for Workstations and Personal Computers," NUREG/CR-0200, Revision 6, ORNL/NUREG/CSD-2/V2/R6. (SCALE 4.4)

J-5 "Characteristics of Potential Repository Wastes," Department of Energy, Office of Civilian Radioactive Waste Management, DOE/RW-0184-R1, July, 1992.

J-6 "Domestic Light Water Reactor Fuel Design Evolution, Volume III," Nuclear Assurance Corporation, September, 1981, DOE/ET/47912-3.

J-7 Roddy, J.W., et.al., "Physical and Decay Characteristics of Commercial LWR Spent Fuel," Oak Ridge National Laboratory October, 1985, ORNL/TM-9591/V1.

J-8 Nuclides and Isotopes, Chart of the Nuclides, 15th Edition, GE Nuclear Energy, 1996.

J-9 Verification and Validation Document SCALE4.4PC: CSAS26X and CSAS26, Transnuclear West Document SCALE4.4PCk-QA, Rev. 1, 6/15/99, Document No. QA040.223.0001.

M.4.2 Summary of Thermal Properties of Materials

The analyses use interpolated values where appropriate for intermediate temperatures. The interpolation assumes a linear relationship between the reported values. The use of linear interpolation between temperature values in the tables for determining intermediate value of property is justified by the near-linear behavior as a function of temperature for the range of interest.

The emissivity of stainless steel is 0.587 [4.7]. For additional conservatism an emissivity of 0.46 for stainless steel is used for the basket steel plates in the analysis. The emissivity values assumed in the analysis for the aluminum sheets (Type 1100) and aluminum based neutron poison plates is 0.85 which is achieved by either anodizing or other processes. The emissivity of the oxidized Zircaloy surface is 0.8 [4.14]. Emissivity for the aluminum rail material (Type 6061) is not required for the analysis because radiation between the rails and the DSC shell is conservatively neglected in the analysis. For the two alternate basket configuration shown in Figure M.4-22, a minimum emissivity value of 0.8 is assumed for the neutron poison plates.

The tables below provide the thermal properties of materials used in the analysis of the NUHOMS®-32PT DSC.

1. PWR Fuel with Helium Backfill

The effective thermal conductivity is the lowest calculated value for the various PWR fuel assembly types that may be stored in this DSC and corresponds to the WE 14x14 PWR assembly. Section M.4.8 presents the calculations that determined WE 14x14 to be the fuel assembly with the lowest effective thermal conductivity in both helium and vacuum environment.

Temperature (°F)	K (Btu/min-in-°F)	ρ (lb_m/in^3)	T (°F)	C_p (Btu/lb_m-°F)
Fuel in Helium, Transverse [Section M.4.8]				
138	2.894E-04	0.1166	80	0.0592
233	3.317E-04		260	0.0654
328	3.968E-04		692	0.0725
423	4.744E-04		1502	0.0778
519	5.668E-04			
616	6.715E-04			
714	7.879E-04			
812	9.208E-04			

Temperature (°F)	K (Btu/min-in-°F)	ρ (lb_m/in^3)	T (°F)	C_p (Btu/lb_m-°F)
Fuel in Helium, Axial [Section M.4.8]				
200	7.949E-04	0.1166	See values above	
300	8.387E-04			
400	8.824E-04			
500	9.189E-04			
600	9.554E-04			
800	1.036E-03			

2. PWR Fuel in Vacuum

Temperature (°F)	K (Btu/min-in-°F)	ρ (lb_m/in^3)	T (°F)	C_p (Btu/lb_m-°F)
Fuel in a Vacuum [Section M.4.8]				
215	9.484E-05	0.1166	80	0.0592
288	1.246E-04		260	0.0654
367	1.633E-04		692	0.0725
452	2.119E-04		1502	0.0778
540	2.701E-04			
632	3.373E-04			
726	4.125E-04			
822	4.949E-04			

3. Zircaloy

Temperature (°F)	K (Btu/min-in-°F) [4.14]	ρ (lbm/in^3) [4.28]	C_p (Btu/lb_m-°F) [4.14]	
200	0.0109	0.237	80	0.067
300	0.0115		260	0.072
400	0.0121		692	0.079
500	0.0126		1502	0.090
600	0.0131		-	
800	0.0142			

4. UO_2 Fuel Pellet

Temperature (°F)	K (Btu/min-in-°F [4.14]	ρ (lbm/in^3) [4.28]	C_p (Btu/lb_m-°F) [4.14]	
200	5.537E-3	0.396	32	0.056
300	5.038E-3		212	0.063
400	4.622E-3		392	0.068
500	4.270E-3		752	0.072
600	3.968E-3		2192	0.079
700	3.707E-3			
800	3.478E-3			

storage and transfer are presented in Figure M.4-9 and Figure M.4-10, respectively. The temperature distribution from the bottom to the top of the DSC at the hottest cross-section is shown in Figure M.4-17 for 70°F ambient storage case.

M.4.4.3 Minimum Temperatures

Under the minimum temperature condition of 0°F ambient, the resulting DSC component temperatures will approach 0°F if no credit is taken for the decay heat load. Since the DSC materials, including confinement structures, continue to function at this temperature, the minimum temperature condition has no adverse effect on the performance of the NUHOMS®-32PT DSC.

M.4.4.4 Maximum Internal Pressures

M.4.4.4.1 Pressure Calculation

This section describes the pressure calculations used to determine maximum internal pressures during storage and transfer within the NUHOMS®-32PT DSC and basket when loaded with a payload of worst case B&W 15x15 fuel assemblies with a maximum burnup of 45 GWd/MTU. The limiting fuel assembly type considered in this evaluation is the B&W 15 x 15 assembly. The fission gasses produced by the WE 17x17 are slightly higher than those from the B&W 15x15, but the B&W 15x15 fuel assembly has the highest heavy metal and fuel assembly weight and therefore displaces the most free volume relative to all the other assembly types considered in Chapter M.2.

The calculations include the DSC free volume, the quantities of DSC backfill gas, fuel rod fill gas, and fission products and the average DSC cavity gas temperature. The 32PT-S100, 32PT-S125, 32PT-L100 and 32PT-L125 canister configurations are considered. The 32PT-L100 and 32PT-L125 DSC internal pressure evaluations also include the contribution due to BPRAs. The internal pressures are then calculated using:

$$P = \frac{nRT}{V}$$

where:

n = Total number of moles of gases,

R = Universal gas constant,

T = Gas temperature (°R),

V = Gas volume, and

P = Internal pressure.

M.4.4.4.2 Free Volume

M.4.4.4.2.1 DSC Cavity

The DSC Cavity free volumes are shown below:

Canister Type	32PT-S100	32PT-S125	32PT-L100	32PT-L125
Cavity Volume (in^3)	583,580	574,977	604,225	595,623
Basket Volume (in^3)	176,312	173,689	182,613	180,008
Fuel Volume (in^3)	181,126	181,126	185,518	185,518
Free Volume (in^3)	226,141	220,163	236,095	230,097

M.4.4.4.3 Quantity of Helium Fill Gas in DSC

The DSC free volume is assumed to be filled with 3.5 psig (18.2 psia) of helium. The maximum temperatures from the 70°F ambient storage case are used to estimate the number of moles of helium backfill.

The average long-term helium fill temperature for the worst case payload, 449°F (909°R) is used. Using the ideal gas law, the quantity of helium in each DSC is calculated and the results are presented in Table M.4-6.

M.4.4.4.4 Quantity of Fill Gas in Fuel Rod

The volume of the helium fill gas in a B&W 15x15 fuel pin at cold, unirradiated conditions is 1.326 in^3, and there are 208 fuel pins in an assembly. The maximum fill pressure is 415 psig (429.7 psia) and the fill temperature is assumed to be room temperature (70°F or 530°R). The quantity of fuel rod fill gas in 32 fuel assemblies is:

$$n_{he} = \frac{(429.7\,psia)(6894.8\,Pa/psi)(32 \cdot 208 \cdot 1.326 in^3)(1.6387 x 10^{-5}\,m^3/in^3)}{(8.314\,J/mol \cdot K)(530°R)(5/9\,K/°R)}$$

$$n_{he} = 175.0\,g-moles$$

Based on NUREG 1536 [4.10], the maximum fraction of the fuel pins that are assumed to rupture and release their fill and fission gas for normal, off-normal and accident events is 1, 10 and 100%, respectively. 100% of the fill gas in each ruptured rod is assumed to be released. The amount of helium fill gas released for each of these conditions is summarized below.

Case	Percentage of Rods Ruptured	Moles of Helium Fill Gas Released
Normal	1	1.75
Off-Normal	10	17.50
Accident	100	175.0

M.4.4.4.5 Quantity of Fission Product Gases in Fuel Rod

The B&W 15x15 fuel assembly used in the pressure calculations is assumed to be burned to 45,000 MWd/MTU, which is the highest burnup proposed for the NUHOMS®-32PT configuration. The maximum burnup creates a bounding case for the amount of fission gases produced in the fuel rod during reactor operation. The amounts of tritium, krypton-85 and xenon-131m at STP for each assembly are summarized below.

Isotope	Volume (liters/assy)	Volume (in^3/assy)
Tritium (H^3)	0.26	16
Kr^{85}	60.4	3,686
Xe^{131m}	547	33,380
Total	607.7	37,081

The total fission gas volume for a fuel assembly is equal to 607.7 liters (37,081 in^3). The total amount of fission gas products produced is calculated using 32°F as:

$$n_{fg} = \frac{(32)(14.7)(6894.8\,Pa/psi)(37{,}081 in^3)(1.6387x10^{-5}\,m^3/in^3)}{(8.314\,J/mol\cdot K)(460°R + 32°F)(5/9\,K/°R)}$$

$$n_{fg} = 867\,g-moles$$

The amount of fission gas released into the DSC cavity for normal, off-normal and accident condition cases assuming a 30% gas release from the fuel pellets and a 1%, 10%, and 100% rod rupture percentage, respectively, is summarized below.

Case	Percentage of Rods Ruptured	Moles of Fission Gas Released
Normal	1	2.6
Off-Normal	10	26.0
Accident	100	260

M.4.4.4.6 Quantity of Gas in Control Components (BPRAs)

The 32PT-L100 and 32PT-L125 DSC configurations may include BPRAs. In the NUHOMS®-32PT DSC, a maximum of 16 BPRAs per DSC are allowed. These BPRAs have an initial helium fill of 14.7 psia, and if 100% of the boron is consumed, and 30% released into the DSC, a total of 53.8 *(16/24) = 35.9 g-moles of gas could be released to the DSC assuming 100% cladding rupture (the 53.8 g-moles is based on 24 BPRAs in the 24P DSC; from Appendix J, Section J.4).

The percentage of BPRA rods ruptured during normal, off-normal and accident conditions is assumed to be 1%, 10% and 100%, respectively, similar to the assumptions for the fuel rod

rupturing. The maximum amount of gas released to the DSC cavity from the BPRAs for normal, off-normal and accident conditions is given below.

Case	Percentage of Rods Ruptured	Moles of Fission Gas Released per DSC from BPRAs
Normal	1	0.359
Off-Normal	10	3.59
Accident	100	35.9

The maximum average helium temperature for normal conditions of storage and transfer occurs when the 32PT DSC is in the TC with an ambient temperature of 100°F and maximum insolation. This case bounds the 100°F ambient case in the HSM. In addition the maximum pressure will occur with the 45,000 MWd/MTU burnup fuel so that lesser burnups will be enveloped by this calculation. The average helium temperature is 545°F (1005°R), however 550°F (1,010°R) is conservatively used. The maximum normal operating condition pressures are summarized in Table M.4-7.

M.4.4.5 Maximum Thermal Stresses

The maximum thermal stresses during normal conditions of storage and transfer are calculated in Section M.3.

M.4.4.6 Evaluation of Cask Performance for Normal Conditions

The NUHOMS®-32PT DSC shell and basket are evaluated for the calculated temperatures and pressures in Section M.3. The maximum fuel cladding temperatures are well below the allowable long-term fuel temperature limits and the short-term limit of 752°F (400°C). The maximum DSC internal pressure remains below 15.0 psig during normal conditions of storage and transfer. Based on the thermal analysis, it is concluded that the NUHOMS®-32PT DSC design meets all applicable normal condition thermal requirements.

M.4.8 Determination of Minimum Effective Fuel Conductivity

In order to determine the bounding effective thermal conductivity of a fuel assembly for use in the thermal analysis of the NUHOMS®-32PT DSC, the fuel assembly with the lowest thermal conductivity at the design basis heat load is selected.

This section presents the methodology for the determination of axial and transverse effective thermal conductivity of spent fuel and the determination of the bounding fuel effective thermal conductivity. In addition, the methodology for calculation of effective specific heat and effective density of the fuel is also presented.

M.4.8.1 Determination of Bounding Effective Fuel Thermal Conductivity

M.4.8.1.1 Fuel Assemblies Evaluated

The fuel assemblies that are considered for storage in the NUHOMS®-32PT DSC are listed in Section M.2. The design data for each of the fuel assemblies are presented in Section M.2.

M.4.8.1.2 Summary of Thermal Properties of Materials

The thermal conductivity and specific heat values of Zircaloy, UO_2 pellets, and Helium are presented in Section M.4.2. The emissivity of Zircaloy is also presented in Section M.4.2.

M.4.8.1.3 Calculation of Fuel Axial Effective Thermal Conductivity

The axial fuel conductivity is assumed to be limited to the cladding conductivity weighted by its fractional area as required in NUREG 1536 [4.10].

$$K_{axl} = (K_{zirc})(A_{zirc}/A_{eff}) \qquad (1)$$

K_{zirc} = Conductivity of Zircaloy 4
A_{eff} = (8.70") x (8.70") = 75.69 in^2
A_{zirc} = Cross section area of Zircaloy cladding in the fuel assembly

Equation (1) is used to calculate axial effective conductivity for the fuel assembly types listed in Section M.2 The results are plotted in Figure M.4-19.

M.4.8.1.4 Calculation of Fuel Transverse Effective Thermal Conductivity

The transverse fuel effective conductivity is determined by creating a two-dimensional finite element model of the fuel assembly centered within a fuel compartment. The outer surfaces, representing the fuel compartment walls, are held at a constant temperature, and heat generating boundary condition is applied to the fuel pellets within the model. A maximum fuel assembly temperature is then determined. The isotropic effective thermal conductivity of a heat generating square, such as the fuel assembly, can be calculated as described in [4.27].

$$K_{eff} = 0.29468 \times \frac{Q'''}{a^2 (T_c - T_o)} \qquad (2)$$

where:

Q''' = heat load per unit volume of fuel assembly (Btu/hr-in^3),
a = half width of fuel compartment opening = 8.7 / 2 = 4.35",
Tc = Maximum Temperature of Fuel Assembly (°F),
To = Compartment Wall Temperature (°F).

with

$$Q''' = \frac{Q}{4a^2 L_a} \qquad (3)$$

where:

Q= decay heat load per assembly = 24 kW/32 = 0.75 kW/assembly, and
L_a = active fuel length

In determining the temperature dependent effective fuel conductivities, an average temperature, equal to $(T_c + T_o)/2$, is used for the fuel temperature.

2-D finite element models of each fuel assembly representing a quarter of the fuel assembly were modeled within ANSYS [4.9]. Plane 55 elements were used to model components such as the fuel pellets, fuel cladding, and the helium back fill gas. The gap between the fuel cladding and the fuel pellets is also included in the model.

Heat generated in the fuel pellets dissipates by conduction and radiation to the fuel compartment walls. Convection is not considered in the model. Radiation between the fuel rods, guide tubes, and basket walls was simulated using the radiation super-element processor (/AUX12). LINK32 elements were used for modeling of radiating surfaces in creating the radiation super-element and were unselected prior to the solution of the model. The compartment walls are not modeled as a solid entity. Only the LINK32 elements aligned with the outermost nodes of the model (not on symmetry lines) are given the emissivity of the compartment walls.

Emissivity of stainless steel was applied to the LINK elements on one compartment wall. The link elements on the other compartment wall were given the emissivity of 0.85 (aluminum with anodized or other processes). To eliminate the radiation heat transfer across the symmetry lines, the link elements on symmetry lines were given a very low emissivity (0.001). Although the symmetry boundaries result in the aluminum surfaces being not adjacent, as it would be in the actual compartment, the impact is negligible.

Since a quarter of fuel assembly is modeled in each case, the reaction solution after solving the 2D model is equal to the heat generated per unit length of the active fuel divided by four.

$$Q_{react} = \frac{Q}{4L_a} \qquad (4)$$

Substitution of equations (3) and (4) in equation (2) gives:

$$K_{eff} = 0.29468 \times \frac{Q_{react}}{(T_c - T_o)} \qquad (5)$$

Equation (5) is used to calculate the transverse effective fuel conductivity for each fuel assembly model.

The heat generating boundary conditions for each assembly is calculated as shown in equation 6.

$$dhl = \frac{Q/N}{n\left(\frac{\pi}{4} d_p^{\,2}\right) L_a} \qquad (6)$$

dhl = Heat generating boundary condition (Btu/min-in-°F)
Q = Total decay heat load = 24 kW = 1364.9 Btu/min
N = Number of assemblies =32
n = Number of fuel rods
d_p = Pellet outer diameter
L_a = Active fuel length

The models were run with a series of isothermal boundary conditions applied to the nodes representing the fuel compartment walls. The symmetry lines going through the center of the fuel assembly are kept at the adiabatic boundary conditions.

A finite element model for B&W 15x15 fuel assembly is shown in Figure M.4-18.

M.4.8.1.5 Results and Conclusion

Figure M.4-19 shows the calculated axial effective conductivities. As Figure M.4-19 shows, WE 14x14 has the minimum (bounding) axial conductivity. Backfill gas property does not have any effect on the axial effective fuel conductivity. Therefore, identical axial effective fuel conductivity values can be used for helium and vacuum conditions.

The calculated bounding axial effective conductivities are listed in the following table:

Temperature °F	k-axial (Btu/min-in-°F)
200	7.949E-04
300	8.387E-04
400	8.824E-04
500	9.189E-04
600	9.554E-04
800	1.036E-03

The calculated transverse conductivities are presented in Figure M.4-20 and Figure M.4-21 for helium and vacuum conditions, respectively. As shown in Figure M.4-20 and Figure M.4-21,

WE 14x14 assembly has the (bounding) minimum transverse conductivity. The bounding transverse effective conductivity values are listed in the following table:

Temperature °F	k-transverse in Helium (Btu/min-in-°F)
138	2.894E-04
233	3.317E-04
328	3.968E-04
423	4.744E-04
519	5.668E-04
616	6.715E-04
714	7.879E-04
812	9.208E-04

Temperature °F	k-transverse in Vacuum (Btu/min-in-°F)
215	9.484E-05
288	1.246E-04
367	1.633E-04
452	2.119E-04
540	2.701E-04
632	3.373E-04
726	4.125E-04
822	4.949E-04

M.4.8.2 Calculation of Fuel Effective Specific Heat and Density

This section presents the calculation of the fuel effective specific heat and density used in the transient thermal analyses.

Volume average density and weight average specific heat are calculated to determine the effective density and specific heat for the fuel assembly.

The equations to determine the fuel effective density ρ_{eff} and specific heat $C_{p\,eff}$ are shown below.

$$\rho_{eff} = \frac{\sum \rho_i V_i}{V_{assembly}} = \frac{\rho_{UO2}\ V_{UO2} + \rho_{Zr4}\ V_{Zr4}}{4a^2 L_a}$$

$$C_{p,eff} = \frac{\sum \rho_i V_i C_{Pi}}{\sum \rho_i V_i} = \frac{\rho_{UO2}\ V_{UO2}\ C_{P,UO2} + \rho_{Zr4}\ V_{Zr4}\ C_{P,Zr4}}{\rho_{UO2}\ V_{UO2} + \rho_{Zr4}\ V_{Zr4}}$$

where:

ρ_i, $C_{p,i}$, V_i = density, specific heat, and volume of component,
L_a = active fuel length, and
a = half of compartment width.

The properties of Zircalloy-4 and UO_2 are provided in Section M.4.2

The calculated values of fuel effective specific heat and fuel effective density are summarized below:

Temperature °F	Fuel Effective Specific Heat (Btu/lbm-F)
80	0.0592
260	0.0654
692	0.0725
1502	0.0778

Fuel Effective Density (lbm/in3)	0.1166

Table M.4-6
32PT DSC Initial Helium Fill Molar Quantities

DSC Configuration	Helium Fill (g-moles)
S100	110.8
S125	107.8
L100	115.6
L125	112.7

Table M.4-7
32PT DSC Maximum Normal Operating Condition Pressures

DSC Configuration	DSC Cavity Free Volume (in^3)	Helium Fill (g-moles)	Plenum Helium (g-moles)	BPRA Gas (g-moles)	Fission Products (g-moles)	Total Gas (g-moles)	Pressure (psig)	DSC Design Pressure (psig)
S100	226,141	110.74	1.75	0.00	2.60	115.11	6.31	15
S125	220,162	107.83	1.75	0.00	2.60	112.18	6.34	15
L100	236,094	115.62	1.75	0.359	2.60	120.34	6.35	15
L125	230,097	112.68	1.75	0.359	2.60	117.41	6.37	15

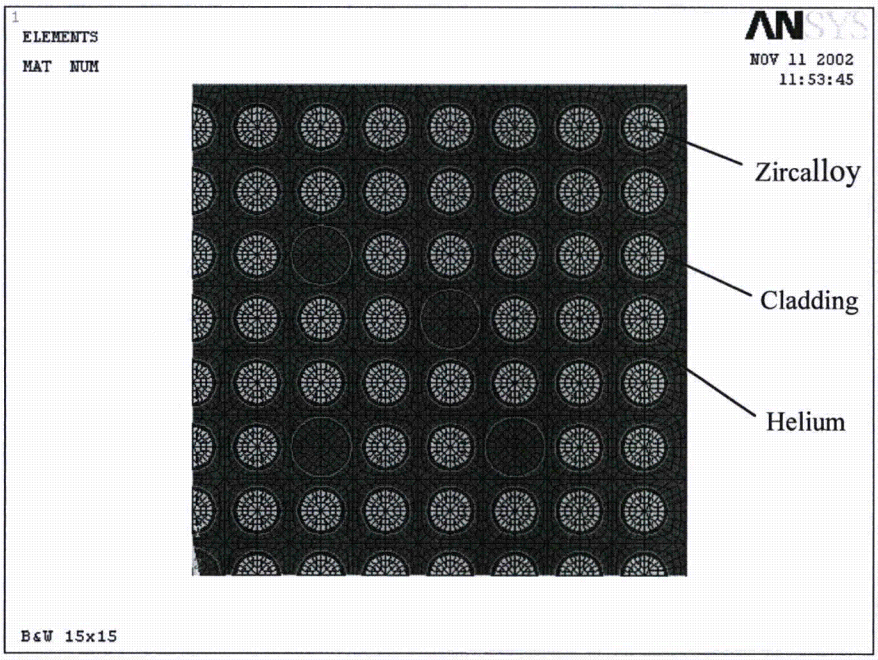

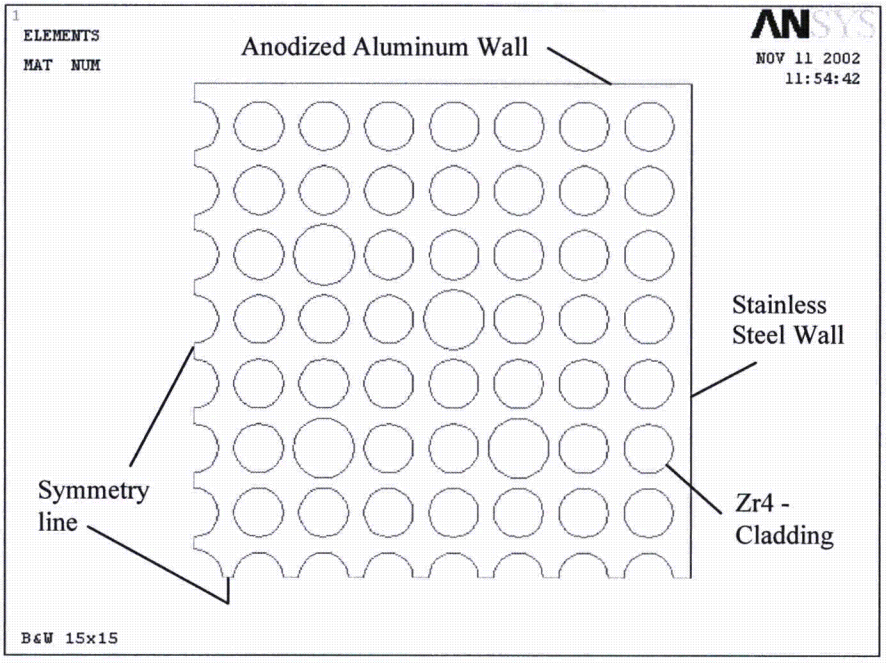

Figure M.4-18
Finite Element Model of B&W 15x15 Fuel Assembly

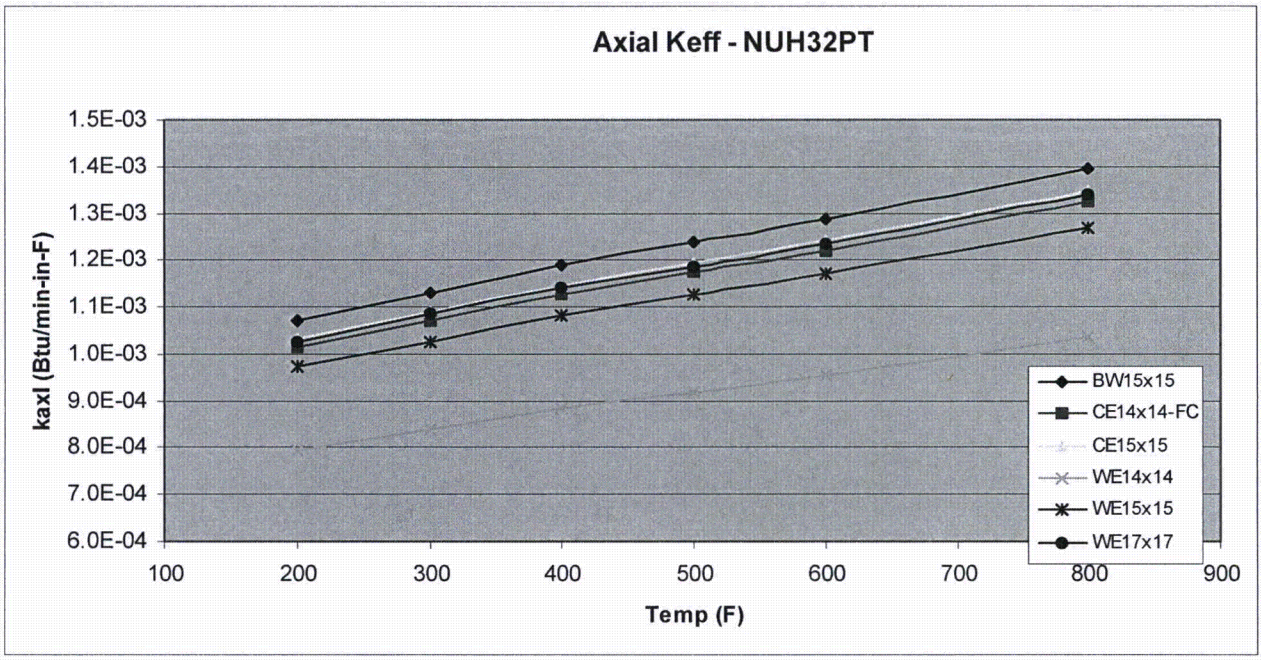

Figure M.4-19
Fuel Axial Effective Conductivity

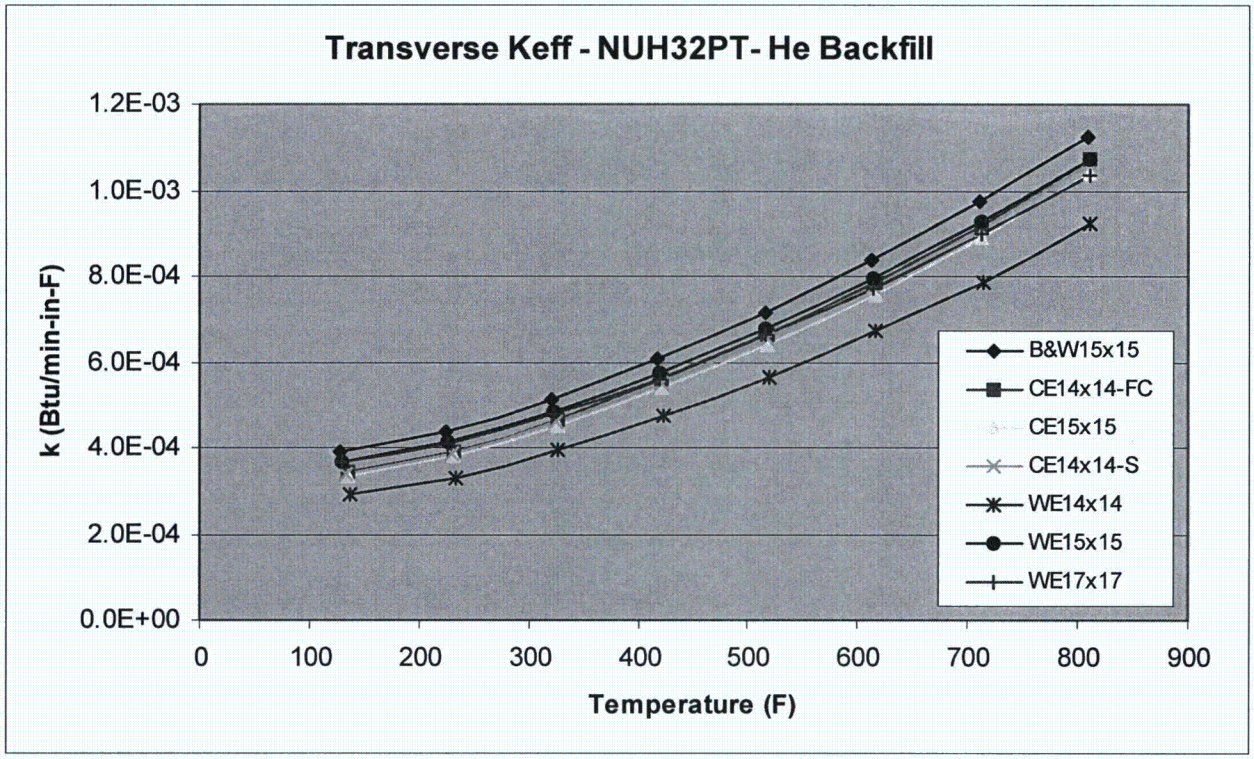

Figure M.4-20
Fuel Transverse Effective Conductivity in Helium

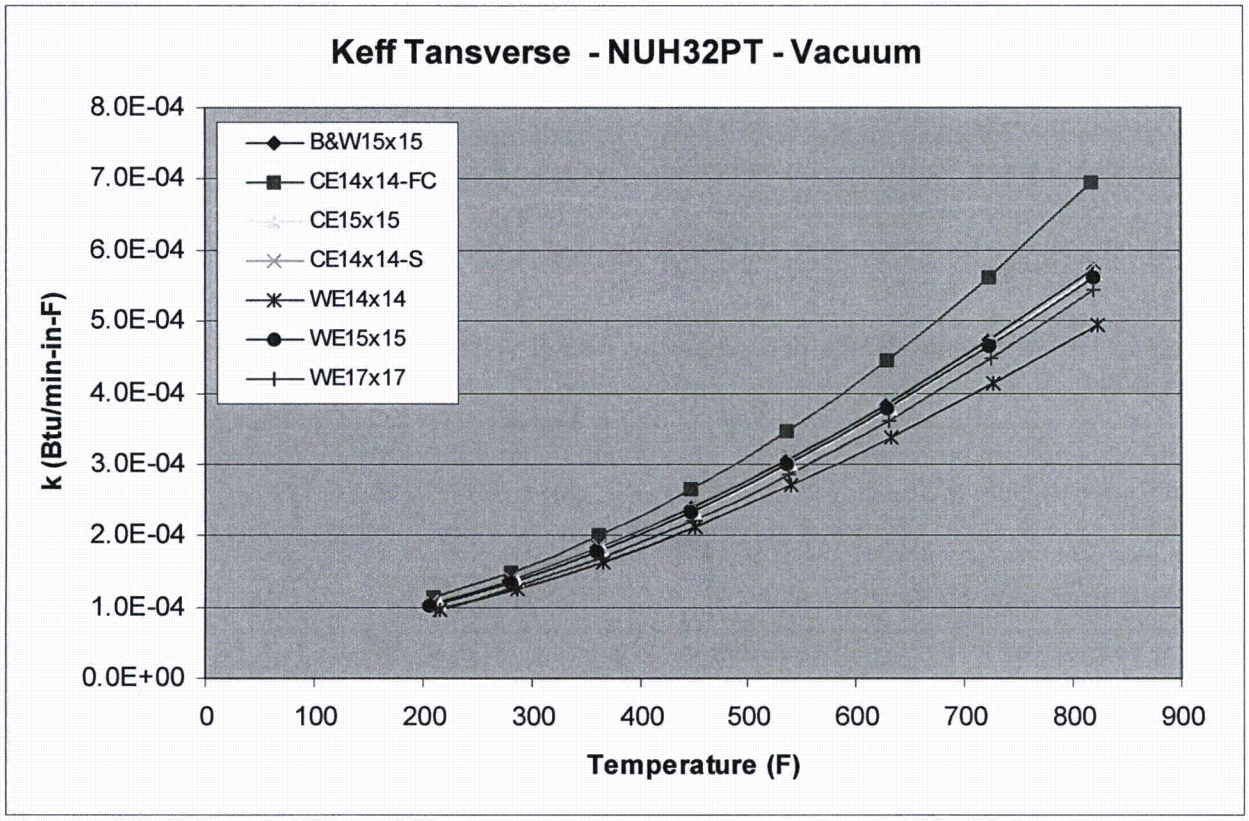

Figure M.4-21
Fuel Transverse Effective Conductivity in Vacuum

P.4.2 Summary of Thermal Properties of Materials

The analyses performed herein use interpolated values where appropriate for intermediate temperatures. The interpolation assumes a linear relationship between the reported values. The use of linear interpolation between temperature values in the tables for determining intermediate value of property is justified by the near-linear behavior as a function of temperature for the range of interest.

The emissivity of stainless steel is 0.587 [4.5]. For additional conservatism an emissivity of 0.46 for stainless steel is used for the basket steel plates in the analysis. The emissivity assumed for oxidized Zircaloy cladding surfaces, including Babcock & Wilcox (B&W) M5 cladding material, is 0.8 [4.11]. The emissivity assumed for anodized and non-anodized aluminum portion of side heat shields are 0.8 and 0.1, respectively [4.26] [4.30] [4.47].

The tables below provide the thermal properties of materials used in the analysis of the NUHOMS®-24PTH DSC.

The effective thermal properties are the lowest calculated values among the various PWR fuel assembly types that may be stored in 24PTH DSC. Since 24PTH-S-LC DSC is designed for storage of B&W 15x15 fuel, an additional subset of bounding effective thermal properties are reported.

1. PWR Fuel with Helium Backfill

Temperature, °F	k, Btu/min-in-°F	ρ, lb_m/in^3	T, °F	C_p,Btu/lb_m-°F
Bounding Fuel in Helium, Transverse (Used in 24PTH-S and 24PTH-L DSC Analysis) **[See Section P.4.8]**				
178	2.798E-04	0.1114	80	0.05924
267	3.257E-04		260	0.06538
357	3.829E-04		692	0.07255
448	4.547E-04		1502	0.07779
541	5.389E-04			
635	6.326E-04			
730	7.398E-04			
826	8.558E-04			

Bounding B&W 15x15 Fuel in Helium, Transverse (Used in 24PTH-S-LC DSC Analysis) **[See Section P.4.8]**				
162	3.560E-04	0.1265	80	0.05931
254	4.064E-04		260	0.06544
346	4.780E-04		692	0.07261
439	5.639E-04		1502	0.07790
533	6.620E-04			
629	7.733E-04			
725	8.957E-04			
822	1.031E-03			

Bounding Fuel in Helium, Axial (Used in 24PTH-S and 24PTH-L DSC Analysis) **[See Section P.4.8]**			
200	7.596E-04	0.1114	See values above (for all fuels)
300	8.014E-04		
400	8.432E-04		
500	8.781E-04		
600	9.129E-04		
800	9.896E-04		

Bounding B&W 15x15 Fuel in Helium, Axial (Used in 24PTH-S-LC DSC Analysis) **[See Section P.4.8]**			
200	9.081E-04	0.1265	See values above (for BW 15x15 fuels)
300	9.581E-04		
400	1.008E-03		
500	1.050E-03		
600	1.091E-03		
800	1.183E-03		

2. PWR Fuel in Vacuum

Bounding Fuel in a Vacuum, Transverse (Used in 24PTH-S and 24PTH-L DSC Analysis) **[See Section P.4.8]**				
250	1.455E-04	0.1114	80	0.05924
321	1.803E-04		260	0.06538
397	2.249E-04		692	0.07255
478	2.797E-04		1502	0.07779
563	3.463E-04			
651	4.278E-04			
742	5.195E-04			
835	6.234E-04			

Bounding B&W 15x15 Fuel in a Vacuum, Transverse (Used in 24PTH-S-LC DSC Analysis) **[See Section P.4.8]**				
233	1.658E-04	0.1265	80	0.05931
307	2.056E-04		260	0.06544
386	2.556E-04		692	0.07261
470	3.176E-04		1502	0.07790
556	3.931E-04			
646	4.830E-04			
738	5.887E-04			
831	7.087E-04			

Bounding Fuel in a Vacuum, Axial (Used in 24PTH-S and 24PTH-L DSC Analysis)			
200	7.596E-04	0.1114	See values above (for all fuels)
300	8.014E-04		
400	8.432E-04		
500	8.781E-04		
600	9.129E-04		
800	9.896E-04		

Bounding B&W 15x15 Fuel, Axial (Used in 24PTH-S-LC DSC Analysis)			
200	9.081E-04	0.1265	See values above (for BW 15x15 fuels)
300	9.581E-04		
400	1.008E-03		
500	1.050E-03		
600	1.091E-03		
800	1.183E-03		

3. Zircaloy

Temperature (°F)	K (Btu/min-in-°F) [4.11]	ρ (lbm/in^3) [4.11]	C_p (Btu/lb$_m$-°F) [4.11]	
200	0.0109	0.237	80	0.067
300	0.0115		260	0.072
400	0.0121		692	0.079
500	0.0126		1502	0.090
600	0.0131			
800	0.0142			

4. B&W 15x15 Mark B11 M5 Cladding Material

Temperature (°F)	K (Btu/min-in-°F) [4.25]	ρ (lbm/in^3)(1)	C_p (Btu/lb$_m$-°F) [4.25]	
-40	0.0142	0.237		
0	0.0141		31.73	0.0671
100	0.0140		100	0.0685
200	0.0140		200	0.0707
300	0.0140		300	0.0728
400	0.0140		400	0.0749
500	0.0142		500	0.0770
600	0.0144		600	0.0791
700	0.0146		700	0.0812
800	0.0149		800	0.0833
900	0.0153		900	0.0854
1000	0.0157		1000	0.0875
1100	0.0162		1100	0.0897

(1) Assumed to be the same as Zircaloy

5. UO2 Fuel Pellet

Temperature (°F)	K (Btu/min-in-°F [4.11]	ρ (lbm/in^3) [4.11]	C_p (Btu/lb$_m$-°F) [4.11]	
200	5.537E-3	0.396	32	0.056
300	5.038E-3		212	0.063
400	4.622E-3		392	0.068
500	4.270E-3		752	0.072
600	3.968E-3		2192	0.079
700	3.707E-3			
800	3.478E-3			

6. SA-240, Type 304 Stainless Steel [4.2]

Temperature (°F)	K (Btu/min-in-°F)	ρ (lbm/in^3)	C_p (Btu/lb$_m$-°F)
70	0.0119	0.284	0.116
100	0.0121		0.117
150	0.0125		0.119
200	0.0129		0.121
250	0.0133		0.124
300	0.0136		0.125
350	0.0140		0.127
400	0.0144		0.128
500	0.0151		0.130
600	0.0157		0.132
700	0.0164		0.134
800	0.0169		0.135

7. A-36, Carbon Steel (C-Mu-Si) [4.2]

Temperature (°F)	K (Btu/min-in-°F)	ρ (lbm/in^3)	C_p (Btu/lb$_m$-°F)
100	0.0383	0.284	0.1098
200	0.0383		0.1157
300	0.0378		0.1224
400	0.0371		0.1271
500	0.0360		0.1326
600	0.0347		0.1362
700	0.0333		0.1413
800	0.0319		0.1474

P.4.8 Determination of Effective Thermal Properties of the Fuel, Basket and Air Within the HSM-H Closed Cavity

This section presents the methodology and determines the effective thermal conductivity, specific heat and density for the fuels to be stored within NUHOMS®-24PTH DSC with helium backfill and vacuum for use in the analysis of the thermal performance of the NUHOMS®-24PTH DSC.

This section also determines the effective thermal conductivity, density and specific heat load of the 24PTH DSC basket for use in the transient thermal analysis in Section P.4.4 and P.4.5.

P.4.8.1 Determination of Bounding Effective Fuel Thermal Conductivity

P.4.8.1.1 Fuel Assemblies Evaluated

The fuel assemblies that are considered for storage in the NUHOMS® 24PTH DSC, including the design data for each fuel assemblies, are listed in Section P.2. This section includes calculation of the bounding properties among fuels to store in 24PTH-S or -L DSC with maximum total decay heat per DSC up to 40.8 kW. The bounding properties of B&W 15x15 fuel assemblies were calculated for thermal analysis of 24PTH-S-LC DSC with maximum total decay heat of 24 kW per DSC.

P.4.8.1.2 Summary of Thermal Properties of Materials

The thermal conductivity and specific heat values of Zircaloy, UO_2 pellets, and Helium are presented in Section P.4.2. The emissivity of Zircaloy is also presented in Section P.4.2.

P.4.8.1.3 Calculation of Fuel Axial Effective Thermal Conductivity

The axial fuel conductivity is assumed to be limited to the cladding conductivity weighted by its fractional area as required in NUREG 1536 [4.7].

$$K_{axl} = (K_{zirc})(A_{zirc}/A_{eff}) \qquad (1)$$

K_{zirc} = Conductivity of Zircaloy 4
A_{eff} = (8.90") x (8.90") = 79.21 in^2
A_{zirc} = Cross section area of Zircaloy cladding in the fuel assembly

Equation (1) is used to calculate axial effective conductivity for the fuel assembly types listed in Section P.2. The results are plotted in Figure P.4-44.

P.4.8.1.4 Calculation of Fuel Transverse Effective Thermal Conductivity

The transverse fuel effective conductivity is determined by creating a two-dimensional finite element model of the fuel assembly centered within a fuel compartment. The outer surfaces, representing the fuel compartment tube walls, are held at a constant temperature and heat generating boundary condition is applied to the fuel pellets within the model. A maximum fuel assembly temperature is

then determined. The isotropic effective thermal conductivity of a heat generating square, such as the fuel assembly, can be calculated as described in [4.22].

$$K_{eff} = 0.29468 \times \frac{Q'''}{a^2 (T_c - T_o)} \qquad (2)$$

where:

Q''' = heat load per unit volume of fuel assembly (Btu/hr-in^3),
a = half width of fuel compartment opening = 8.9 / 2 = 4.45",
Tc = maximum temperature of fuel assembly (°F),
To = compartment wall temperature (°F).

with

$$Q''' = \frac{Q}{4a^2 L_a} \qquad (3)$$

where:

Q= decay heat load per assembly,
L_a = active fuel length

In determining the temperature dependent effective fuel conductivities, an average temperature, equal to $(T_c + T_o)/2$, is used for the fuel temperature.

2-D finite element models of each fuel assembly representing a quarter of the fuel assembly were modeled within ANSYS [4.6]. Plane 55 elements were used to model components such as the fuel pellets, fuel cladding, and the helium back fill gas. The gap between the fuel cladding and the fuel pellets is also included in the model.

Heat generated in the fuel pellets dissipates by conduction and radiation to the fuel compartment walls. Convection is not considered in the model. Radiation between the fuel rods, guide tubes, and basket walls was simulated using the radiation super-element processor (/AUX12). LINK32 elements were used for modeling of radiating surfaces in creating the radiation super-element and were unselected prior to the solution of the model. The compartment walls are not modeled as a solid entity. Only the LINK32 elements aligned with the outermost nodes of the model (not on symmetry lines) are given the emissivity of the compartment walls.

Emissivity of stainless steel (0.46) was applied to the LINK elements on fuel compartment tube walls. To eliminate the radiation heat transfer across the symmetry lines, the link elements on symmetry lines were given a very low emissivity (0.001).

The B&W 15x15 fuel assembly finite element model is shown in Figure P.4-43 as a typical for all the fuel types considered.

Since a quarter of fuel assembly is modeled in each case, the reaction solution after solving the 2D model is equal to the heat generated per unit length of the active fuel divided by four.

$$Q_{react} = \frac{Q}{4L_a} \qquad (4)$$

Substitution of equations (3) and (4) in equation (2) gives:

$$K_{eff} = 0.29468 \times \frac{Q_{react}}{(T_c - T_o)} \qquad (5)$$

Equation (5) is used to calculate the transverse effective fuel conductivity for each fuel assembly model.

The heat generating boundary conditions for each assembly is calculated as shown in equation 6.

$$dhl = \frac{Q/N}{n\left(\frac{\pi}{4} d_p^{\,2}\right) L_a} \qquad (6)$$

dhl = Heat generating boundary condition, Btu/min-in-°F
Q = Total decay heat load, Btu/min
N = Number of assemblies, 24
n = Number of fuel rods
d_p = Pellet outer diameter, in
L_a = Active fuel length, in

The models were run with a series of isothermal boundary conditions applied to the nodes representing the fuel compartment walls. The symmetry lines going through the center of the fuel assembly are kept at the adiabatic boundary conditions.

P.4.8.1.5 Results

Figure P.4-44 shows the calculated axial effective conductivities for fuel to store in 24PTH-S DSC and –L DSC. As Figure P.4-44 shows, WE 14x14 has the minimum (bounding) axial conductivity. Backfill gas property does not have any effect on the axial effective fuel conductivity. Therefore, identical axial effective fuel conductivity values can be used for helium and vacuum conditions.

Figure P.4-45 shows the calculated axial effective conductivities for the B&W 15x15 fuel to be stored in 24PTH-S-LC DSC. As Figure P.4-45 shows, BW 15x15 Mk-11 has the minimum (bounding) axial conductivity among BW 15x15 fuels. Backfill gas property does not have any effect on the axial effective fuel conductivity. Therefore, identical axial effective fuel conductivity values can be used for helium and vacuum conditions.

The calculated bounding axial effective conductivities for fuels to store in 24PTH-S DSC, -L DSC, and –S-LC DSC are listed in Section P.4.2.

The calculated transverse conductivities for fuels to store in 24PTH-S and –L DSC are presented in Figure P.4-46 and Figure P.4-47for helium and vacuum conditions, respectively. As shown herein, WE 14x14 assembly has the (bounding) minimum transverse conductivity for helium and vacuum conditions. The bounding transverse effective conductivity values for fuels to store in 24PTH-S DSC and -L DSC are listed in Section P.4.2.

The calculated transverse conductivities for B&W 15x15 fuels to store in 24PTH-S-LC DSC are presented in Figure P.4-48 and Figure P.4-49 for helium and vacuum conditions, respectively. The bounding transverse effective conductivity values for fuels to store in 24PTH-S-LC DSC are listed in Section P.4.2.

P.4.8.2 Calculation of Fuel Effective Specific Heat and Density

This section presents the calculation of the fuel effective specific heat and density used in the transient thermal analyses.

Volume average density and weight average specific heat are calculated to determine the effective density and specific heat for the fuel assembly.

The equations to determine the fuel effective density ρ_{eff} and specific heat $C_{p\,eff}$ are shown below.

$$\rho_{eff} = \frac{\sum \rho_i V_i}{V_{assembly}} = \frac{\rho_{UO2}\ V_{UO2} + \rho_{Zr4}\ V_{Zr4}}{4a^2 L_a}$$

$$C_{p,eff} = \frac{\sum \rho_i V_i C_{Pi}}{\sum \rho_i V_i} = \frac{\rho_{UO2}\ V_{UO2}\ C_{P,UO2} + \rho_{Zr4}\ V_{Zr4}\ C_{P,Zr4}}{\rho_{UO2}\ V_{UO2} + \rho_{Zr4}\ V_{Zr4}}$$

where:

ρ_i, $C_{p,i}$, V_i = density, specific heat, and volume of component,
L_a = active fuel length, and
a = half of compartment width.

The properties of Zircaloy-4 and UO_2 are provided in Section P.4.2.

The calculated minimum (bounding) values of fuel effective specific heat and fuel effective density for fuel to store in 24PTH-S DSC, -L DSC and -S-LC DSC are summarized in Section P.4.2.

P.4.11 References

4.1 Report, "Topical Report on Actinide-Only Burnup Credit for PWR Spent Nuclear Fuel Packages," Office of Civilian Radioactive Waste Management, DOE/RW-0472, Revision 2, September 1998.

4.2 ASME Boiler and Pressure Vessel Code, Section II, Part D, Properties, 1998, including 2000 addenda.

4.3 Roshenow, W. M., J. P. Hartnett, and Y. I. Cho, *Handbook of Heat Transfer*, 3rd Edition, 1998.

4.4 Bolz, R. E., G. L. Tuve, *CRC Handbook of Tables for Applied Engineering Science*, 2nd Edition, 1973. Transfer, McGraw Hill, 1989.

4.5 Bucholz, J. A., *Scoping Design Analysis for Optimized Shipping Casks Containing 1-, 2-, 3-, 5-, 7-, or 10-Year old PWR Spent Fuel*, Oak Ridge National Laboratory, January, 1983, ORNL/CSD/TM-149.

4.6 ANSYS, Inc., ANSYS Engineering Analysis System User's Manual for ANSYS, Houston, PA.

4.7 NUREG-1536, *Standard Review Plan for Dry Cask Storage Systems,* January 1997.

4.8 Consolidated Safety Analysis Report for IF-300 Shipping Cask, CoC 9001.

4.9 J.P. Holman, Heat Transfer, McGraw Hill, 1989.

4.10 Chun, Ramsey; Witte, Monika; Schwartz, Martin, "Dynamic Impact Effects on Spent Fuel Assemblies," Lawrence Livermore National Laboratory, Report UCID-21246, October, 1987.

4.11 NUREG/CR-0497, "MATPRO-Version 11: "A Handbook of Materials Properties for Use in the Analysis of Light Water Reactor, Fuel Rod Behavior," EG&G, Inc. February, 1979.

4.12 Glasstone, S., Seasonske, A., "Nuclear Reactor Engineering," Third Edition, 1981.

4.13 Young, W.C., "Roark's Formulas for Stress and Strain," Sixth Edition, McGraw Hill.

4.14 Kreith, "The CRC Handbook of Thermal Engineering", 2000.

4.15 Aluminum. Volume 1, Properties, Physical Metallurgy and Phase Diagrams, edited by Kent R. Van Horn, American Society for Metals, Metals Park, Ohio, 1967.

4.16 ASHRAE Handbook, 1981 Fundamentals, 4th Printing, 1983.

4.17 Rohsenow, Hartnett, "Handbook of Heat Transfer Fundamentals, " 2nd Edition, 1985.

4.18 Roth, A., "Vacuum Technology," 2nd Edition, 1982.

4.19 Interim Staff Guidance No. 11, Revision 2, "Cladding Considerations for the Transportation and Storage of Spent Fuel," July 30, 2002.

4.20 TN Response to RAI No. 2 and Submittal of Revision 4 of Application for Amendment No. 5 to the NUHOMS® Certificate of Compliance No. 1004 (TAC No. L23343), January 24, 2003 (Docket 72-1004).

4.21 J. M. Creer, et al, "The TN-24 PWR Spent Fuel Storage Cask: Testing and Analyses," PNL Report, Report No. PNL-6054, 1987.

4.22 SAND90–2806, Sanders, T. L., et al., "A Method for Determining the Spent Fuel Contribution to Transport Cask Containment Requirements," TTC-1019, UC-820, November 1992.

4.23 Oak Ridge National Laboratory, RSIC Computer Code Collection, "SCALE, A Modular Code System for Performing Standardized Computer Analysis for Licensing Evaluation for Workstations and Personal Computers", NUREG/CR-0200, Rev. 6, ORNL/NUREG/CSD-2/V3/R6.

4.24 Report, Azzazy, M., Emissivity Measurements of 304 Stainless Steel, Prepared for Southern California Edison, September 6, 2000, Transnuclear File No. NUH32PT.0100-01

4.25 Duke Energy's letter, Transnuclear, Inc., File No. NUH24PTH-0100-01.

4.26 Frank Kreith, Principles of Heat Transfer, Third Edition, Harper and Row Publishers.

4.27 Incropera and DeWitt, Handbook of Heat And Mass Transfer Fundamentals, 5th edition, Wiley Publishers, 2002, Table A.6 pp 924.

4.28 Bentz, "A Computer Model to Predict the Surface Temperature and Time-of-wetness of Concrete Pavements and Bridge Decks", Report # NISTIR 6551, National Institute of Standards and Technology, 2000.

4.29 Zoldners, "Thermal Properties of Concrete under Sustained Elevated Temperatures", ACI Publications, Paper SP 25-1, American Concrete Institute, Detroit, MI, 1970, Cavanaugh, Guide to Thermal Properties of Concrete and Masonry Systems, Reported by ACI Committee 122, Report #ACI 122R-02, American Concrete Institute, Detroit, MI, 2002.

4.30 Siegel, Howell, "Thermal Radiation Heat Transfer", 4th Edition, 2002.

4.31 ANSYS Computer Code and User's Manuals, Rev. 6.0, See Test Report E-19197, Rev. 0 and E-20184, Rev. 0 for validation of computer code.

4.32 NRC, Code of Federal Regulations, Part 71, "Packaging and Transportation of Radioactive Material", 2003.

4.33 I.E. Idelchik, Handbook of Hydraulic Resistance, 3rd Edition, 1994.

4.34 Not used.

4.35 David R. Lide, *CRC Handbook of Chemistry and Physics*, 83rd edition, 2002-2003, CRC Press.

4.36 SINDA/FLUINT™, Systems Improved Numerical Differencing Analyzer and Fluid Integrator, *Version 4.5, Cullimore & Ring Technologies, Inc., Littleton, CO, 2002*

4.37 Thermal Desktop™, *Version 4.5, Cullimore & Ring Technologies, Inc., Littleton, CO, 2002.*

4.38 Section M.4 of Appendix M, Revision 6 of Application for Amendment No. 5 to the NUHOMS® Certificate of Compliance No. 1004, (TAC NO. L23343).

4.39 "ASHRAE Handbook, Fundamentals" – SI Edition, 1997

4.40 White, F. M., Fluid Mechanics, 2nd Edition, McGraw-Hill, 1986.

4.41 Incropera, F. P., D. P. DeWitt, *Fundamentals of Heat and Mass Transfer*, 3rd Edition, Wiley, 1990.

4.42 Cavanaugh et al., *Guide to Thermal Properties of Concrete and Masonry Systems,* Reported by ACI Committee 122, Report # ACI 122R-02, American Concrete Institute, Detroit, MI, 2002.

4.43 Transnuclear, Inc., TN-68 Dry Storage Cask Final Safety Analysis Report, Revision 0, Hawthorne, NY, 2000 (Docket 72-1027).

4.44 FLUENT™, Version 5.6, Fluent Inc., Lebanon, NH, 2003.

4.45 ICEPAK™, Version 4.08, Fluent Inc., Lebanon, NH, 2003.

4.46 TN Calculation, NUH32PT.0414, Rev. 1, "Validation of FLUENT™/ICEPAK™ for Convective Flow in Enclosures."

4.47 Perry, Chilton, et al, "Chemical Engineer's Handbook," 5th Edition, 1973.

4.48 "Thermal Testing of the NUHOMS® Horizontal Storage Module, Model HSM-H," Transnuclear Report No. E-21625, Revision 1.

4.49 Misumi, Toshiyuki, & Suzuki, Koji, & Kitamura, Kenzo, *Fluid Flow and Heat Transfer of Natural Convection Around Large Horizontal Cylinders: Experiments with Air*, Heat Transfer – Asian Research, Volume 32, 2003.

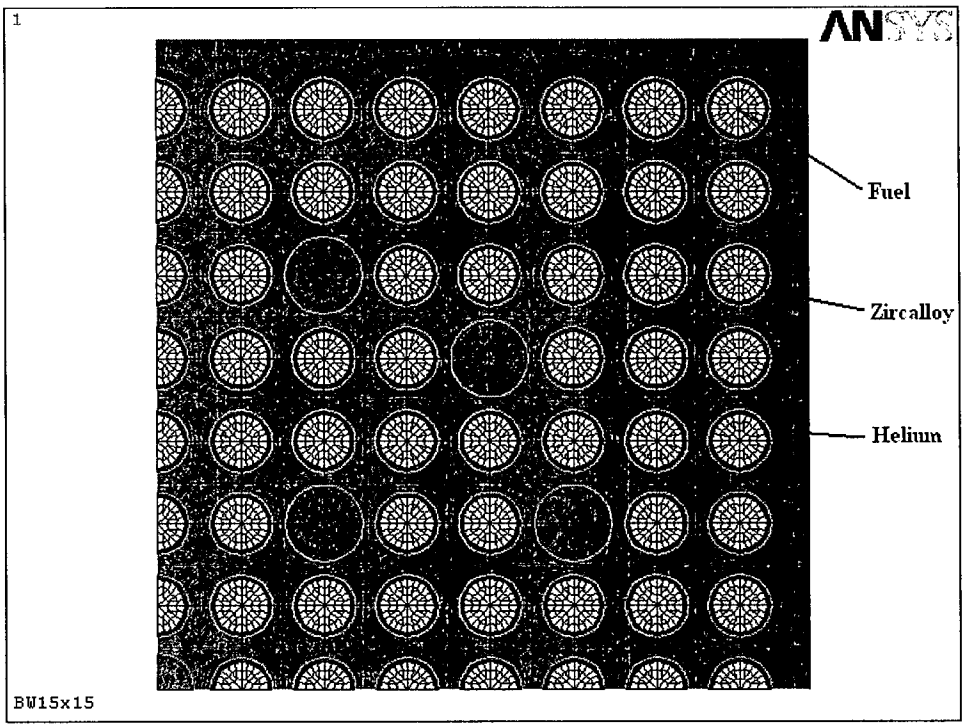

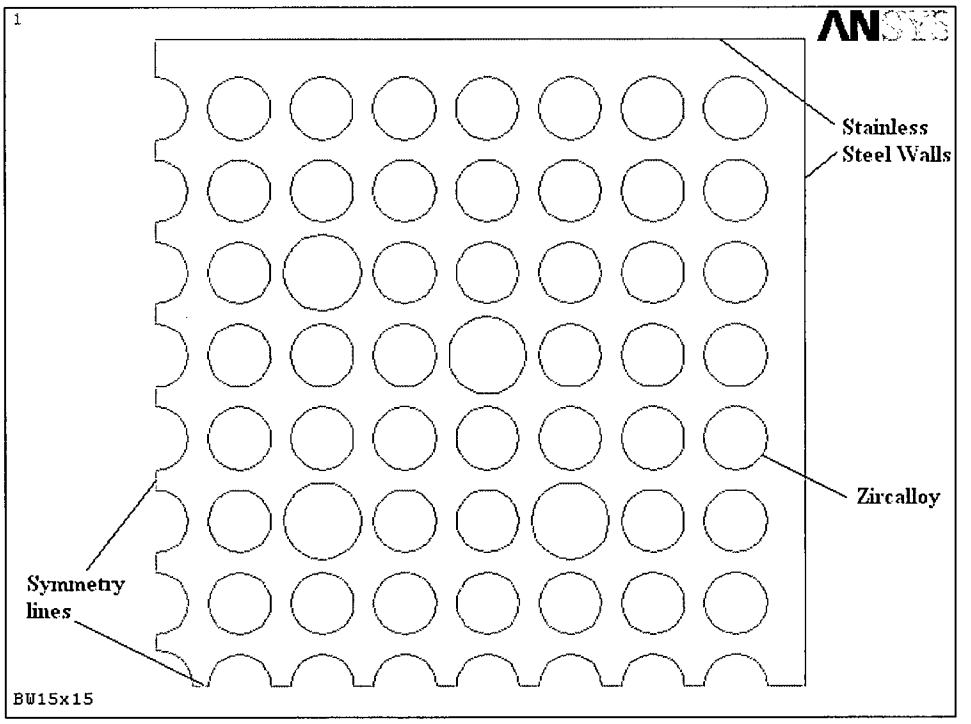

Figure P.4-43 Finite Element Model of B&W 15x15 Fuel Assembly

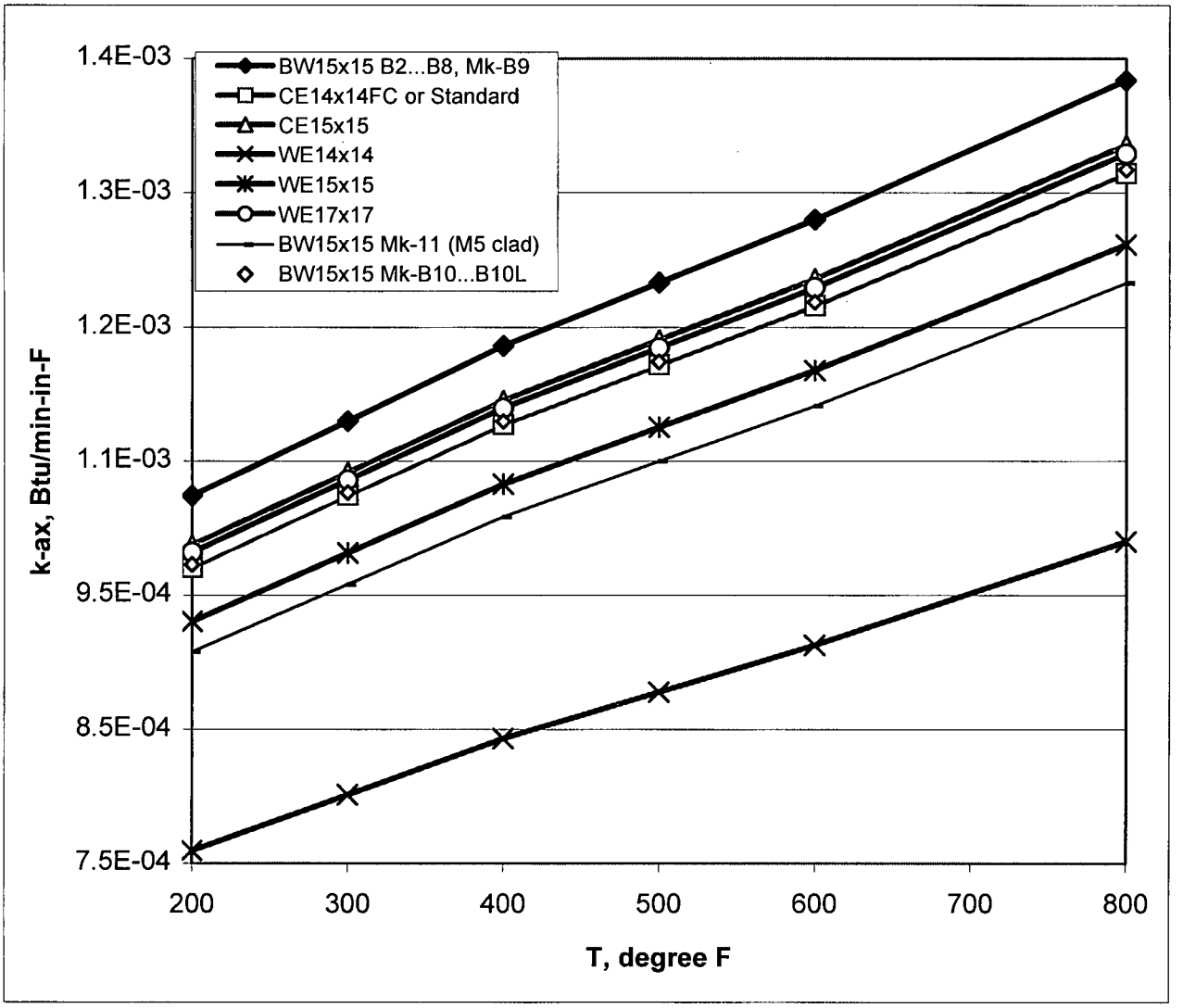

Figure P.4-44 Axial Fuel Effective Thermal Conductivity, All Fuels

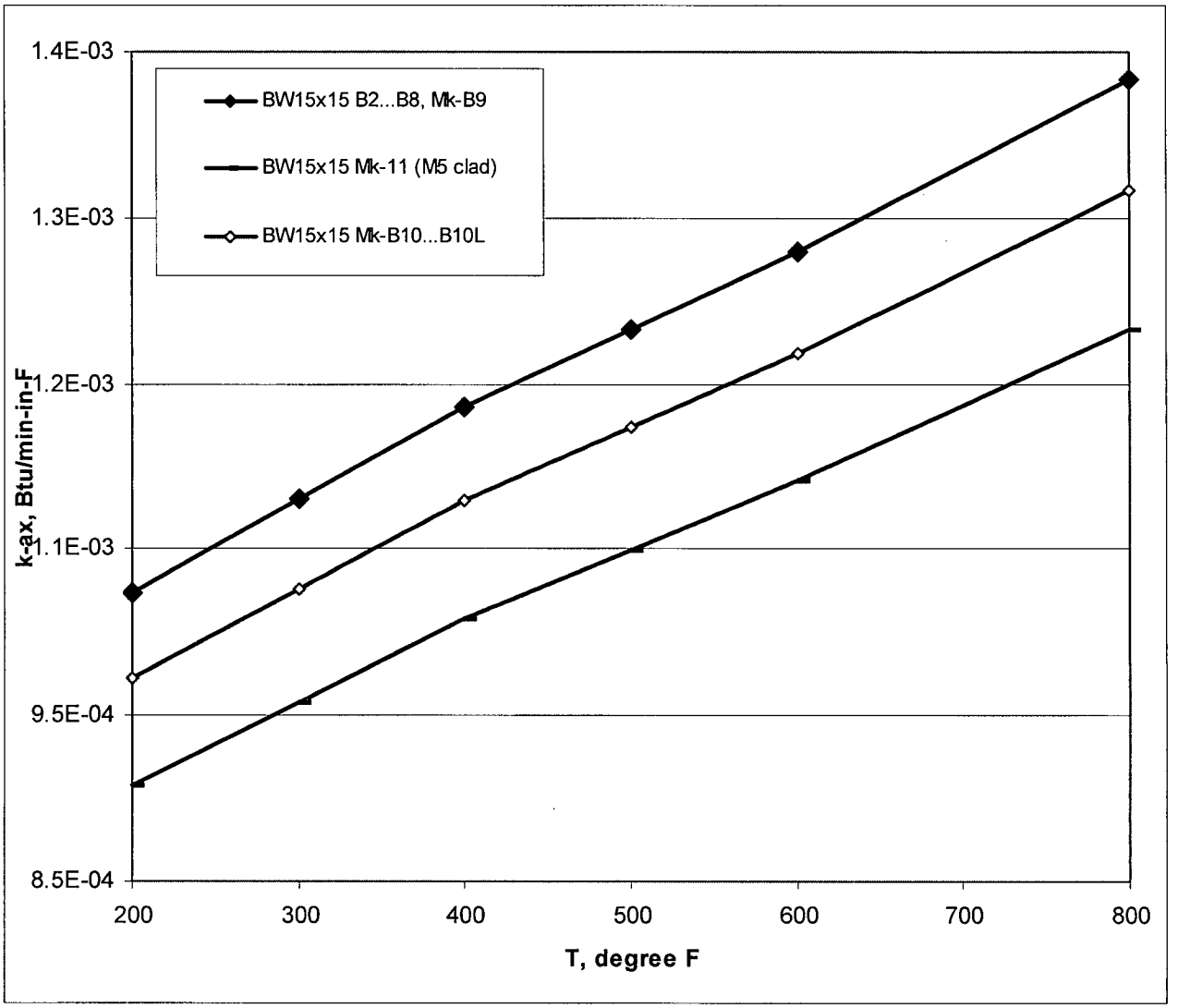

Figure P.4-45 Axial Fuel Effective Thermal Conductivity, B&W 15x15 Fuel Types

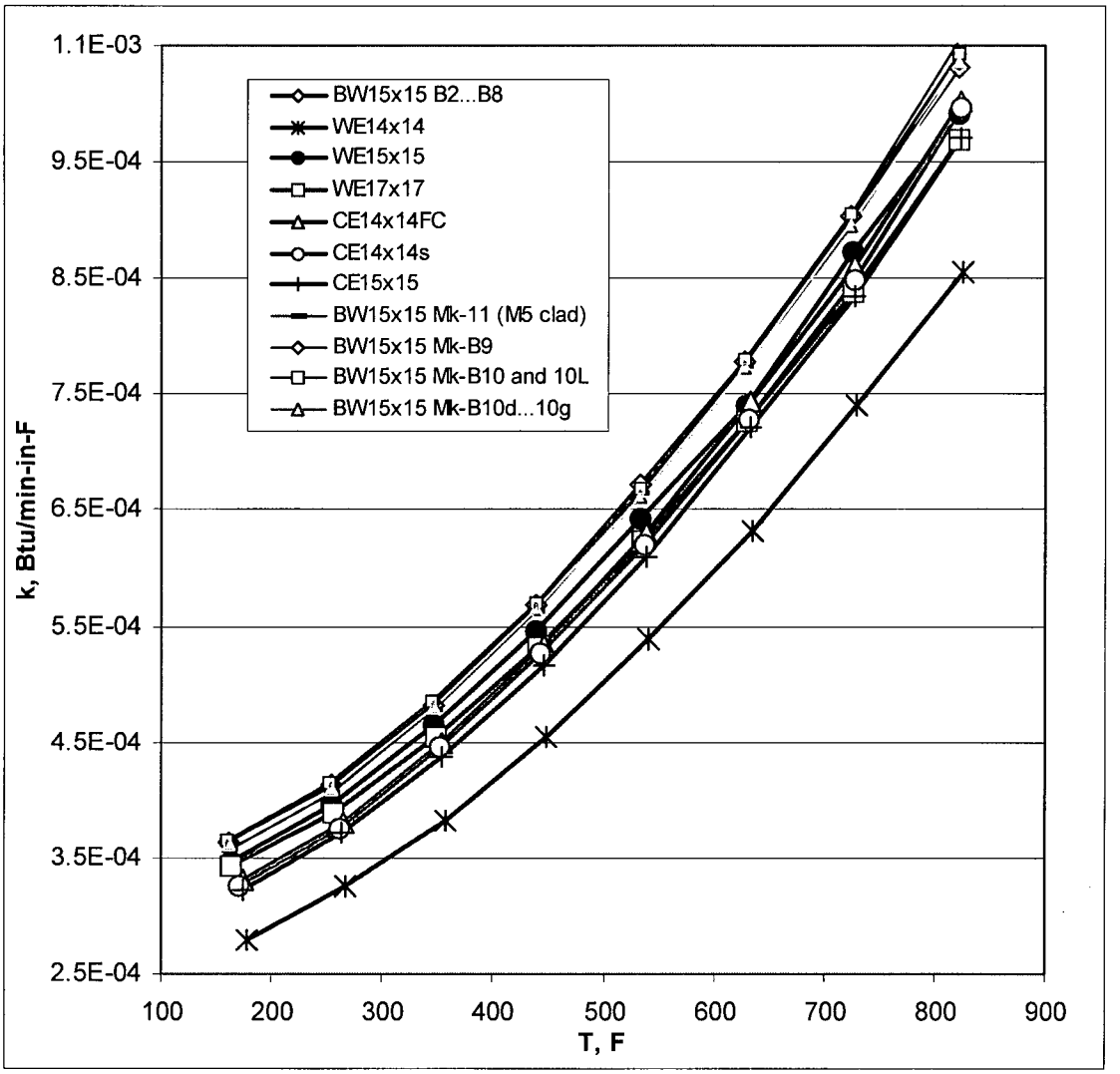

Figure P.4-46 Fuel Transverse Effective Thermal Conductivity in Helium, All Fuels

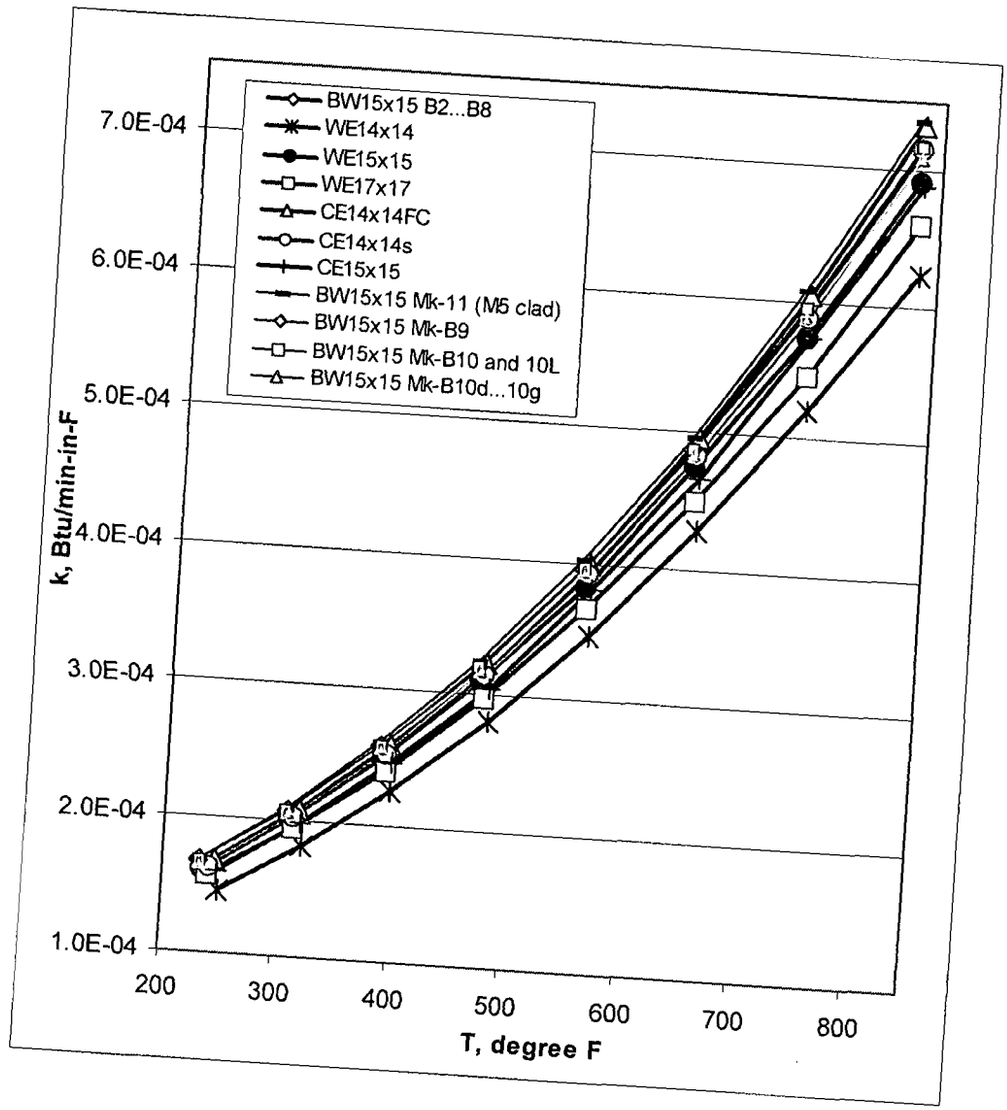

Figure P.4-47 Fuel Transverse Effective Thermal Conductivity in Vacuum, All Fuels

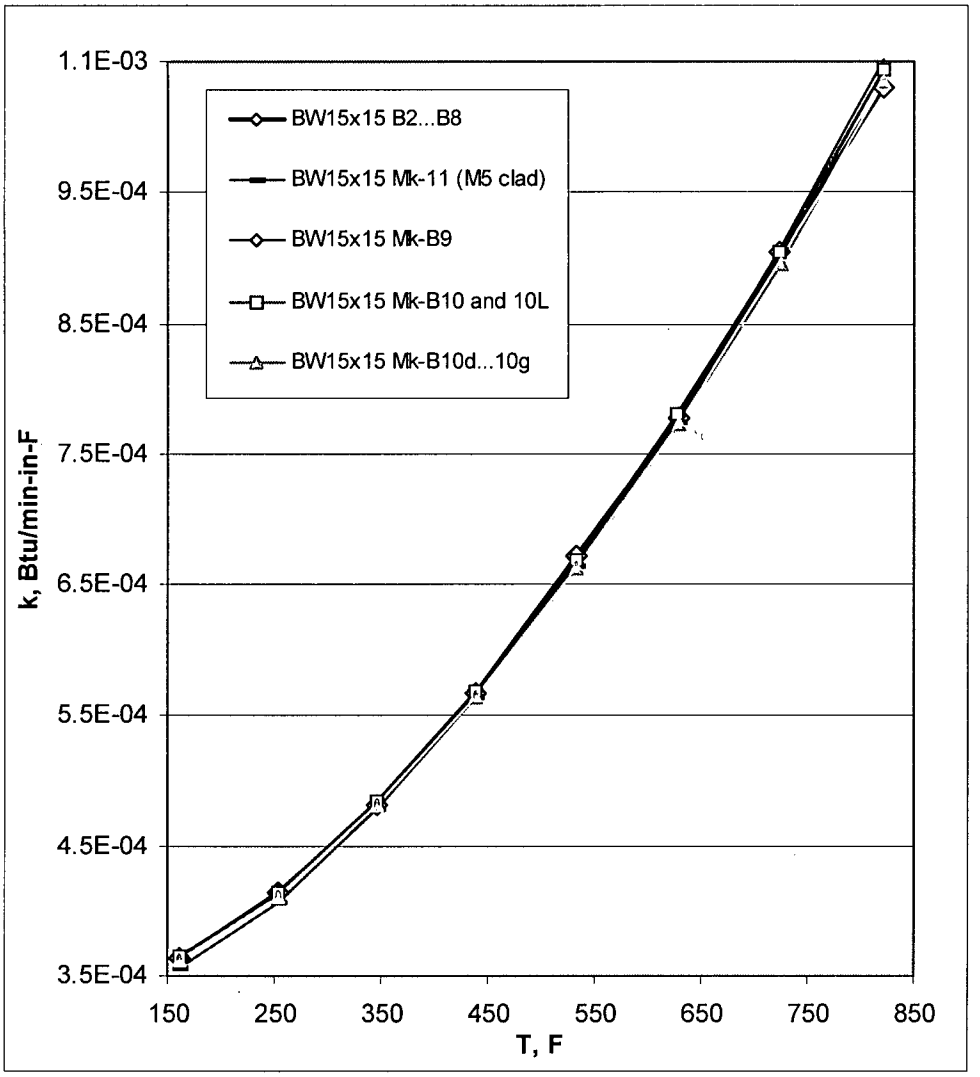

Figure P.4-48 Fuel Transverse Effective Thermal Conductivity in Helium, B&W 15x15 Fuels

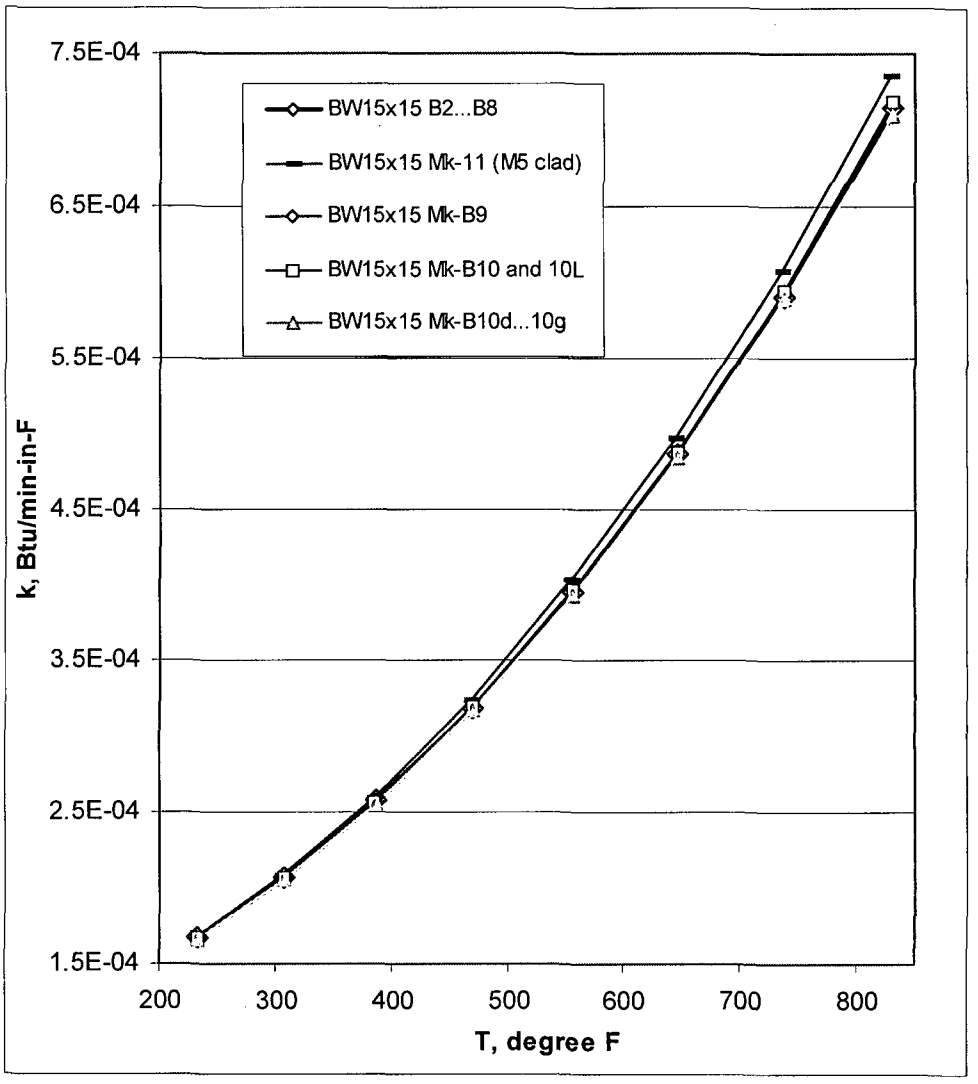

Figure P.4-49 Fuel Transverse Effective Thermal Conductivity in Vacuum, B&W 15x15 Fuels

T.4.2 Summary of Thermal Properties of Materials

The analyses performed herein use interpolated values where appropriate for intermediate temperatures. The interpolation assumes a linear relationship between the reported values. The use of linear interpolation between temperature values in the tables for determining intermediate value of property is justified by the near-linear behavior as a function of temperature for the range of interest.

The emissivities of the different materials used in the analyses are provided in the following table.

Component	Material	Fuel Assembly Effective Properties	TC and DSC Thermal Analysis	HSM-H Thermal Analysis
Fuel cladding	Zircaloy	0.74	-	-
Fuel compartment wall	Stainless steel	0.2	-	-
HSM roof and walls	Concrete	-	-	0.9
Heat Shield	Stainless steel	-	-	0.46(1)
Support structure	Carbon steel	-	-	0.55
DSC shell	Stainless steel	-	0.6	0.6
TC inner shell		-	0.6	-
Structural shell inner surface		-	0.6	-
TC exterior		-	0.6, 0.8(2)	-
TC top and bottom forgings		-	0.46(3)	-

Notes:
1. Used for surfaces of the side and top heat shields based on test report,
2. Used for all exterior surfaces of the cask during and after the 15-minute fire accident to account for the potential oxidation and sooting of the surfaces,
3. Used for the machined surfaces of the top and bottom forgings of the cask.

The tables below provide the thermal properties of materials used in the analysis of the NUHOMS®-61BTH DSC.

The effective thermal properties are the lowest calculated values among the various BWR fuel assembly types that may be stored in 61BTH DSC as described in Section T.4.8.

1. **Bounding BWR Fuel with Helium Backfill (from Section T.4.8)**

Temperature (°F)	Transverse Conductivity (Btu/min-in-°F)	Axial Conductivity (Btu/min-in-°F)	Density (lb_m/in^3)	Specific Heat (Btu/lb_m-°F)
200	2.618E-04	6.700E-04	0.103	0.0575
300	3.021E-04			
400	3.520E-04			
500	4.104E-04			
600	4.756E-04			
700	5.468E-04			
800	6.250E-04			

2. **Bounding BWR Fuel in Vacuum (from Section T.4.8)**

Temperature (°F)	Transverse Conductivity (Btu/min-in-°F)	Axial Conductivity (Btu/min-in-°F)	Density (lb_m/in^3)	Specific Heat (Btu/lb_m-°F)
200	8.693E-05	6.700E-04	0.103	0.0575
300	1.137E-04			
400	1.460E-04			
500	1.842E-04			
600	2.257E-04			
700	2.736E-04			
800	3.295E-04			

3. **Zircaloy [4.8]**

Temperature (°F)	Conductivity (Btu/min-in-°F)	Density (lb_m/in^3)	Specific Heat (Btu/lb_m-°F)
All	0.0100	0.237	0.0657

4. **UO_2 Fuel Pellet [4.8]**

Temperature (°F)	Conductivity (Btu/min-in-°F	Density (lb_m/in^3)	Specific Heat (Btu/lb_m-°F)
All	2.210E-3	0.396	0.05

Modulus of Elasticity, E (psi) = 11.1 x10^6 [from Figure 4 of Reference [4.7]]
Coefficient of thermal expansion, α, (in/in/°F) = 3.73 x 10-6 [4.8]
Poisson's Ratio, ν, = 0.38 [4.9]
Yield Stress (irradiated), Sy, = 50,500 psi [4.10] [4.7]

The fuel cladding is evaluated as a hollow cylinder with an outer surface temperature of T (50°F), and the inner surface temperature of T+ΔT (750°F) using Reference [4.10] equations. The maximum thermal stress in the fuel cladding due to the temperature gradient during reflooding is calculated as follows:

The maximum circumferential stress at the outer surface is given by:

$$\sigma_t = \frac{\Delta T * \alpha \cdot E}{2(1-\nu)\log_e(c/b)} * (1 - \frac{2 * b^2}{(c^2 - b^2)} * \log_e c/b)$$

The maximum circumferential stress at the inner surface is given by:

$$\sigma_t = \frac{\Delta T * \alpha \cdot E}{2(1-\nu)\log_e(c/b)} * (1 - \frac{2 * c^2}{(c^2 - b^2)} * \log_e c/b)$$

The maximum stresses are calculated as 22,420 psi (outer surface) and 24,325 psi (inner surface). Based on the results of the thermal stress analysis, these stresses in the cladding during reflood are much less than the yield stress of 50,500 psi [4.7]. Therefore, cladding integrity is maintained during reflood operations.

Therefore, no cladding damage is expected due to the reflood event. This is also substantiated by the operating experience gained with the loading and unloading of transportation packages like IF-300 [4.6] which show that fuel cladding integrity is maintained during these operations and fuel handling and retrieval is not impacted.

T.4.8 Determination of Effective Thermal Properties of the Fuel, Basket and Air Within the HSM-H Closed Cavity

This section presents the methodology and determines the effective thermal conductivity, specific heat and density for the fuels to be stored within NUHOMS®-61BTH DSC with helium backfill and vacuum for use in the analysis of the thermal performance of the NUHOMS®-61BTH DSC.

This section also determines the effective thermal conductivity, density and specific heat load of the 61BTH DSC basket for use in the transient thermal analysis in Sections T.4.4 and T.4.5.

T.4.8.1 Determination of Bounding Effective Fuel Thermal Conductivity

T.4.8.1.1 Fuel Assemblies Evaluated

The fuel assemblies that are considered for storage in the NUHOMS® 61BTH DSC, including the design data for each fuel assemblies, are listed in Section T.2. This section includes calculation of the bounding properties among fuels to store in the 61BTH DSC with maximum total decay heat per DSC up to 31.2 kW.

T.4.8.1.2 Summary of Thermal Properties of Materials

The thermal conductivity and specific heat values of Zircaloy, UO_2 pellets, and Helium are presented in Section T.4.2. The emissivity of Zircaloy is also presented in Section T.4.2.

T.4.8.1.3 Calculation of Fuel Axial Effective Thermal Conductivity

The axial fuel conductivity is assumed to be limited to the cladding conductivity weighted by its fractional area as required in NUREG 1536 [4.5].

$$K_{axl} = (K_{zirc})(A_{zirc}/A_{eff}) \qquad (1)$$

K_{zirc} = Conductivity of Zircaloy
A_{eff} = (6") x (6") = 36 in^2
A_{zirc} = Cross section area of Zircaloy cladding in the fuel assembly

Equation (1) is used to calculate axial effective conductivity for the fuel assembly types listed in Section T.2.

T.4.8.1.4 Calculation of Fuel Transverse Effective Thermal Conductivity

The transverse fuel effective conductivity is determined by creating a two-dimensional finite element model of the fuel assembly centered within a fuel compartment. The outer surfaces, representing the fuel compartment tube walls, are held at a constant temperature and heat generating boundary condition is applied to the fuel pellets within the model. A maximum fuel assembly temperature is

then determined. The isotropic effective thermal conductivity of a heat generating square, such as the fuel assembly, can be calculated as described in Reference [4.16].

$$K_{eff} = 0.29468 \times \frac{Q'''a^2}{T_c - T_o} \qquad (2)$$

where:

Q''' = heat load per unit volume of fuel assembly (Btu/hr-in^3),
a = half width of fuel compartment opening = 6 / 2 = 3",
T_c = maximum temperature of fuel assembly (°F),
T_o = compartment wall temperature (°F).

with:

$$Q''' = \frac{Q}{4a^2 L_a} \qquad (3)$$

where:

Q = decay heat load per fuel assembly,
L_a = active fuel length

In determining the temperature dependent effective fuel conductivities, an average temperature, equal to $(T_c + T_o)/2$, is used for the fuel temperature.

2-D finite element models of each fuel assembly representing a quarter of the fuel assembly were modeled within ANSYS [4.22]. Plane 55 elements were used to model components such as the fuel pellets, fuel cladding, and the helium back fill gas. The gap between the fuel cladding and the fuel pellets is also included in the model.

Heat generated in the fuel pellets dissipates by conduction and radiation to the fuel compartment walls. Convection is not considered in the model. Radiation between the fuel rods, guide tubes, and basket walls was simulated using the radiation super-element processor (/AUX12). LINK32 elements were used for modeling of radiating surfaces in creating the radiation super-element and were unselected prior to the solution of the model. The compartment walls are not modeled as a solid entity. Only the LINK32 elements aligned with the outermost nodes of the model (not on symmetry lines) are given the emissivity of the compartment walls.

The emissivity of stainless steel (0.46) was applied to the LINK elements on fuel compartment tube walls. To eliminate the radiation heat transfer across the symmetry lines, the link elements on symmetry lines were given a very low emissivity (0.001).

The FANP9 9x9-2 fuel assembly finite element model is shown in Figure T.4-35 as a typical model for all the fuel types considered.

Since a quarter of fuel assembly is modeled in each case, the reaction solution after solving the 2D model is equal to the heat generated per unit length of the active fuel divided by four.

$$Q_{react} = \frac{Q}{4L_a} \qquad (4)$$

Substitution of equations (3) and (4) in equation (2) gives:

$$K_{eff} = 0.29468 \times \frac{Q_{react}}{(T_c - T_o)} \qquad (5)$$

Equation (5) is used to calculate the transverse effective fuel conductivity for each fuel assembly model.

The heat generating boundary conditions for each fuel assembly is calculated as shown in equation 6.

$$dhl = \frac{Q/N}{n\left(\frac{\pi}{4}d_p^{\,2}\right)L_a} \qquad (6)$$

dhl = Heat generating boundary condition, Btu/min-in-°F
Q = Total decay heat load, Btu/min
N = Number of assemblies, 61
n = Number of fuel rods
d_p = Pellet outer diameter, in
L_a = Active fuel length, in

The models were run with a series of isothermal boundary conditions applied to the nodes representing the fuel compartment walls. The symmetry lines going through the center of the fuel assembly are kept at the adiabatic boundary conditions.

T.4.8.1.5 Results

The Siemens QFA 9x9 assembly has the minimum (bounding) axial conductivity. Backfill gas property does not have any effect on the axial effective fuel conductivity. Therefore, identical axial effective fuel conductivity values can be used for helium and vacuum conditions.

The calculated transverse conductivities for fuels to store in the 61BTH DSC are presented in Figure T.4-36 for a helium environment. As shown herein, the FANP9 9 x 9-2 assembly has the (bounding) minimum transverse conductivity. The bounding transverse effective conductivity values for fuels to store in the 61BTH DSC are listed in Section T.4.2.

T.4.8.2 Calculation of Fuel Effective Specific Heat and Density

This section presents the calculation of the fuel effective specific heat and density used in the transient thermal analyses.

Volume average density and weight average specific heat are calculated to determine the effective density and specific heat for the fuel assembly.

The equations to determine the fuel effective density ρ_{eff} and specific heat $C_{p\,eff}$ are shown below.

$$\rho_{eff} = \frac{\sum \rho_i V_i}{V_{assembly}} = \frac{\rho_{UO_2}\ V_{UO_2} + \rho_{Zr}\ V_{Zr}}{4a^2 L_a}$$

$$C_{p,eff} = \frac{\sum \rho_i V_i C_{Pi}}{\sum \rho_i V_i} = \frac{\rho_{UO_2}\ V_{UO_2}\ C_{P,UO_2} + \rho_{Zr}\ V_{Zr}\ C_{P,Zr}}{\rho_{UO_2}\ V_{UO_2} + \rho_{Zr}\ V_{Zr}}$$

where:

ρ_i, $C_{p,i}$, V_i = density, specific heat, and volume of component,
L_a = active fuel length, and
a = half of compartment width.

The properties of Zircaloy and UO_2 are provided in Section T.4.2.

The calculated minimum (bounding) values of fuel effective specific heat and fuel effective density for fuel to store in the 61BTH DSC are summarized in Section T.4.2.

T.4.8.3 61BTH DSC Basket Effective Thermal Properties

The 61BTH DSC basket effective density, thermal conductivity and specific heat are calculated for use in the transient analyses of the 61BTH DSC in the OS197/OS197H/OS197FC-B transfer cask and in the HSM or HSM-H. The calculation of these thermal effective properties is based on the DSC component weights.

The 61BTH DSC effective density $\rho_{eff\ DSC\ basket}$, and specific heat $c_{p\ eff\ DSC\ basket}$ are calculated as volumetric and weight average values, respectively.

The effective transverse thermal conductivity is determined by theoretical solution for conduction in an infinite cylinder with uniform heat generation [4.28]:

$$k_{eff-basket} = \frac{Q}{4\pi \cdot L \cdot (T_c - T_s)}$$

where Q is total heat load, W
L is cylinder (DSC cavity) length, m
T_C is temperature at the cylinder center, $°C$
T_S is temperature at the cylinder surface, $°C$

The effective transverse thermal conductivities of the 61BTH DSC basket $k_{eff\text{-}basket}$ are calculated for the Type 1 and Type 2 DSCs, using the corresponding ANSYS models.

The heat generation is applied to the fuel assemblies uniformly without a peaking factor. The temperatures from 100°F to 800°F are applied uniformly to the DSC shell.

An average, $(T_s+T_c)/2$, is used as the reference temperature, for which $k_{eff\text{-}basket}$ is reported.

The bounding radial and axial thermal conductivity values for 61BTH DSCs are shown in Section T.4.2.

T.4.8.4 Effective Air Conductivity in the HSM-H Closed Cavity

During blockage of the inlet and outlet vents, the air within the HSM-H is trapped. The convection heat transfer under these circumstances reduces to free convection in closed cavities. For conservatism, no convection is considered within the HSM-H cavity during blockage of the vents.

T.4.9 References

4.1 Report, "Topical Report on Actinide-Only Burnup Credit for PWR Spent Nuclear Fuel Packages," Office of Civilian Radioactive Waste Management, DOE/RW-0472, Revision 2, September 1998.

4.2 ASME Boiler and Pressure Vessel Code, Section II, Part D, Properties, 1998, including 2000 addenda.

4.3 Roshenow, W. M., J. P. Hartnett, and Y. I. Cho, "Handbook of Heat Transfer," 3rd Edition, 1998.

4.4 Bolz, R. E., G. L. Tuve, "CRC Handbook of Tables for Applied Engineering Science," 2nd Edition, 1973. Transfer, McGraw Hill, 1989.

4.5 NUREG-1536, "Standard Review Plan for Dry Cask Storage Systems," January 1997.

4.6 Consolidated Safety Analysis Report for IF-300 Shipping Cask, CoC 9001.

4.7 Chun, Ramsey; Witte, Monika; Schwartz, Martin, "Dynamic Impact Effects on Spent Fuel Assemblies," Lawrence Livermore National Laboratory, Report UCID-21246, October, 1987.

4.8 NUREG/CR-0497, "MATPRO-Version 11: "A Handbook of Materials Properties for Use in the Analysis of Light Water Reactor, Fuel Rod Behavior," EG&G, Inc. February, 1979.

4.9 Glasstone, S., Seasonske, A., "Nuclear Reactor Engineering," Third Edition, 1981.

4.10 Young, W.C., "Roark's Formulas for Stress and Strain," Sixth Edition, McGraw Hill.

4.11 Kreith, "The CRC Handbook of Thermal Engineering," 2000.

4.12 GESC NS-3, NAC International, Atlanta Corporate Headquarters (Test Report NS-3-001, while BISCO Products, Inc.).

4.13 Rohsenow, Hartnett, "Handbook of Heat Transfer Fundamentals," 2nd Edition, 1985.

4.14 Roth, A., "Vacuum Technology," 2nd Edition, 1982.

4.15 Interim Staff Guidance No. 11, Revision 3, "Cladding Considerations for the Transportation and Storage of Spent Fuel," November 17, 2003.

4.16 SAND90 2806, Sanders, T. L., et al., "A Method for Determining the Spent Fuel Contribution to Transport Cask Containment Requirements," TTC1019, UC 820, November 1992.

4.17 Not used.

4.18 Incropera and DeWitt, Handbook of Heat And Mass Transfer Fundamentals, 5th edition, Wiley Publishers, 2002, Table A.6, pp 924.

4.19 Bentz, "A Computer Model to Predict the Surface Temperature and Time-of-wetness of Concrete Pavements and Bridge Decks," Report # NISTIR 6551, National Institute of Standards and Technology, 2000.

4.20 Zoldners, "Thermal Properties of Concrete under Sustained Elevated Temperatures," ACI Publications, Paper SP 25-1, American Concrete Institute, Detroit, MI, 1970, Cavanaugh, Guide to Thermal Properties of Concrete and Masonry Systems, Reported by ACI Committee 122, Report #ACI 122R-02, American Concrete Institute, Detroit, MI, 2002.

4.21 Siegel, Howell, "Thermal Radiation Heat Transfer," 4th Edition, 2002.

4.22 ANSYS 8.1 Computer Code and Online User's Manuals.

4.23 NRC, Code of Federal Regulations, Part 71, "Packaging and Transportation of Radioactive Material," 2003.

4.24 I.E. Idelchik, "Handbook of Hydraulic Resistance," 3rd Edition, 1994.

4.25 David R. Lide, "CRC Handbook of Chemistry and Physics," 83rd edition, 2002-2003, CRC Press.

4.26 SINDA/FLUINT™, "Systems Improved Numerical Differencing Analyzer and Fluid Integrator," Version 4.7, Cullimore & Ring Technologies, Inc., Littleton, CO, 2004.

4.27 Thermal Desktop™, Version 4.7, Cullimore & Ring Technologies, Inc., Littleton, CO, 2004.

4.28 Incropera, F. P. M. D P. DeWitt, "Fundamentals of Heat and Mass Transfer," 3rd Edition, Wiley, 1990.

4.29 Not used.

4.30 "Thermal Testing of the NUHOMS® Horizontal Storage Module, Model HSM-H," Transnuclear Report No. E-21625, Revision 1.

4.31 Misumi, Toshiyuki, & Suzuki, Koji, & Kitamura, Kenzo, "Fluid Flow and Heat Transfer of Natural Convection Around Large Horizontal Cylinders: Experiments with Air, Heat Transfer – Asian Research," Volume 32, 2003.

Y.4.2 Summary of Thermal Properties of Materials

The analyses performed herein use interpolated values where appropriate for intermediate temperatures. The interpolation assumes a linear relationship between the reported values. The use of linear interpolation between temperature values in the tables for determining intermediate value of property is justified by the near-linear behavior as a function of temperature for the range of interest.

The emissivities of the different materials used in the analyses are provided in the following table.

1. Surface Emissivity

Component	Material	Fuel Assembly Effective Properties	HSM-H Thermal Analysis
Fuel cladding	zircaloy	0.74	-
Fuel compartment wall	stainless steel	0.2	-
HSM roof and walls	concrete	-	0.9
Heat shield	stainless steel	-	0.46 [1]
Support structure	carbon steel	-	0.55
DSC shell	stainless steel	-	0.587

[1] Used for surfaces of the side and top heat shields based on test report.

The tables below provide the thermal properties of materials used in the analysis of the NUHOMS®-69BTH DSC.

The effective thermal properties are the lowest calculated values among the various BWR fuel assembly types that may be stored in 69BTH DSC as described in Section Y.4.9.

2. Bounding Effective Properties for BWR Fuel Assembly

(See Section Y.4.9 for calculation of effective fuel properties)

Temperature (°F)	Transverse Conductivity (Btu/hr-in-°F)	Axial Conductivity (Btu/hr-in-°F)	Specific Heat (Btu/lb$_m$-°F)	Density (lb$_m$/in^3)
200	0.0157	0.0402	0.0575	0.103
300	0.0181			
400	0.0210			
500	0.0245			
600	0.0282			
700	0.0324			
800	0.0369			

Y.4.9 Determination of Effective Thermal Properties of the Fuel Assemblies

This section presents the methodologies and determines the bounding effective thermal conductivity, specific heat, and density of the fuel assemblies for use in the thermal analysis of the NUHOMS® 69BTH DSC.

The fuel assemblies that are considered for storage in the 69BTH DSC, including the design data for each fuel assembly, are listed in Section Y.2. Most of these fuel assemblies are previously studied in Appendix T, Section T.4.8 for 61BTH DSC. The characteristics of the fuel assemblies studied in Appendix T are identical to those listed in Section Y.2 for 69BTH DSC. Based on the study in Appendix T, FANP 9x9-2 fuel assembly has the bounding transverse effective conductivity and fuel assembly Siemens QFA has the bounding axial effective conductivity, bounding effective density, and bounding effective specific heat. The transverse effective conductivities of the bounding FANP 9x9-2 fuel assembly from Appendix T, Section T.4.8 are recalculated using irradiated UO_2 properties and listed in Section Y.4.2, Table 2.

The fuel assemblies listed in Section Y.2 for 69BTH DSC that are not studied in Appendix T, Section T.4.8 are:

- FANP 9x9, TN ID 9x9-81;
- LaCrosse, TN ID 10x10-100;
- SVEA fuel assemblies;
- MOX fuel assemblies.

The effective properties for these fuel assemblies are evaluated in this section to determine the bounding effective properties to use in the 69BTH DSC thermal analysis. The effective properties in Appendix T, Section T.4.8 are calculated for stainless steel fuel compartments with a nominal opening size of 6″. The same compartment material and size are considered in evaluation of the effective properties in this analysis.

Effective properties for the above four fuel assemblies are calculated using the methodologies and material properties approved in Appendices M, P, and T. For the LaCrosse fuel assembly, a stainless steel cladding emissivity of 0.70 is considered in this evaluation. Perry in [4.5], Table 10-17, gives an emissivity between 0.62 and 0.82 for steel/stainless steel sheets heated or covered with shiny oxide layer. The assumed emissivity for the stainless steel cladding of the LaCrosse fuel assembly remain with this range and is therefore acceptable.

Y.4.9.1 Effective Properties for Fuel Assembly FANP 9x9

The characteristics of fuel assembly FANP 9x9 (TN ID 9x9-81), shown in Section Y.2, are identical to those for the fuel assembly FANP 9x9-2 (TN ID 9x9-79/2) except for the number of fuel rods. The number of fuel rods for fuel assembly FANP 9x9 varies between 72 and 81 while fuel assembly FANP 9x9-2 has 79 fuel rods.

Due to the higher number of fuel rods in FANP 9x9 in comparison to FANP 9x9-2, the effective axial conductivity, density, and specific heat for FANP 9x9 is higher than those for FANP 9x9-2 and does not represent the bounding minimum values.

The two-dimensional finite element model used to determine the transverse effective conductivity of the fuel assembly FANP 9x9 is shown in the following figure. A correction factor of 1.0262 is used to increase the heat generation rate in the 2D model. This correction factor compensates the imperfection of the pellet cross section area in the model.

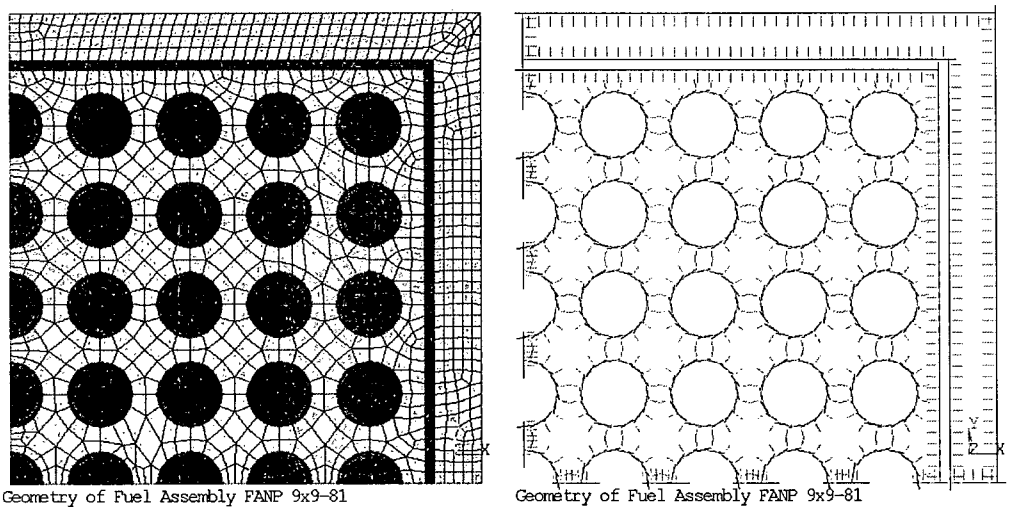

Quarter Symmetric FE Model for Fuel Assembly FANP 9x9

Y.4.9.2 Effective Properties for the LaCrosse Fuel Assembly

The LaCrosse fuel assembly consists of stainless steel cladding as indicated in Section Y.2. This evaluation uses a fuel cladding temperature limit of 752 °F (400 °C) for stainless steel cladding, which is identical to the limit for the zircaloy cladding as noted in NUREG-1536 [4.1].

The two-dimensional finite element model used to determine the transverse effective conductivity of the LaCrosse fuel assembly is shown in the following figure. A correction factor of 1.0262 is used to increase the heat generation rate in the 2D model. This correction factor compensates the imperfection of the pellet cross section area in the model.

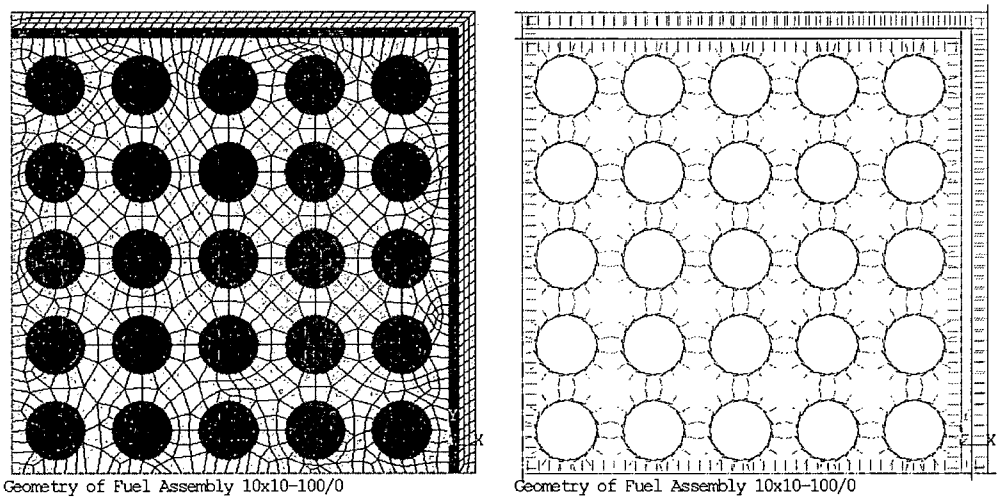

Quarter Symmetric FE Model for Fuel Assembly LaCrosse

Y.4.9.3 Effective Properties for SVEA Fuel Assemblies

SVEA fuel assemblies are described in detail in [4.14]. Based on [4.14], the SVEA fuel assemblies provide larger heat transfer areas and lower heat fluxes in comparison to conventional BWR fuel assemblies with similar fuel rod arrays. In addition, the SVEA fuel assemblies consist of sub-channels which arrange the fuel rods closer to the periphery of the assembly. These factors result in higher transverse effective conductivity for these fuel types.

The sub-channels in SVEA fuel assemblies provide also more zircaloy in comparison to conventional BWR fuel assemblies with similar fuel rod arrays. Therefore, the axial effective conductivity, effective density, and effective specific heat of the SVEA fuel assemblies are higher than those for comparable conventional BWR fuel assemblies.

To verify that the effective properties of SVEA fuel assemblies are bounded by comparable conventional BWR fuel assemblies, the effective properties of fuel assembly SVEA-92 (TN ID ABB-10-2) with four 5x5 sub-bundles are evaluated in this section.

The two-dimensional finite element model of the fuel assembly SVEA-92 used to determine the transverse effective conductivity is shown in the following figure. A correction factor of 1.0262 is used to increase the heat generation rate in the 2D model. This correction factor compensates the imperfection of the pellet cross section area in the model.

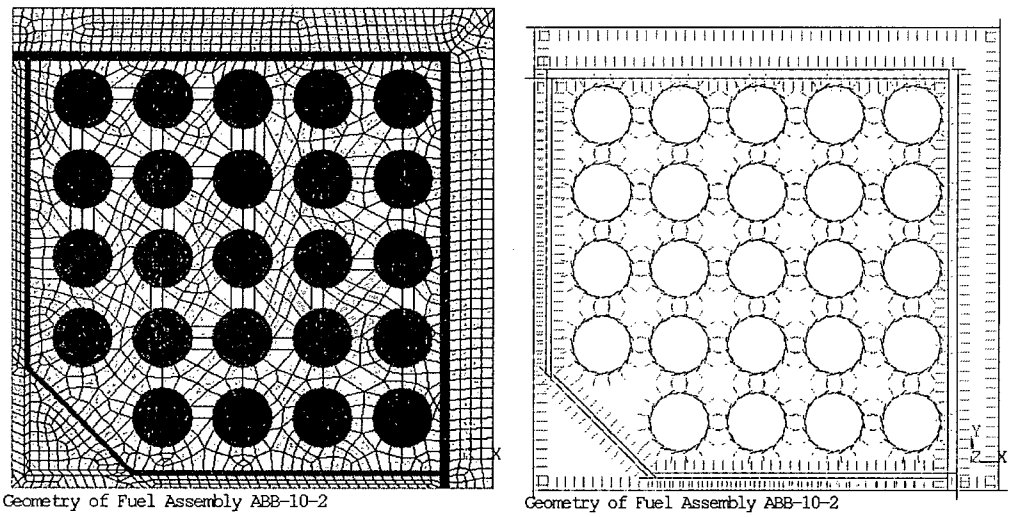

Quarter Symmetric FE Model for Fuel Assembly SVEA-92

Y.4.9.4 Effective Properties for MOX Fuel Assemblies

The MOX fuel assemblies are used to replace fuel assemblies with UO_2 pellets. The characteristics of the MOX fuel assemblies are almost identical to the fuel assemblies they are replacing. The only significant difference in regard to the effective properties is the conductivity of the MOX fuel pellets versus the conductivity of UO_2 pellets. Therefore, the effective axial conductivity, specific heat and density of the MOX fuel assemblies remain the same as the UO_2 fuel assemblies.

The transverse effective conductivity of a MOX fuel assembly is calculated using the model for the bounding FAN 9x9-2 fuel assembly. It is assumed that the reduction of MOX fuel pellet conductivity due to irradiation is the same as for UO_2 such that:

$k_{MOX\ irrd} = k_{MOX\ un\text{-}irrd} \times k_{UO2\ irr} / k_{UO2\ un\text{-}irrd}$.

The thermal conductivity values of irradiated UO_2 based on the bounding maximum allowable burnup of 70 GWd/MTU for BWR fuel assemblies in 69BTH DSC is obtained by interpolation of the data from [4.16] for irradiation temperature ≥1300 K and burnups between 51 and 92 GWd/MTU. The results of irradiated MOX fuel thermal conductivity are summarized below.

Calculation of Irradiated MOX Fuel Thermal Conductivity

T (°F)	$k_{UO2\ un\text{-}irrd}$ [4.11] (Btu/hr-in-°F)	$k_{UO2\ irrd}$ (1) (Btu/hr-in-°F)	$k_{UO2\ irrd}/k_{UO2\ un\text{-}irrd}$	$k_{MOX\ un\text{-}irrd}$ (2) (Btu/hr-in-°F)	$k_{MOX\ irrd}$ (used in analysis) (Btu/hr-in-°F)	$k_{MOX\ irrd}$ [4.15] (Btu/hr-in-°F)
200	3.322E-01	1.69E-01	51%	2.354E-01	**1.201E-01**	-
300	3.023E-01	1.63E-01	54%	2.204E-01	**1.186E-01**	-
400	2.773E-01	1.56E-01	56%	2.078E-01	**1.167E-01**	-
500	2.562E-01	1.49E-01	58%	1.967E-01	**1.143E-01**	-
600	2.381E-01	1.42E-01	60%	1.866E-01	**1.113E-01**	-
700	2.224E-01	1.36E-01	61%	1.785E-01	**1.092E-01**	-
800	2.087E-01	1.30E-01	62%	1.709E-01	**1.067E-01**	1.248E-01

(1) Interpolated values from [4.16] based on bounding maximum burnup of 70 GWd/MTU.
(2) Interpolated values from Table 3.6-2 of [4.19].

The irradiated conductivity for a MOX pellet calculated based on the above assumption is compared to the irradiated conductivity of a MOX pellet taken from ORNL report [4.15] at 800 °F with 4% enrichment and ~5% PuO_2 in the mixed-oxide (UO_2-PuO_2). As shown in the above table, the calculated $k_{MOX\ irrd}$ value is lower than the value given in [4.15]. This comparison verifies that the calculated $k_{MOX\ irrd}$ values provided in the above table can be used conservatively to calculate the transverse effective conductivities for a MOX fuel assembly.

Y.4.9.5 Transverse Effective Conductivity

The results of the two-dimensional models for fuel assemblies FANP 9x9, LaCrosse, SVEA-92, and MOX fuel assemblies are summarized in the following table.

Fuel Assembly Transverse Effective Conductivity

FANP 9x9 (9x9-81)			
Fuel Compartment Wall Temperature (°F)	**Maximum Fuel Temperature (°F)**	**Average Fuel Temperature (°F)**	**Transverse Conductivity $K_{eff, FANP9x9}$ (Btu/hr-in-°F)**
200	228	214	0.0156
300	324	312	0.0184
400	420	410	0.0217
500	517	509	0.0255
600	615	607	0.0299
700	713	706	0.0348
800	811	805	0.0402
LaCrosse (10x10-100/0)			
Fuel Compartment Wall Temperature (°F)	**Maximum Fuel Temperature (°F)**	**Average Fuel Temperature (°F)**	**Transverse Conductivity $K_{eff, LaCrosse}$ (Btu/hr-in-°F)**
200	240	220	0.0194
300	334	317	0.0228
400	429	415	0.0267
500	525	512	0.0313
600	621	611	0.0365
700	719	709	0.0421
800	816	808	0.0483
SVEA-92 (ABB-10-2)			
Fuel Compartment Wall Temperature (°F)	**Maximum Fuel Temperature (°F)**	**Average Fuel Temperature (°F)**	**Transverse Conductivity $K_{eff, SVEA-92}$ (Btu/hr-in-°F)**
100	122	111	0.0199
200	220	210	0.0226
300	317	309	0.0255
400	415	408	0.0289
500	513	507	0.0327
600	612	606	0.0370
MOX Fuel Assembly (FAN 9x9-2)			
Fuel Compartment Wall Temperature (°F)	**Maximum Fuel Temperature (°F)**	**Average Fuel Temperature (°F)**	**Transverse Conductivity $K_{eff, MOX, 9x9-2}$ (Btu/hr-in-°F)**
200	228	214	0.0158
300	324	312	0.0184
400	421	410	0.0213
500	518	509	0.0246
600	616	608	0.0285
700	714	707	0.0325
800	812	806	0.0370

The transverse effective conductivities used in the thermal analysis as listed in Section Y.4.2, Table 2 present lower values in comparison to the transverse effective conductivities for LaCrosse and SVEA-92 fuel assemblies as listed in the above table. The transverse effective listed in Section Y.4.2, Table 2 remain also bounding for FANP 9x9 fuel assemblies except for low operating temperatures below ~315°F (~157°C). For all practical purposes, the operating

temperature of fuel assemblies within the 69BTH DSC is above 315°F. Therefore, the values listed in Section Y.4.2, Table 2 remains the bounding values to be used in the thermal analysis.

The transverse effective conductivities of a FANP 9x9-2 fuel assembly with MOX pellets are compared to the bounding values from Section Y.4.2, Table 2 and listed in the following table.

Transverse K_{eff} for MOX and Bounding Values

Average Fuel Temperature (°F)	Transverse Conductivity $K_{eff, MOX}$ [1] (Btu/hr-in-°F)	Transverse Conductivity $K_{eff, bounding}$ [2] (Btu/hr-in-°F)	$K_{eff, MOX} / K_{eff, bounding}$ (---)
200	0.0155	0.0157	0.99
300	0.0180	0.0181	1.00
400	0.0209	0.0210	1.00
500	0.0243	0.0245	0.99
600	0.0281	0.0282	1.00
700	0.0322	0.0324	0.99
800	0.0367	0.0369	0.99

(1) Interpolated for comparison purpose
(2) Bounding values from Section Y.4.2, Table 2 based on FANP 9x9-2 FA with irradiated UO_2

The above table shows that the transverse fuel effective conductivities for MOX fuel assembly (based on FANP 9x9-2 characteristics) are at most 1% lower than the comparable UO_2 Fuel assembly (FANP 9x9-2), which is the design basis BWR fuel assembly used in 69BTH DSC thermal evaluation. However, this small decrease in effective conductivity for BWR fuel assemblies has negligible effect on 69BTH DSC thermal evaluation. Therefore, using the transverse effective conductivities as listed in Section Y.4.2, Table 2 remains acceptable for thermal analysis of 69BTH DSC.

Y.4.9.6 Axial Effective Conductivity

The axial effective conductivities calculated for fuel assemblies FANP 9x9, LaCrosse, and SVEA-92 are compared to the bounding values from Appendix T, Section T.4.8 in the following table. Since the axial effective conductivity is calculated based on cladding area only, the axial effective conductivities for MOX and UO_2 fuel assemblies are identical.

Fuel Assembly Axial Effective Conductivity

	FANP 9x9 (9x9-81)	LaCrosse (10x10-100/0)	SVEA-92 (ABB-10-2)	
No of fuel rods	81	100	96	
OD fuel rod (in.)	0.424	0.395	0.378	
Clad thickness (in.)	0.03	0.0210	0.0243	
Sub-channel area (in^2)[1]	N/A	N/A	0.59	
Cladding area (in^2)	3.01	2.47	3.18	
Compartment area (in^2)	36.0	36.0	36.0	
Temp (°F)	**$K_{eff,axial}$ (Btu/hr-in-°F)**	**$K_{eff,axial}$ (Btu/hr-in-°F)**	**$K_{eff,axial}$ (Btu/hr-in-°F)**	**Bounding Value[2] $K_{eff,axial}$ (Btu/hr-in-°F)**
70	0.0503	0.0491	0.0532	0.0402
100		0.0497		
200		0.0531		
300		0.0560		
700		0.0674		
1000		0.0748		

(1) The area of sub-channel is determined using the FE model of SVEA-92.
(2) Bounding values are from Appendix T, Section T.4.8

As seen, the axial effective fuel conductivity from Appendix T, Section T.4.8 remains the bounding value to be used in the thermal analysis.

Y.4.9.7 Effective Density and Specific Heat

The effective density (ρ_{eff}) and specific heat ($c_{P,\,eff}$) calculated for fuel assemblies FANP 9x9, LaCrosse, and SVEA-92 are compared to the bounding values from Appendix T, Section T.4.8 in the following table. As discussed in Section Y.4.9.4, the effective density and specific heat for MOX fuel assemblies are equivalent to those for UO_2 fuel assemblies.

Fuel Assembly Effective Density and Specific Heat

	FANP 9x9 (9x9-81)	LaCrosse (10x10-100/0)	SVEA-92 (ABB-10-2)	
No. of fuel rods	96 [1]	81	96	Bounding values[2]
OD fuel rod (in.)	0.395	0.424	0.378	
Clad thickness (in.)	0.0210	0.03	0.0243	
No. of water tubes	4 [1]	0	0.59	
Pellet OD (in.)	0.3465	0.3565	0.3224	
Fuel length (in.)	85	150	150.59	
Cladding area (in^2)	2.47	3.01	3.18	
UO_2 area (in^2)	9.05	8.09	7.84	
Compartment area (in^2)	36.0	36.0	36.0	
Cladding volume (in^3)	210	451	479	
UO_2 volume (in^3)	769	1213	1180	
Compartment volume (in^3)	3060	5400	5421	
$Density_{eff}$ (lbm/in^3)	0.119	0.109	0.107	0.103
$c_{P,\,eff}$ (Btu/lbm-°F)	0.0658	0.0578	0.0579	0.0575

[1] Fuel assembly FANP 9x9 can optionally contain up to four water rods. To determine the lowest possible density and specific heat, four water rods are considered for fuel assembly FA FANP 9x9.

[2] Bounding values are from Appendix T, Section T.4.8.

As seen, the effective density and specific heat from Appendix T, Section T.4.8 remain the bounding values to be used in the thermal analysis.

The effective conductivities along with specific heat and density used for BWR fuel assemblies are summarized in Section Y.4.2, Table 2.

Y.4.10 References

4.1 U.S. NRC, NUREG-1536, "Standard Review Plan for Dry Cask Storage Systems – Final Report," Revision 1, July 2010.

4.2 American Concrete Institute, "Code Requirements for Nuclear Safety Related Concrete Structures (ACI 349-90)," March 1, 1990.

4.3 ASME Boiler and Pressure Vessel Code, Section II, Part D, "Material Properties," 2004, including 2006 addenda.

4.4 Roshenow, Hartnett, Cho, "Handbook of Heat Transfer," 3rd Edition, 1998.

4.5 Perry, Chilton, "Chemical Engineers' Handbook," 5th Edition, 1973.

4.6 Zoldners, "Thermal Properties of Concrete under Sustained Elevated Temperatures," ACI Publications, Paper SP 25-1, American Concrete Institute, Detroit, MI, 1970, Cavanaugh, Guide to Thermal Properties of Concrete and Masonry Systems, Reported by ACI Committee 122, Report #ACI 122R-02, American Concrete Institute, Detroit, MI, 2002.

4.7 Cavanaugh et al., "Guide to Thermal Properties of Concrete and Masonry Systems," Reported by ACI Committee 122, ACI 122 R-02.

4.8 Bentz, "A Computer Model to Predict the Surface Temperature and Time-of-wetness of Concrete Pavements and Bridge Decks," Report # NISTIR 6551, National Institute of Standards and Technology, 2000.

4.9 Kreith, Frank, "Principles of Heat Transfer," 3rd Edition, 1973.

4.10 U.S. DOE, Office of Civilian Radioactive Waste Management, "Topical Report on Actinide-Only Burnup Credit for PWR Spent Nuclear Fuel Packages," DOE/RW-0472, Revision 2, September 1998.

4.11 U.S. NRC, NUREG/CR-0497, "MATPRO-Version 11: "A Handbook of Materials Properties for Use in the Analysis of Light Water Reactor, Fuel Rod Behavior," EG&G, Inc. February, 1979.

4.12 Oak Ridge National Laboratory, "Effect of Fuel Failure on Criticality Safety and Radiation Dose for Spent Fuel Casks," by K.R. Elam, J.C. Wagner and C.V. Parks, NUREG/CR-6835 (ORNL/TM-2002/255), September 2003.

4.13 Oak Ridge National Laboratory, "Physical Characteristics of GE BWR Fuel Assemblies," by Moore and Notz, Report No. ORNL/TM-10902, June 1989.

4.14 Nylund, Hjarne, "The SVEA BWR Fuel, Eight Years of Further development," ABB atom AB, Fuel Division, Vaesteras, Sweden.

4.15 Oak Ridge National Laboratory, "Thermophysical Properties of MOX and UO_2 Fuels including the Effect of Irradiation," by Popov, Carbajo, Ivanov, and Yoder, ORNL/TM-2000/351.

4.16 Ronchi et al., "Effect of Burn-up on the Thermal Conductivity of Uranium Dioxide up to 100,000 MWd/t," Journal of Nuclear Materials 327 (2004) 58-76.

4.17 AAR Brooks & Perkins, Advanced Structural Division, "Boral® The Neutron Absorber," Product Performance Report 624.

4.18 ANSYS Computer Code and Online User's Manuals, Versions 8.1 and 10.0.

4.19 Safety Analysis Report Mixed Oxide Fresh Fuel Package, Volume 1, Revision 4, January 2007, Docket No. 71-9295.

4.20 Updated Final Safety Analysis Report for TN-68 Dry Storage Cask, Revision 4, Certificate of Compliance No. 1027, Amendment 1.

4.21 Transnuclear, Inc., "Application for Revision to Certificate of Compliance No. 9302 for the Model No. NUHOMS®-MP197 Packaging," Docket No. 71-9302, Transnuclear Report No. E-27814 dated April 14, 2009, plus supplemental submittals on June 22, 2009, April 20, 2010, and July 15, 2010.

4.22 Transnuclear, Inc., "Thermal Testing of the NUHOMS® Horizontal Storage Module, Model HSM-H," Transnuclear Report No. E-21625, Revision 1.

4.23 Transnuclear, Inc., Calculation, "TN-24P Benchmarking Analysis Using ANSYS," Transnuclear Calculation No. NUH32PT.0408, Revision 0, provided to USNRC in TN Letter NUH03-03-04, Dated January 24, 2003, "Response to Request for Additional Information (RAI) and Submittal of Revision 4 of Application for Amendment No. 5 to the NUHOMS® Certificate of Compliance No. 1004 (TAC NO. L23343)," Docket No. 72-1004.

Z.4.2 Summary of Thermal Properties of Materials

The analyses performed herein use interpolated values which are appropriate for intermediate temperatures. The interpolation assumes a linear relationship between the reported values. The use of linear interpolation between temperature values in the tables for determining intermediate value of property is justified by the near-linear behavior as a function of temperature for the range of interest.

The tables below provide the thermal properties of materials used in the analysis of the NUHOMS®-37PTH DSC.

The effective thermal properties are the lowest calculated values among the various PWR fuel assembly types that may be stored in the 37PTH DSC as described in Section Z.4.9.

1. Bounding Effective Properties for PWR Fuel Assemblies

(See Section Z.4.9 for calculation of effective fuel properties)

Homogenized PWR Fuel Assemblies in Four Corner Fuel Compartments in 37PTH DSC

Temp (°F)	Transverse Conductivity (Btu/hr-in-°F)	Temp (°F)	Axial Conductivity (Btu/hr-in-°F)	Temp (°F)	Specific Heat (Btu/lbm-°F)	Density (lbm/in^3)
178	0.0168	200	0.0456	80	0.05924	0.1114
267	0.0195	300	0.0481	260	0.06538	
357	0.0230	400	0.0506	692	0.07255	
448	0.0273	500	0.0527	1502	0.07779	
541	0.0323	600	0.0548			
635	0.0380	800	0.0594			
730	0.0444					
826	0.0513					

Homogenized PWR Fuel Assemblies in Other Fuel Compartments in 37PTH DSC

Temp (°F)	Transverse Conductivity (Btu/hr-in-°F)	Temp (°F)	Axial Conductivity (Btu/hr-in-°F) [1]	Bounding effective specific heat and density are the same as those for corner fuel assemblies.
138	0.0174	200	0.0454	
233	0.0199	300	0.0478	
328	0.0238	400	0.0503	
423	0.0285	500	0.0524	
519	0.0340	600	0.0545	
616	0.0403	800	0.0591	
714	0.0473			
812	0.0552			

[1] Only 95% of the axial effective conductivity calculated in Appendix M, Section M.4.8 for the 32PT DSC is considered in the 37PTH DSC model for conservatism.

Z.4.9 Determination of Effective Thermal Properties of the Fuel Assemblies

This section discusses the bounding effective thermal conductivity, specific heat, and density of the fuel assemblies for use in the thermal analysis of the NUHOMS®-37PTH DSC.

The PWR fuel assemblies proposed for storage in the 37PTH DSC are listed in Appendix Z.2. The UO_2 based PWR fuel assemblies are studied in Appendix M, Section M.4.8 and Appendix P, Section P.4.8. There are minor deviations between the dimensions of the fuel assemblies listed in Appendix Z.2 and those studied in Appendices M and P, which have no effect on the bounding effective PWR fuel properties.

For the UO_2 based PWR fuel assemblies, the effective fuel properties of WE 14x14 fuel assembly are the bounding minimum values for all PWR fuel assemblies based on the studies in Appendices M and P. The conductivities of the MOX fuel assemblies are discussed in Section Z.4.9.1.

For the 37PTH DSC, there are two kinds of nominal opening sizes for fuel compartments: 8.875″ for four corner fuel compartments and 8.6″ for the other fuel compartments. In addition, two of the compartment walls are covered with anodized aluminum/poison plates. Since the emissivity of the anodized plates is higher than the emissivity of stainless steel and the compartment opening size is smaller than 9.0″ for the corner compartments, the effective fuel properties calculated in Appendix P, Section P.4.2 based on 9.0″ nominal opening size with WE 14x14 fuel assembly for the 24PTH DSC represent the bounding values for the fuel assemblies in the corner compartments in the 37PTH DSC.

The configurations of the other fuel compartments in the 37PTH DSC are identical to those in the 32PT DSC described in Appendix M. Since the compartment opening in the 37PTH DSC (8.6″) is smaller than the compartment opening in the 32PT DSC (8.7″) and the compartment configurations are identical, the effective fuel properties calculated in Appendix M, Section M.4.2 based on 8.7″ nominal opening size with WE 14x14 fuel assembly for the 32PT DSC represent the bounding values for the fuel assemblies in the compartments other than the four corner ones in the 37PTH DSC.

Based on the above discussion, no further analysis is required for the UO_2 based PWR fuel assemblies for the 37PTH DSC model. The bounding effective properties for these PWR fuel assemblies to use in the thermal analysis of the 37PTH DSC are listed in Section Z.4.2, Table 1.

Z.4.9.1 Effective Properties for MOX Fuel Assemblies

The MOX fuel assemblies are used to replace fuel assemblies with UO_2 pellets. The characteristics used to determine the effective fuel conductivities of the MOX fuel assemblies are almost identical to the fuel assemblies they are replacing. The only significant difference in regard the effective properties is the conductivity of the MOX fuel pellets versus the conductivity of the UO_2 pellets. The effective axial fuel conductivity is calculated based on cladding area only. Therefore, the effective axial conductivity, specific heat and density of the MOX fuel assemblies remain the same as the UO_2 fuel assemblies.

The transverse effective conductivity of a MOX fuel assembly is calculated using the model for the bounding WE 14x14 fuel assembly. It is assumed that the reduction of MOX fuel pellet conductivity due to irradiation is the same as for UO_2 such that:

$k_{MOX\ irrd} = k_{MOX\ un\text{-}irrd} \times k_{UO2\ irrd} / k_{UO2\ un\text{-}irrd}$

The thermal conductivity values of irradiated UO_2 are obtained by interpolation of the data from [4.11] for irradiation temperature ≥1300 K and burnups between 51 and 92 GWD/MTU. The conductivity values are calculated based on a burnup of 70 GWD/MTU for conservatism since the maximum allowable burn up of fuel assemblies in the 37PTH DSC is 62 GWD/MTU. The results of irradiated MOX fuel thermal conductivity calculation are summarized below.

Calculation of Irradiated MOX Fuel Thermal Conductivity

T (°F)	$k_{UO2\ un\text{-}irrd}$ [4.6] (Btu/hr-in-°F)	$k_{UO2\ irrd}$ [1] (Btu/hr-in-°F)	$k_{UO2\ irrd}/k_{UO2\ un\text{-}irrd}$	$k_{MOX\ un\text{-}irrd}$ [2] (Btu/hr-in-°F)	$k_{MOX\ irrd}$ (used in analysis) (Btu/hr-in-°F)	$k_{MOX\ irrd}$ [4.10] (Btu/hr-in-°F)
200	3.322E-01	1.69E-01	51%	2.354E-01	**1.201E-01**	-
300	3.023E-01	1.63E-01	54%	2.204E-01	**1.186E-01**	-
400	2.773E-01	1.56E-01	56%	2.078E-01	**1.167E-01**	-
500	2.562E-01	1.49E-01	58%	1.967E-01	**1.143E-01**	-
600	2.381E-01	1.42E-01	60%	1.866E-01	**1.113E-01**	-
700	2.224E-01	1.36E-01	61%	1.785E-01	**1.092E-01**	-
800	2.087E-01	1.30E-01	62%	1.709E-01	**1.067E-01**	1.248E-01

[1] Interpolated values from [4.11] based on bounding maximum burnup of 70 GWD/MTU.
[2] Interpolated values from Table 3.6-2 of [4.14].

The results of the two-dimensional models for WE 14x14 fuel assemblies with irradiated MOX pellets and design basis PWR fuel assembly used in the thermal analysis (listed in Section Z.4.2, Table 1) are compared in the following table.

The irradiated conductivity for a MOX pellet calculated based on the above assumption is compared to the irradiated conductivity of a MOX pellet taken from ORNL report [4.10] at 800 °F with 4% enrichment and ~5% PuO_2 in the mixed-oxide (UO_2- PuO_2). As shown in the above table, the calculated $k_{MOXirrd}$ value is lower than the value given in [4.10]. This comparison verifies that the calculated $k_{MOXirrd}$ values provided in the above table can be used conservatively to calculate the transverse effective conductivities for a MOX fuel assembly.

Fuel Assembly Transverse Effective Conductivity
(WE14x14)

Average Fuel Temperature (°F)	MOX FA Transverse Conductivity $K_{PWR\ MOX}$ (Btu/hr-in-°F)	Design Basis Transverse Conductivity $K_{PWR\ Design}$ (Btu/hr-in-°F)	$K_{PWR\ MOX}/K_{,PWR\ Design}$ (---)
200	0.0186	0.0190	0.98
300	0.0221	0.0227	0.98
400	0.0267	0.0273	0.97
500	0.0320	0.0329	0.97
600	0.0381	0.0392	0.97
700	0.0449	0.0463	0.97
800	0.0525	0.0543	0.97

As seen in the above table, the transverse fuel effective conductivities for PWR MOX fuel assembly (based on WE 14x14 dimensions) are approximately 3% lower than those for design basis PWR fuel assemblies used in the 37PTH DSC thermal evaluation. However, this small decrease in effective conductivity for PWR fuel assemblies has negligible (less than 1°F) effect on the maximum fuel cladding temperature. Therefore, using the transverse effective conductivities as reported in Section Z.4.2, Table 1 remains acceptable for thermal analysis of the 37PTH DSC.

Z.4.10 References

4.1 U.S. NRC, "Standard Review Plan for Dry Cask Storage Systems–Final Report," NUREG-1536, Revision 1, July 2010.

4.2 American Concrete Institute, "Code Requirements for Nuclear Safety Related Concrete Structures (ACI 349-90)," March 1, 1990.

4.3 ASME Boiler and Pressure Vessel Code, Section II, Part D, Properties, 2004, including 2006 addenda.

4.4 Roshenow, W. M., J. P. Hartnett, and Y. I. Cho, "Handbook of Heat Transfer," 3rd Edition, 1998.

4.5 U.S. DOE, Office of Civilian Radioactive Waste Management, "Topical Report on Actinide-Only Burnup Credit for PWR Spent Nuclear Fuel Packages," DOE/RW-0472, Revision 2, September 1998.

4.6 U.S. NRC, "MATPRO-Version 11: "A Handbook of Materials Properties for Use in the Analysis of Light Water Reactor, Fuel Rod Behavior," NUREG/CR-0497, EG&G, Inc. February, 1979.

4.7 Oak Ridge National Laboratory, "Effect of Fuel Failure on Criticality Safety and Radiation Dose for Spent Fuel Casks," by K.R. Elam, J.C. Wagner and C.V. Parks, NUREG/CR-6835 (ORNL/TM-2002/255), September 2003.

4.8 U.S. Department of Energy, Office of Civilian Radioactive Waste Management, "Characteristics of Spent Nuclear Fuel, High- Level Waste, and Other Radioactive Wastes Which May Require Long-Term Isolation, Appendix 2A," DOE/RW-0184, Volume 3 of 6, December, 1987.

4.9 Not Used.

4.10 Oak Ridge National Laboratory, "Thermophysical Properties of MOX and UO_2 Fuels including the Effect of Irradiation," by Popov S. G., Carbajo J. J., Ivanov V. K., Yoder G. L., ORNL/TM-2000/351.

4.11 Ronchi et al., "Effect of Burn-up on the Thermal Conductivity of Uranium Dioxide up to 100,000 MWd/t," Journal of Nuclear Materials 327 (2004) 58-76.

4.12 AAR Brooks & Perkins, Advanced Structural Division, "Boral® The Neutron Absorber," Product Performance Report 624.

4.13 ANSYS Computer Code and Online User's Manuals, Versions 8.1 and 10.0.

4.14 Safety Analysis Report Mixed Oxide Fresh Fuel Package, Volume 1, Revision 4, January 2007, Docket No. 71-9295.

4.15 Transnuclear, Inc., "Application for Revision to Certificate of Compliance No. 9302 for the Model No. NUHOMS®-MP197 Packaging, Docket No. 71-9302," Transnuclear Report No. E-27814 dated April 14, 2009, plus supplemental submittals on June 22, 2009, April 20, 2010, and July 15, 2010.

4.16 Transnuclear, Inc., Calculation, "TN-24P Benchmarking Analysis Using ANSYS," Transnuclear Calculation No. NUH32PT.0408, Revision 0, provided to USNRC in TN Letter NUH03-03-04, Dated January 24, 2003, "Response to Request for Additional Information (RAI) and Submittal of Revision 4 of Application for Amendment No. 5 to the NUHOMS® Certificate of Compliance No. 1004 (TAC NO. L23343), Docket No. 72-1004."

AFFIDAVIT PURSUANT
TO 10 CFR 2.390

Transnuclear, Inc.)
State of Maryland) SS.
County of Howard)

I, Jayant Bondre, depose and say that I am a Vice President of Transnuclear, Inc., duly authorized to execute this affidavit, and have reviewed or caused to have reviewed the information which is identified as proprietary and referenced in the paragraph immediately below. I am submitting this affidavit in conformance with the provisions of 10 CFR 2.390 of the Commission's regulations for withholding this information.

The information for which proprietary treatment is sought is contained in Enclosures 1 and 5 and is listed below:

- Portions of the RSI responses for TN-LC Transportation Package Application
- Portions of the SAR Sections 1, 2, and 5 for TN-LC Transportation Package Application

These documents have been appropriately designated as proprietary.

I have personal knowledge of the criteria and procedures utilized by Transnuclear, Inc. in designating information as a trade secret, privileged or as confidential commercial or financial information.

Pursuant to the provisions of paragraph (b) (4) of Section 2.390 of the Commission's regulations, the following is furnished for consideration by the Commission in determining whether the information sought to be withheld from public disclosure, included in the above referenced document, should be withheld.

1) The information sought to be withheld from public disclosure involves drawings related to the design of transportation cask, portions of the safety analysis report related to the structural and shielding evaluations, which are owned and have been held in confidence by Transnuclear, Inc.

2) The information is of a type customarily held in confidence by Transnuclear, Inc. and not customarily disclosed to the public. Transnuclear, Inc. has a rational basis for determining the types of information customarily held in confidence by it.

3) Public disclosure of the information is likely to cause substantial harm to the competitive position of Transnuclear, Inc. because the information consists of descriptions of the design of transportation cask, the application of which provide a competitive economic advantage. The availability of such information to competitors would enable them to modify their product to better compete with Transnuclear, Inc., take marketing or other actions to improve their product's position or impair the position of Transnuclear, Inc.'s product, and avoid developing similar data and analyses in support of their processes, methods or apparatus.

Further the deponent sayeth not.

Jayant Bondre
Vice President, Transnuclear, Inc.

Subscribed and sworn to me before this 17th day of August, 2011.

Notary Public

My Commission Expires

Lauren McKee
NOTARY PUBLIC
Anne Arundel County, Maryland
My Commission Expires 2/12/2015